NOVA SCHOOL OF SCIENCE & TECHNOLOGY

DEPARTAMENTO DE ENGENHARIA CIVIL

SAMUEL ALEXANDRE CORADO COSME

Licenciado em Ciências de Engenharia Civil

NUMERICAL SIMULATION OF RETROFITTED MASONRY BUILDINGS

RETROFITTING SOLUTIONS FOR UNREINFORCED MASONRY BUILDINGS

MESTRADO INTEGRADO EM ENGENHARIA CIVIL

Universidade NOVA de Lisboa

Março, 2022

NOVA SCHOOL OF SCIENCE & TECHNOLOGY

DEPARTAMENTO DE ENGENHARIA CIVIL

NUMERICAL SIMULATION OF RETROFITTED MASONRY BUILDINGS

RETROFITTING SOLUTIONS FOR UNREINFORCED MASONRY BUILDINGS

SAMUEL ALEXANDRE CORADO COSME
Licenciado em Ciências de Engenharia Civil

Advisor: Igor Tomic,
PhD Student,
École polytechnique fédérale de Lausanne (EPFL)

Co-advisors: António Pinho Ramos,
Associate Professor with Habilitation,
NOVA University Lisbon

Júri:

Presidente: Fernando Farinha da Silva Pinho,
Associate Professor with Habilitation,
NOVA University Lisbon

Arguentes: Ildi Cismasiu,
Associate Professor with Habilitation,
NOVA University Lisbon

Vogais: António Pinho Ramos,
Associate Professor with Habilitation,
NOVA University Lisbon

MESTRADO INTEGRADO EM ENGENHARIA CIVIL

Universidade NOVA de Lisboa
Março, 2022

Numerical Simulation of Retrofitted Masonry Buildings

ACKNOWLEDGMENTS

First, I would like to endorse my sincere appreciation and gratitude to Professor Katrin Beyer for the opportunity of working with the Earthquake Engineering and Structural Dynamics Laboratory in EPFL. All the knowledge and experiences shared by this fantastic group took my master's degree to another level.

A special thanks to Igor Tomic, PhD candidate at EPFL, for all the help, patience, and empathy during this project. All the words that I can write will never be enough to thank him for his support. This endeavour would never be accomplished without his help, shared knowledge, and contribution.

In addition, I would like to thank Professor António Pinho Ramos from NOVA School of Science and Technology, for his assistance, observations and revisions that considerably contributed to the present research.

My deepest gratitude to my parents, Elisabete and Samuel, for always supporting my academic studies, and for always providing the best conditions to finish my master's degree. To all my family, I want to thank for all the positive thoughts throughout these years.

I want to thank my classmates Catarina, Filipe, João Pedro and Pedro Silva for the memories and work created from the start of the bachelor's till the end of the master's degree. To all my friends, especially the close ones, I want to thank for their friendship, ideas, and support during my master's degree.

Finally, but not least, I want to thank my girlfriend Inês, for all the support and company on this long academic journey.

ABSTRACT

Unreinforced masonry buildings are very common all over Europe, including Portugal and Switzerland. Old and unreinforced masonry buildings are typically constructed with stone masonry and timber floors. The in-plane stiffness and the fixing connections of these floors can have a considerable impact on the global seismic response of the building. As these buildings are normally considered cultural heritage, their safety and the preservation of their original characteristics are key elements to consider.

The main objective of this thesis is to evaluate and study the behaviour of timber floors, considering possible retrofitting and reinforcement interventions, to enhance the building's resistance to seismic events. For this purpose, two numerical models were created, using the software OpenSEES (Open System for Earthquake Engineering Simulation). The first model replicates the original characteristics of unreinforced masonry buildings with stone masonry walls and timber floors. The second model simulates strengthening techniques that are used to enhance the seismic response of the building. The models were developed based on an experimental campaign performed on two half-scale building specimens. Similar to what happens in the development of the numerical models, the first experimental specimen was built based on the typical characteristics of unreinforced masonry buildings. After the first set of experimental tests, this specimen was strengthened. These experimental models were developed and constructed in Athens and were used for a set of shake table tests. The experimental data obtained on these tests is present in the paper *Vintzileou and Mouzakis, 2014* [14]. All the data present in this paper was used for the validation of the numerical models.

The two numerical models were calibrated and subjected to a set of incremental dynamic analyses that replicate the ground motion used in the experimental shake-table tests. After the analyses, conclusions, and results about the behaviour of the timber floors and the seismic enhancement of the retrofitting interventions are presented.

Keywords: unreinforced masonry; equivalent frame models; timber floors; flexible diaphragms; retrofitting.

RESUMO

Os edifícios de alvenaria são bastante comuns em todo o território Português, assim como são também na Suíça. Quando antigos, os edifícios de alvenaria são tradicionalmente constituídos por alvenarias de pedra e pavimentos de madeira. A rigidez no próprio plano e as características de fixação destes pavimentos de madeira, podem ter um impacto considerável no comportamento sísmico dos edifícios. Uma vez que estes edifícios são normalmente considerandos património cultural, a sua segurança e a conservação das suas características originais deve ser considerados.

O principal objetivo desta tese é avaliar e estudar o comportamento dos pavimentos de madeira, considerando possíveis reforços, para aumentar a resistência sísmica do edifício. Neste intuito, foram criados dois modelos numéricos, utilizando o software OpenSEES (Open System for Earthquake Engineering Simulation). O primeiro modelo simula as características originais dos edifícios de alvenaria de pedra com pavimentos de madeira. O segundo modelo simula técnicas de reforço que são usadas para melhorar a resposta sísmica do edifício. Os modelos foram desenvolvidos a partir de uma campanha experimental realizada em dois protótipos de escala 1:2. À semelhança do que acontece no desenvolvimento dos modelos numéricos, o primeiro protótipo experimental foi construído com base nas características comuns dos edifícios de alvenaria de pedra. Após o primeiro conjunto de testes sísmicos, o protótipo original foi reforçado dando origem ao segundo caso de estudo. Estes modelos experimentais foram desenvolvidos e construídos em Atenas e foram usados para um conjunto de testes em mesa sísmica. Os dados experimentais obtidos nestes testes estão presentes no artigo *Vintzileou and Mouzakis, 2014* [14]. Todos os dados presentes neste artigo foram utilizados para a validação dos modelos numéricos.

Os dois modelos numéricos foram calibrados e submetidos a um conjunto de análises dinâmicas incrementais que pretendem simular os testes experimentais realizado em mesa-sísmica. Após as análises, são apresentadas as conclusões e os resultados sobre o comportamento dos pavimentos de madeira e das intervenções de reforço.

Palavras-chave: alvenarias de pedra; modelação por pórtico equivalente; pavimentos de madeira; diafragmas flexíveis; reforços de estruturas.

LIST OF CONTENTS

LIST OF FIGURES

LIST OF TABLES

1. INTRODUCTION

1.1. Context and motivation

Masonry has been the most used construction material throughout time. Nowadays, masonry buildings from different epochs can be seen all around the world. Generally, old masonry buildings were built based on common knowledge and using basic and traditional materials and techniques. In many cases, these buildings are considered to be cultural heritage. In recent years, increased importance has been given to the conservation of cultural and historical heritage. In this way, the assessment and evaluation of the old masonry buildings are crucial to preserve and conserve the historical and cultural legacy.

Ancient masonry buildings are typically stone or brick masonry buildings with timber floors and are resistant to deformations and stresses caused by gravity loads, being considered safe when constructed in non-seismic zones. This situation changes when the building is constructed in a seismic active zone. When subjected to seismic loads, the additional bending and shear stresses developed on the building, could provoke severe damages, often causing a structural collapse [1]. Not being considered an earthquake-resistant construction, in the last decades, research works were done to characterize the real behaviour of masonry buildings while subjected to earthquake ground motion. This type of research originated new types of retrofitting interventions and an upgrade on the quality of masonry products.

The seismic assessment of old masonry buildings is still considered to be a challenge to civil engineers. According to Beyer et al. 2017 [2], this challenge is associated with their flexible floors and ceilings (timber floors/ceilings), which largely prevent the transfer of forces between walls and favour local out-of-plane failure mechanisms [3], the largely unknown deformation capacity of stone masonry walls under in-plane loading [4], and the interaction between adjacent buildings in building aggregates. Moreover, the information about the used materials and constructions techniques can be missing increasing the number of uncertainty variables of the assessment. The seismic assessment of this type of building can be done experimentally, by testing scaled models [5]–[9], or by numerically simulating the behaviour of the building [10]–[13].

Even with the research advances in this field, engineers often lack the tools to capture the expected earthquake behaviour of an existing building. As a result, conservative assessments of the earthquake behaviour are often carried out and too extensive reinforcement concepts and interventions are proposed [2]. As considered being cultural heritage, the interventions and reinforcement techniques need to be as less intrusive as possible to preserve and conserve the cultural and historical legacy. In this way, the development of tools and studies to assess this type of building is crucial for the preservation of cultural heritage.

1.2. **Problem and goals**

Timber floors play an important role in the seismic behaviour of old and unreinforced masonry buildings. Their stiffness has a direct impact on the distribution of the vertical loads to the load-bearing walls and the detailing of the connections between the timber floors and the masonry walls must be adequate to prevent possible out-of-plane failures. Generally, the timber floors present in old unreinforced masonry buildings consist of flexible diaphragms with poor connections to the load-bearing walls. These characteristics can easily jeopardize the behaviour of the building under seismic excitation.

The goal of this thesis is to study the seismic behaviour of unreinforced masonry buildings and timber floors, considering their original state and strengthening interventions that are designed to enhance the global seismic response of the buildings.

1.3. **Approach and contributions**

For this purpose, a pair of numerical models were created and analysed. These models are based on two experimental specimens built and tested in the shake-table of the Laboratory for Earthquake Engineering/National Technical University of Athens (LEE/NTUA). This set of experimental tests performed to the case study is detailed and explained in the paper *Vintzileou and Mouzakis, 2014* [14].

First, a bibliographic study was conducted to obtain information about masonry buildings, timber floors and numerical modelling used to assess this type of structure. A study on OpenSEES was also carried out, through lessons given by EESD, to gain knowledge and practice on the software.

Second, the case-study paper was analysed to gather information on the case-study specimens and to evaluate the possible comparison between numerical and experimental results.

Third, a numerical model was created based on the as-built case-study specimen. The numerical model was developed using the OpenSEES software. The numerical model was then subjected to three types of analysis: modal analysis, self-weight analysis and incremental dynamic

analysis. The incremental dynamic analysis was used to replicate the seismic ground motion used in the experimental campaign. All the results extracted from the performed analyses were then organized and treated using self-written MATLAB coding. Some of the results were then compared with the experimental data detailed in [14].

Fourth, a numerical model was created based on the strengthened case-study specimen. Similar to what was done to the as-built numerical model, the strengthened numerical model was developed using the OpenSEES software and was subjected to three types of analysis: modal analysis, self-weight analysis and incremental dynamic analysis. The incremental dynamic analysis was used to replicate the seismic ground motion used in the experimental campaign. All the results extracted from the performed analyses were then organized and treated using MATLAB coding. Some of the results were then compared with the results obtained from the as-built numerical model and the experimental data detailed in [14].

1.4. **Document organization**

Considering the objectives previously described, the current thesis is organized and divided into eight chapters, including the introduction and conclusion, which are briefly described:

Chapter 1 contains the introduction of the thesis establishing the main objectives and guidelines.

Chapter 2 presents a description of masonry buildings. The seismic performance of masonry buildings is an important topic to understand the typical behaviour of this type of building and is described in this chapter. The bibliographical study of the types of masonry buildings, materials and construction systems is also present in this chapter.

Chapter 3 is dedicated to the description of timber floors. In this chapter, detailed information on the influence that timber floors have on the seismic behaviour of unreinforced masonry buildings is presented. A description of the most common strengthening techniques designed for timber floors is also present in this chapter.

Chapter 4 contains a concise description of the numerical modelling techniques used to develop the numerical models.

Chapter 5 details and describes the information present in the case-study paper. As already described, this information was used to develop the numerical models.

In **Chapter 6**, and based on the previous knowledge acquired, the as-built numerical model was developed and calibrated. All the results extracted from the performed analyses are present in this chapter. The results of the numerical modelling were compared with experimental data, and the conclusions are also described in this chapter.

In **Chapter 7**, the strengthened model was developed and calibrated. All the results extracted from the performed analyses were compared with the experimental results to assess and validate the numerical model. The strengthened model results were also compared to the results from the as-built numerical model to get conclusions on the enhancement of the seismic behaviour of the building.

Finally, **Chapter 8** resumes all the conclusions reached throughout all the research done. Some suggestions are also proposed in this section, leading the way for future work related to this subject.

2. MASONRY BUILDINGS

2.1. Introduction

Being one of the oldest, most important, and widely used construction materials in human history, masonry has been used in the construction of a wide variety of buildings, from historical monuments to residential buildings. Nowadays, we can confirm that many old and historical masonry buildings are still in a good state of preservation, even without substantial repairs or retrofitting interventions. The good resistance to environmental deteriorations combined with the good mechanical properties of this material made it very reliable for construction throughout history.

This kind of structure can be constructed with various materials, whereas masonry units are constructed of different types of materials and bonded with numerous types of mortar. There is a large variety of construction systems, where the materials can be assembled in many ways. Depending on the construction's age, technology and procedures, the building can be considered an old masonry building or a modern masonry building [15].

Modern masonry buildings, that were constructed more recently, generally meet the safety-related requirements of European standards. As these norms were developed more recently, old masonry buildings were constructed without considering safety requirements, being based just on the constructer's experience, which in many cases, can jeopardize the safety of the buildings. However, in the past, the scientific community did not show interest in more advanced testing and analysis on these types of structures. More recently, with the development of new modelling and analysis tools, new research work is being done on this topic. Nevertheless, the lack of experience in this field is considerable when compared to other topics. In this chapter, a brief resume of the characterization of masonry buildings, describing the most common construction systems, masonry materials, and their mechanical properties is presented. At the start of the chapter, description of the seismic performance of masonry buildings is also presented.

2.2. **Seismic Performance of Masonry Buildings**

Earthquakes generate seismic waves that induce ground movements, which in turn affect buildings. The prediction of this kind of occurrence can be done based on geological studies.

These studies have been done for decades and have concluded that seismic events are more common in certain regions of the world. Buildings that are built in these so-called seismic zones, should be constructed under special requirements to increase their seismic resistance and safety. The damages caused by the occurrence of an earthquake depend on several factors, such as the intensity of the earthquake, the foundation soil characteristics, and the response of the structure to seismic ground motion.

Figure 2.1 - Damaged and collapsed masonry buildings: collapsed buildings after the 2020 earthquake in Petrinja, Croatia (Reuters, 2020).

Nevertheless, a major percentage of the existing masonry buildings were built before the creation of these studies and requirements. Adding to unknown construction procedures, the age of the buildings implies possible degradations and existing damages caused by various effects such as natural disasters, armed conflicts, architectural alterations, or bad construction interventions (Figure 2.1). In this way, the behaviour of these buildings while under an earthquake is many times, hard to predict [16].

Despite their longevity, old and historic masonry buildings are usually not resistant to seismic activities. Often showing a brittle behaviour, with non-linear behaviour and structural discontinuities, earthquakes can easily jeopardize their safety. Damage patterns can be observed in the aftermaths of previous earthquakes.

During the observation of strong earthquakes, we can easily conclude that a major percentage of the masonry buildings are easily damaged or collapsed [1]. The oldest types of masonry buildings (stone and adobe masonry buildings) are the ones that normally suffer the most damages due to their poor construction and material quality.

These buildings' behaviour under seismic events, can cause safety issues for not only their occupants but also for those that are in their surroundings or adjacent buildings, due to collapse and/or falling debris. Elements like gable walls, chimneys, cornices, or other exterior ornamentation and exterior walls are particularly vulnerable to collapse, which could be potentially lethal. In more recent masonry buildings, the layout in plan and existing openings have an influence on the building behaviour during an earthquake, as the material and construction quality is theoretically better. Nevertheless, if not built according to the seismic standards, referenced in Eurocode 8 [17] and other standard guides, masonry buildings, in general, are not considered suitable for construction in seismic zones.

Despite the variety of construction typologies and systems, the damage types are similar in every masonry building under an earthquake, and are [1]:

- Cracks in the floor-to-wall interface and sliding of the beams (Figure 2.2, b and c).
- Vertical cracks at wall intersections (Figure 2.2, c).
- Out-of-plane deformations and collapse of the walls perpendicular to the seismic load (Figure 2.2, c).
- Diagonal cracks in piers and spandrels (Figure 2.2, a).
- Flexural cracks in piers and spandrels (Figure 2.2, b).
- Partial collapse of load-bearing walls (Figure 2.2, c).
- Partial or complete collapse of the masonry building (Figure 2.2, d).

(a)

(b)

(c)

(d)

Figure 2.2 - Damaged buildings after 2020 earthquake in Petrinja, Croatia: (a) shear cracks, (b) flexural cracks in piers, (c) out-of-plane deformations and (d) total collapse.

These typical damage patterns are dependent on the type of collapse mechanism that happens in the structure. These mechanisms can happen in the plane of a wall or out of its plane. Only if the out-of-plane failure is prevented, due to the good wall-to-wall connections, appropriate floor-to-wall connections paired with sufficient diaphragm stiffness, will the in-plane damage occur (if the seismic excitation is strong enough)

There are three main types of in-plane mechanisms [18]:

- Flexural mechanism (Rocking) - in this mechanism, the typically observed damages are cracks in a pier base joint, caused by the wall flexural bending, leading to a possible excessive wall overturning and collapse (Figure 2.3 a).

- Shear mechanism - normally characterized by a diagonal crack mechanism, originated by shear stresses, this mechanism reduces the wall's resistant capacity and stiffness (Figure 2.3, b).

- Sliding mechanism - caused by the induced horizontal forces, this mechanism is characterized by the formation of horizontal cracks at the element's bed joints. These cracks form a mechanism throughout the wall that can slide. This failure mode is exclusively found in piers (Figure 2.3, c).

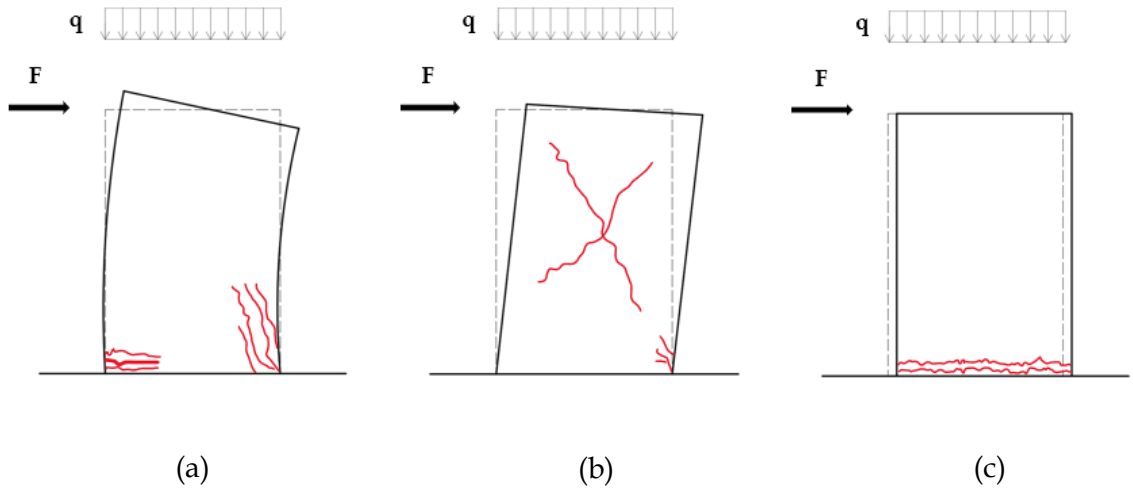

Figure 2.3 - In-plane mechanisms: (a) flexural mechanism, (b) shear mechanism and (c) sliding mechanism.

The out-of-plane failure modes are normally associated with the poor quality of the connections between structural elements and the lack of load-bearing elements. To prevent this so-called out-of-plane mechanism, the building behaviour should be like a closed box-type behaviour (Figure 2.4, b). This behaviour can be achieved, for example, with good connections between orthogonal walls and in the interface between floors and masonry walls.

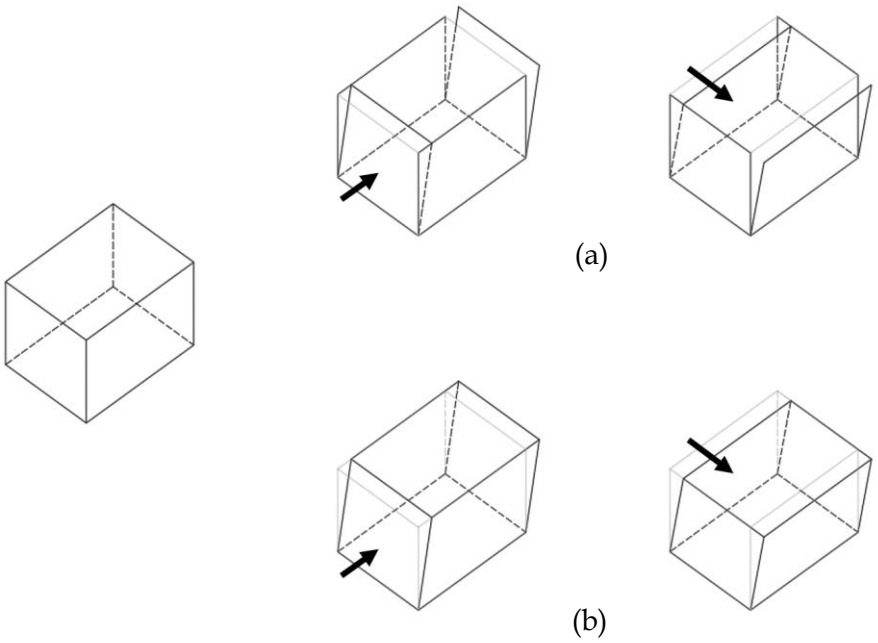

Figure 2.4 - Box behaviour in unreinforced masonry buildings: (a) building behaviour with no "closed box" behaviour and (b) building behaviour with "closed box" behaviour.

If the building has a good structural capacity, then usually the simple overturning of walls is prevented, but other types of out-of-plane mechanisms relayed on arch effects can still occur. This type of mechanism can be prevented using strengthening devices [4].

With this chapter, we can conclude that old and unreinforced masonry buildings are not considered earthquake resistant, especially when unreinforced. Old and historical buildings were many times constructed under no technical knowledge and just by construction experience, making the building safety vulnerable [19]. Nowadays engineers that are working with this type of building have to overcome a major contradiction, making the best decision between safety requirements and cultural heritage preservation. The seismic behaviour of these buildings needs to be considered safe and resistant, and at the same time the interventions needed to reach these requirements, cannot alter the values of the cultural heritage structures [4].

2.3. **Masonry Materials**

The oldest masonry buildings were constructed millenniums ago and consist of adobe or natural stone walls. Due to good resistance and properties, some of these primitive materials are still used nowadays [20].

Adobe walls consist of clayey earth mixed with water, that when dried, becomes solid and robust (Figure 2.5). This material could be dried into bricks or used directly in the walls. In some cases, this type of material was used as mortar or plaster. A common practice on this kind of construction was to add dung or straw into the adobe units and let them dry in the shade, to prevent cracking. Although being load-bearing, adobe is not considered earthquake resistant. This type of masonry can be very durable and reliable when used in dry climate zones.

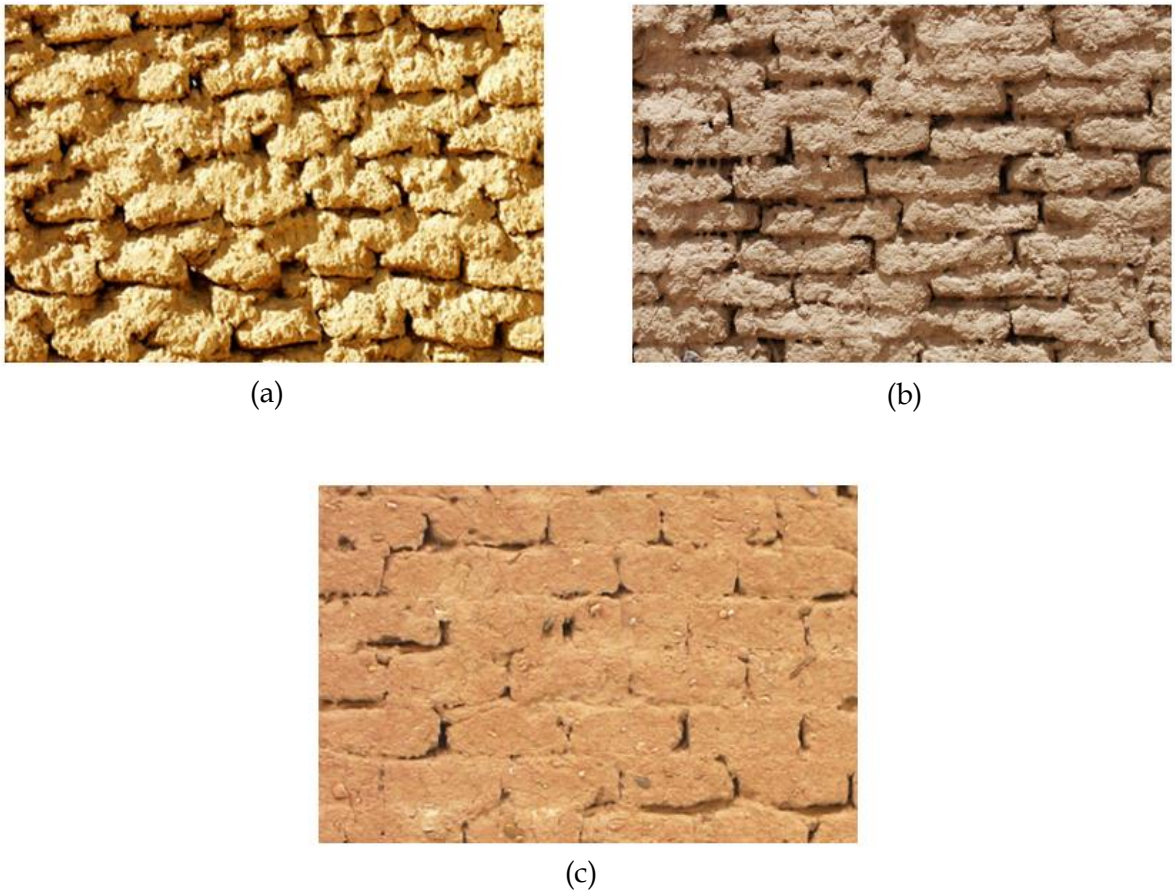

(a) (b)

(c)

Figure 2.5 - Example images of adobe walls: (a) irregular hand-shaped adobe units, (b) irregular adobe blocks and (c) regular adobe blocks.

Stone masonry has provided shelter and comfort to humanity for thousands of years. This heavy and dense material was locally extracted and used on various types of construction, such as various structural elements like arches, columns, beams, and most commonly, walls.

The quality of the stones varies with the type of stone, and to be used for stone masonry should be hard and durable. These walls can be classified based on the used stones (dimensions, geometry, and properties), the mortar, the arrangement of the units, and the wall section.:

- Dry Masonry Walls - this type of masonry wall is characterized by the absence of mortar. In these walls, the strength of the connection between stones is fully dependent on stones geometry and arrangement (Figure 2.6, a).

- Rubble Masonry Walls - in this type of masonry wall, the stones are in their most natural state, roughly without dressing or polishing. These walls can be called coursed or non-coursed walls, depending on the arrangement of the stones. If the stones are placed respecting a course this wall is a coursed masonry wall. If the stones are placed without respecting a predetermined course, the wall can be defined as a non-coursed masonry wall. Either the case, the joints and possible voids between stones and courses are normally filled with mortar. Long vertical joints are normally avoided, and each stone is carefully selected according to its future placement. (Figure 2.6, b).

- Ashlar Masonry Walls - this type of masonry wall consists of cut masonry units that were dressed on a specific geometry. This stone masonry wall is characterized by smooth and parallel faces. This type of masonry uses a lesser quantity of mortar when compared to other types of walls, because of the regularity of the interfaces between masonry units. This type of wall can also be called Dressed Stone Masonry Walls. (Figure 2.6, c).

(a)

(b)

(c)

Figure 2.6 - Example images of masonry walls: (a) dry masonry wall, (b) rubble masonry wall and (c) ashlar masonry wall.

Stone walls can have different settings in terms of their section. The number of leaves is an important parameter that characterizes these sections. There are various leaf settings for stone masonry walls [21]:

- Single leaf stone masonry walls - as the name suggests, this wall consists of one leaf of stone masonry units (Figure 2.7, a).

- Two leaves stone masonry walls - a wall that has two leaves of stone masonry with smaller stones and mortar filling the irregular gaps and voids (Figure 2.7, b).

- Three leaves masonry walls - a wall with two outer high-quality leaves separated by a lesser resistant stone masonry leave (Figure 2.7, c).

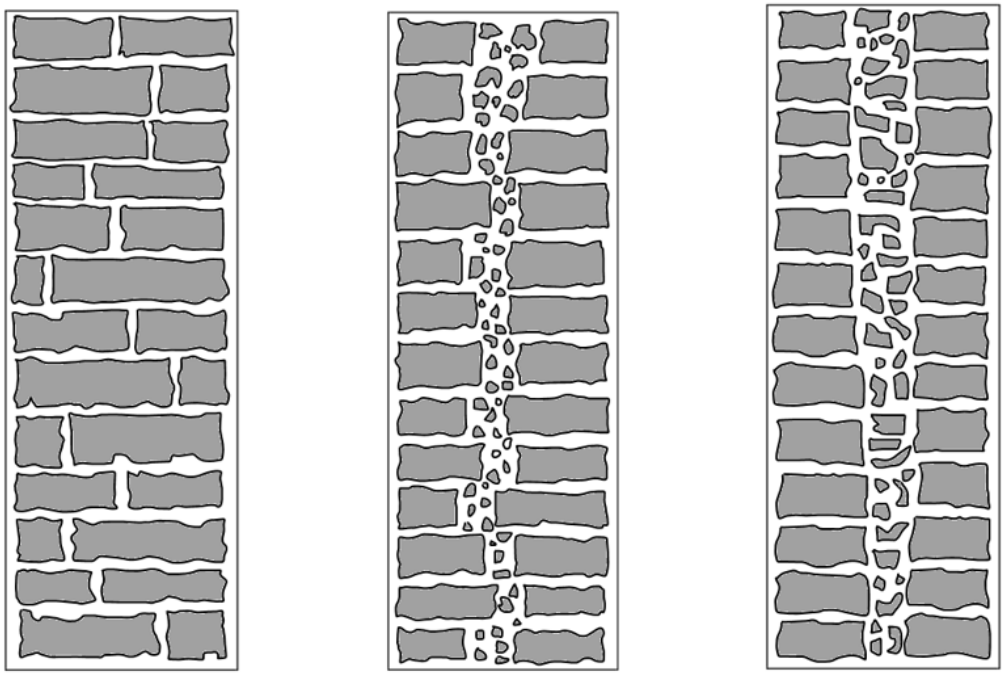

Figure 2.7 - Leaf settings of the masonry walls: (a) single leaf masonry wall, (b) two leaves masonry wall and (c) three leaves masonry wall.

With the advancement of human technology, newly manufactured masonry units were created, originating new and better solutions for the construction of masonry buildings. From fired clay units to concrete and autoclaved concrete units, the weight was reduced compared to traditional solutions such as natural stone. In the past decades, hollow and perforated masonry units were manufactured turning the material more cost-effective and material efficient. A description of the existing types of units is present in

Table 2.1.

Masonry Material	Description
Fired clay units (Figure 2.8, a)	Manufactured from a similar material as adobe, that is cooked in high-temperature ovens. These units have good resistance to abrasion and corrosion, high mechanical strengths, and good thermal performance. Are considered lightweight masonry units.
Concrete units (Figure 2.8, b)	Manufactured from casted concrete, normally composed of Portland cement and sand or fine gravel. Other materials can be used on this type of units, such as recycled materials and industrial waste. These blocks inherit the mechanical properties of the concrete, making them a resistant and reliable construction material.
Autoclaved aerated concrete units (Figure 2.8, c)	Manufactured from casted lightweight cellular concrete, cured under heat and pressure in an autoclave. As the composing concrete suggests, this is a lightweight unit, with high thermal insulation, good fire resistance, and good workability.

Table 2.1 - Industrial masonry units: description and information.

The classification of these units is dependent on the volume of holes and cavities. If the unit has no holes/cavities or has up to 25% by volume of vertical holes they are considered solid masonry units. If more than 50% of the volume of the units consists of cavities or holes, the units are considered hollow masonry units. If the percentage by volume of vertical holes is in the interval defined by the last two values (25%-50%), the unit is considered a perforated masonry unit.

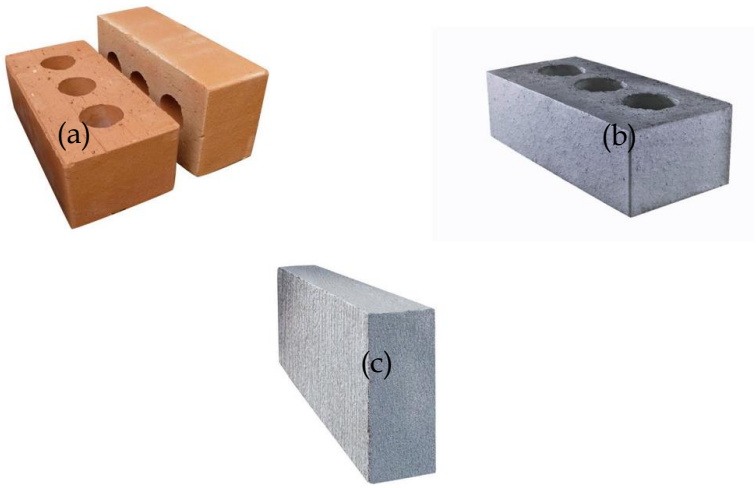

Figure 2.8 - Example images of industrial masonry units: (a) fired clay units, (b) concrete units and (c) autoclaved aerated concrete units.

Specifications and requirements such as dimensions and tolerances, and properties like mechanical strength, water absorption, frost resistance, etc., about these materials, are described in more detail in the Eurocode 6 [22].

Mortar has been used for centuries as a block biding material. Due to its properties, this material hardens when dried, giving a strong connection between elements and strength to the structure. With good workability, this material is used to fill and seal gaps between masonry units, reducing discontinuities on the masonry walls. The combination of masonry blocks and mortar is one of the oldest constructions methods of human history, and due to its success, is still used nowadays. There are numerous types of mortar (Table 2.2). From clay and mud mortar to pozzolanic mortar, their characteristics, and commonly their names, are inherited from their constituents. Also, for the same constituents, mortars can be distinguished depending on their mix ratio. This ratio influences the mechanical properties of the mortar.

Table 2.2 - Common types of mortar: description and information.

Gypsum mortar	- ancient mortar, made with a mixture of gypsum and fine aggregate mixed with water, this mortar is still used nowadays, mainly for decoration purposes. Was used in the past in many historical buildings. Has poor mechanical properties and environmental resistance. [23]
Lime mortar	- common in old and historical buildings, this mortar is composed of lime and sand mixed with water. Depending on the cure and set time, hydraulic and non-hydraulic limes can be used. Low compressive strength material with good porous properties. [24], [25]
Portland Cement mortar	- being developed more recently, this mortar is composed of cement and fine aggregate mixed with water. Having a higher compressive strength, settling hard and quickly is very used on new masonry constructions.
Pozzolanic mortar	- by mixing pozzolana with lime or cement with water, a strong and quickly hardened mortar is created. The reaction between this volcanic ash and the calcium hydroxide gives this mortar its mechanical properties.
Polymer modified mortar	- polymer-based materials were recently developed and when added to existing mor-

	tars, they improve their mechanical properties. From tensile strength to workability, the enhancement of the mortar depends on the type of polymer modified used. [26]

Lime mortar is still used nowadays, mostly when retrofitting and reinforcing historical buildings. This old used mortar is normally characterized by low compressive strength, normally between 0.5-3.0 N/mm2 [27] and good adhesion to masonry units. This mortar is common to be found in unreinforced masonry buildings that were constructed in the past, being important to the seismic behaviour of the building. The usage of cement-based mortars is more common in recent constructions, due to the good mechanical properties of the material. These properties are fully dependent on the mix ratio of the constituents. The compressive strength and the adhesion are the two most important properties of this material. In Eurocode 6 [28], the reader can find extra information on the mechanical properties of this material.

2.4. **Masonry construction systems**

2.4.1. **Unreinforced masonry buildings**

Unreinforced masonry buildings consist of walls (typically bearing and non-bearing walls) often made of bricks, hollow concrete blocks, hollow clay tiles, or stones, and more commonly of timber floors. The masonry units are normally connected using mortar, which most of the time, is not strong enough to withstand much impact or stress. Being constructed using a vertical arrangement of masonry units, the walls tend to be heavy, with discontinuities, and are normally considered a heterogeneous material. This type of buildings normally has other structural elements like ceilings, or stairs, that are normally constructed using timber, or in some cases, using concrete.

This type of construction system is old, and with his development and user experience, a set of good mason workmanship rules was created. This set of rules aims to enhance the construction properties and procedures. Some examples of these rules are:

- Masonry units should be overlapped on alternate courses so that the wall acts as a single structural element.

- Water can be used to soak the masonry units before the construction to prevent the burning of the mortar, especially cement.

- The settling surfaces, for the walls, should be regularly flat and with the appropriate roughness

This set of rules is still used nowadays and should be used on every masonry construction system.

As described in the previous sections, unreinforced masonry walls have no reinforced materials and are vulnerable to damage and collapse in an earthquake. Due to material geometrical and mechanical properties, the unreinforced masonry walls are normally very resistant to compressive strengths, having poor resistance to traction stresses. When subjected to ground motion, the seismic forces will be higher than in other types of buildings, caused by the heavyweight of the used materials. Being such weak and brittle material, these masonry structures are normally not able to absorb the energy from an earthquake, and in this way, this traditional construction system is not considered earthquake-resistant by the Eurocode 8 [17].

2.4.2. Confined masonry buildings

The confined masonry system was developed more recently, stimulated by the appearance of new and more resistant construction materials like concrete and steel. This type of masonry wall, as the name suggests, is normally confined in all four sides, by reinforced concrete elements or reinforced masonry elements. This construction system is very similar to the masonry-infilled frames, except that on confined masonry, the masonry walls are designed to carry both gravitational and seismic loads. For this purpose, during construction, the bearing walls are constructed first, second, the floors are added into the structure and in the last step the confining elements, both vertical and horizontal are constructed, to connect everything, confining the structural walls.

By confining the walls and using tie-columns and bond beams the connection between bearing walls is improved. Following the upgrade on the connections, the stability of the building is increased, making it slenderer. The ductility and strength of the structure increase as well. Under seismic activity, the brittleness of masonry is reduced, elevating the in-plane resistance of the structural walls. These statements are confirmed with past studies and research works, carried out considering static loads and seismic loads, and with real experience during seismic events.

In this way, this kind of construction system has been performing well in past seismic events, compared with other systems, such as unreinforced masonry. This system can be considered a simple solution where both traditional construction materials and procedures can be used.

In Eurocode 6 [28], the reader can find some additional information about this type of construction system. As this system is not used on the developed models for this thesis, the information present in this sub-chapter is brief and concise.

2.4.3. **Reinforced masonry buildings**

When a masonry wall is strengthened or fortified using other construction materials, we can call that wall a reinforced masonry wall. There are many solutions related to this type of construction system. Each solution is applied considering all the stresses and loads that will be applied to the structure.

Reinforced hollow unit masonry is one of the most used solutions. In this method, steel bars and meshes are embedded in the mortar. With this reinforcement, the walls display increased resistance to seismic loads, increasing the energy dissipation capacity of the walls substantially. The steel reinforcements can be vertical or horizontal. To get better seismic performance, wall construction can be done using both types of reinforcements. After the steel placement, the vertical cavities, are normally infilled with grout or concrete to get a good connection between materials, the horizontal groove is normally filled with either grout or mortar. By grouting the masonry walls, the compressive strength capacity is increased, bonding all the masonry units and other possible reinforcement materials together and filling all the voids that can cause discontinuities in the walls. While using steel to reinforce masonry walls, there are a few things that have to be accounted for. One is the possible corrosion that the reinforcement steel can suffer, if not protected against environmental threats.

Depending on the loads and stresses that will act on the structure, various types of reinforcement materials can be chosen. The Eurocode 6 [28] and the Eurocode 8 [17] have some more information and descriptions about this type of construction system.

3.
TIMBER FLOORS

3.1. Introduction

Floors play an important role in the performance of masonry buildings during a seismic event. These elements are designed to withstand extra masses that are present on the building and are responsible for the bracing of the vertical elements, preventing possible out-of-plane mechanisms.

Figure 3.1 - Timber floor of a school building in Zagreb Croatia, this image belongs to the EESD repository.

If the quality of the connections between the floors and the walls is poor, and/or the floors stiffness is not sufficient (Figure 3.1), the building can be vulnerable to various out-of-plane mechanisms [29]. The floor-to-wall connections need to be sufficiently resistant to withstand lateral forces and displacements, caused by an earthquake. If the force capacity of this connection is not sufficient, the floor will not brace the vertical elements, making them vulnerable to out-of-plane bending and overturning.

Depending on the construction materials of the floors, and construction procedure, they can be more flexible or rigid, meaning that different kinds of responses can happen. Assuming that the floor-to-wall connections are appropriate and a more flexible floor (Figure 3.2, a) the walls that are perpendicular to the main direction of the earthquake will be susceptible to higher displacements and out-of-plane stresses. In the case of a more rigid floor (Figure 3.2, b), the building will develop higher in-plane stresses, acting in the walls that are parallel to the earthquake's main direction [29]. The adequate stiffness of these elements plays a key role in the overall behaviour of the building, but recent studies proved that in some cases, the stiffening of the diaphragm can negatively influence the building's performance [30].

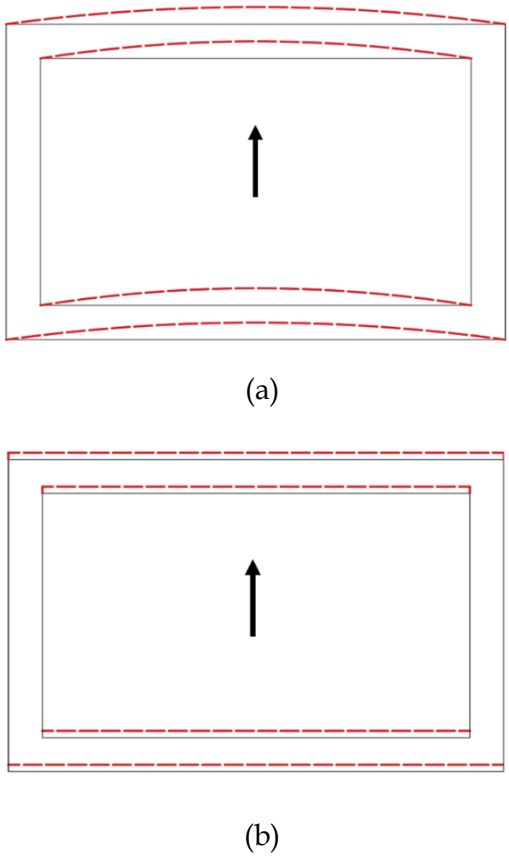

Figure 3.2 - Diaphragm behavior: (a) flexible diaphragm; (b) rigid diaphragm.

In many cases, an enhancement of the global seismic performance of unreinforced masonry buildings is needed. Reinforcing the floors is often less invasive than other forms of retrofitting, and as they play an important role in the building's behaviour, these elements are usually the first to be retrofitted. To achieve this, various strengthening techniques can be used.

In this chapter, the reader can find a resume on timber floors, and on reinforcements/strengthening interventions that can be done to enhance the building's global response under seismic events.

3.2. **Timber Floors**

Timber floors are the most common slabs used in unreinforced masonry buildings. These elements are composed of a set of parallel joist beams that sustain a wooden floor. The floors normally consist of timber boards that are laid perpendicularly to the joist beams and nailed at intersections (Figure 3.3). The dimensions of the beams and the thickness of the floor timber boards can vary and influence the floor stiffness and load-bearing capacity. Being the main structural element, beams are normally laid in the shortest length direction of the walls. The behaviour of the diaphragm is different in the two orthogonal directions: perpendicular and parallel to the main beam's axis [31].

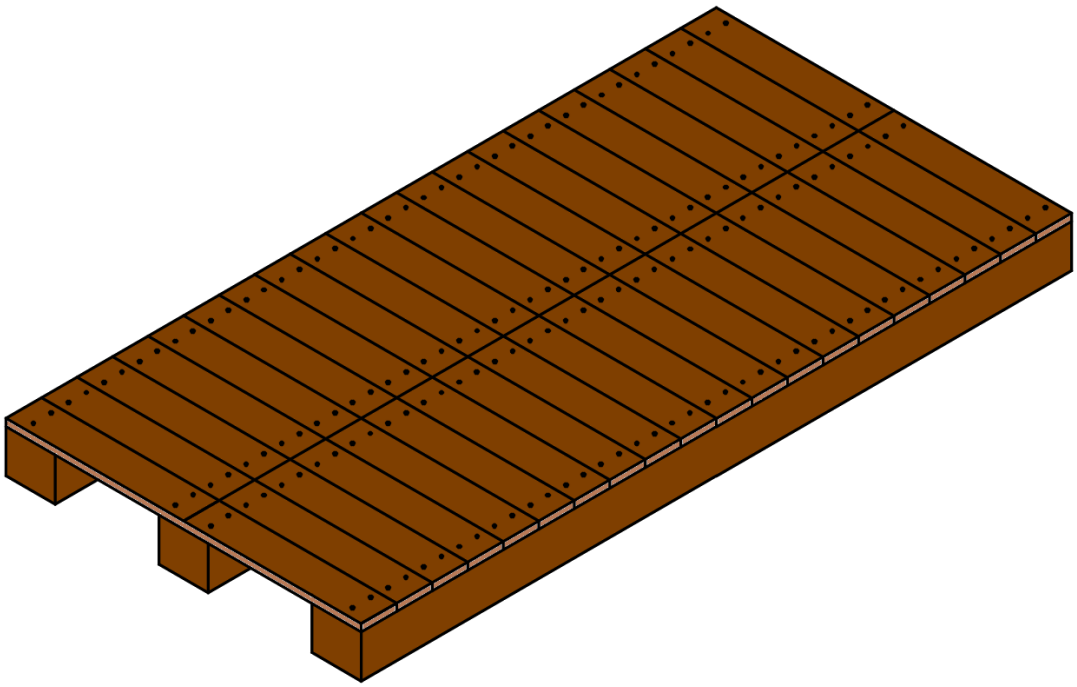

Figure 3.3 - Common timber floor layout used in unreinforced masonry buildings.

The role of the timber diaphragms on the seismic performance of a masonry building mainly depends on their in-plane stiffness and the quality of their connections to the load-bearing walls [31]. Timber floors present in unreinforced masonry buildings, normally behave like a flexible membrane, where the flexibility depends on numerous factors:

- Timber characteristics and mechanical properties
- Floor plan dimensions
- Beam section dimensions
- Distance between horizontal elements
- Type of wall-diaphragm connection
- State of preservation of the floors

The flexibility of the floors has an influence on the mechanisms that can occur, caused by lateral seismic actions. In excessively flexible timber floors, the distributions of the seismic loads to the shear resistance elements can be unbalanced, causing higher out-of-plane stresses and possible bending, and overturning of the perimeter out-of-plane walls (Figure 3.4). In a stiffer timber floor, the out-of-plane mechanisms are less probable to happen, as the shear forces will be transferred to the walls, causing higher in-plane stresses, and increasing the probability of in-planes mechanisms [30]. Overturning of the perimeter out-of-plane (OOP) walls is considered the first mode of failure and the least desirable in historical buildings [32].

Figure 3.4 - Out-of-plane mechanism of a damaged building in Petrinja, Croatia, this image belongs to the EESD repository.

On the floor-to-wall connections side, when these are not adequate, the load-bearing walls can vibrate and be susceptible to out-of-plane failure. Moreover, if the out-of-plane displacements of the walls are substantial, there can be a potential loss of support that can cause total or partial collapse of the floors [31]. In this way, the proper connections need to be established to ensure the box-type behaviour of the building.

The typical connections between the floors and the walls, in URM buildings, are done in various ways, depending on the building layout and geometrical properties. These connections can be done in two major ways: by embedding the beams directly into the walls or supporting them in secondary elements:

- Directly embedded beams into the masonry walls
- Masonry bracket supported beams
- Collector timber beam supported floors

The directly embedded beams are, as the name implies, embedded into a cavity that exists in the wall (Figure 3.5). These are considered the most elementary connections used for fixing the floors. The cavity could be filled with poor grout or mortar to enhance the connection. From post-earthquake assessment experience, constructers could include a gap between the beam and the wall to prevent damage from pounding.

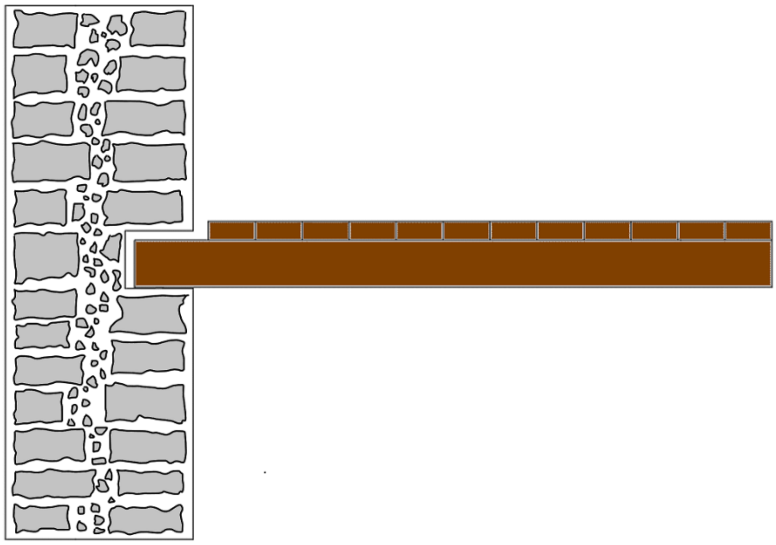

Figure 3.5 - Connection detailing with directly embedded beams.

Another type of connection that is widely used, is the connection where the beams lay on top of a corbel, generally constructed with an arrangement of stones, or using a single masonry structure, that gives a stable and plane support for the beam (Figure 3.6). This bracket element can be made of other materials like timber or metal. By laying the floors on these brackets, better support for the beams is provided, redistributing stresses, and improving their connection with the walls.

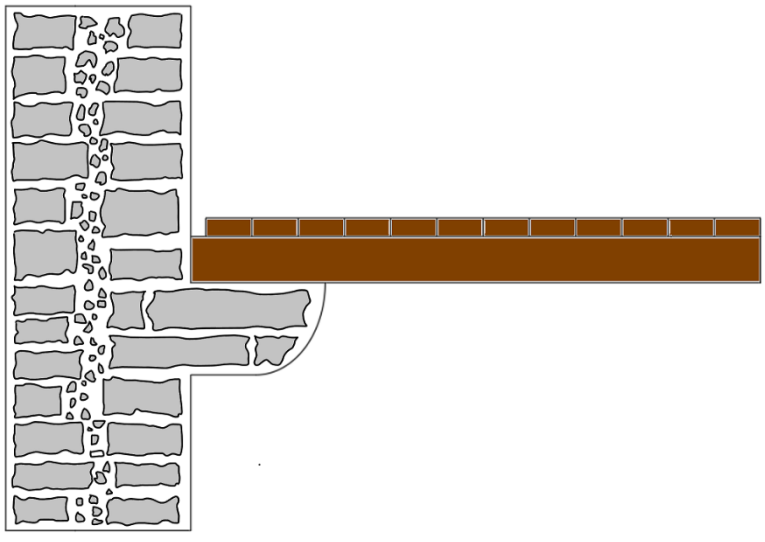

Figure 3.6 - Connection detailing where the beams are laid in bracket elements.

The usage of a collector beam to lay the joist beams is very common in unreinforced masonry buildings and leads to a better distribution of the loads (Figure 3.7). This type of connection could be constructed in various ways, mainly depending on the structural layout of the building. The laying of the main beams or joist beams on top of the collector beam allows a better distribution of vertical and horizontal loads [33].

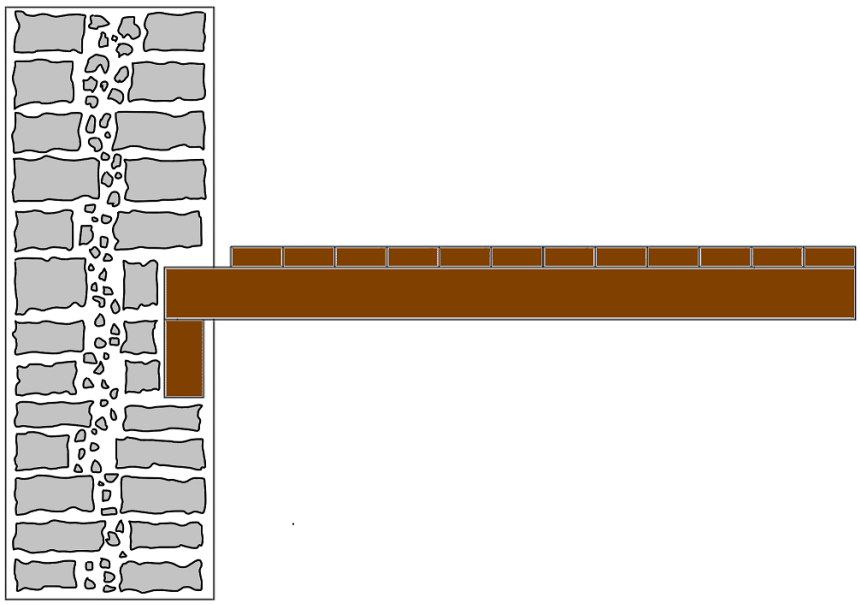

Figure 3.7 - Connection detailing where the beams are laid on the collector beam.

Not being fixed for all degrees of freedom, these traditional connections work through a friction mechanism between elements, where the self-weight of the beams, the friction coefficient, and the surface of contact play the main roles, meaning that the load transmission can be poor [32].

As lateral forces cause high deformations on timber floors, these properties can be affected, making the slab vulnerable to damage or collapse during an earthquake. To avoid high deformations, it was already concluded that these floors need adequate stiffness [29]. The proper detailing of the floor-to-wall connections is also important to ensure the shear transfer between the diaphragm and the masonry walls [31].

In cases where both the good quality of the connections and the proper stiffness of the floors are assured, the walls parallel to the seismic actions will be bearing these actions. This load will act in-plane and will test the in-plane resistance of the masonry walls. As already described, this resistance can be dependent on numerous factors, and if not sufficient can cause in-plane mechanisms normally characterized by the X-cracking in the direction of wall length or flexural cracks (Figure 3.8). Globally the in-plane mechanisms are preferred over OOP failures, as the in-plane resistances of the walls are higher.

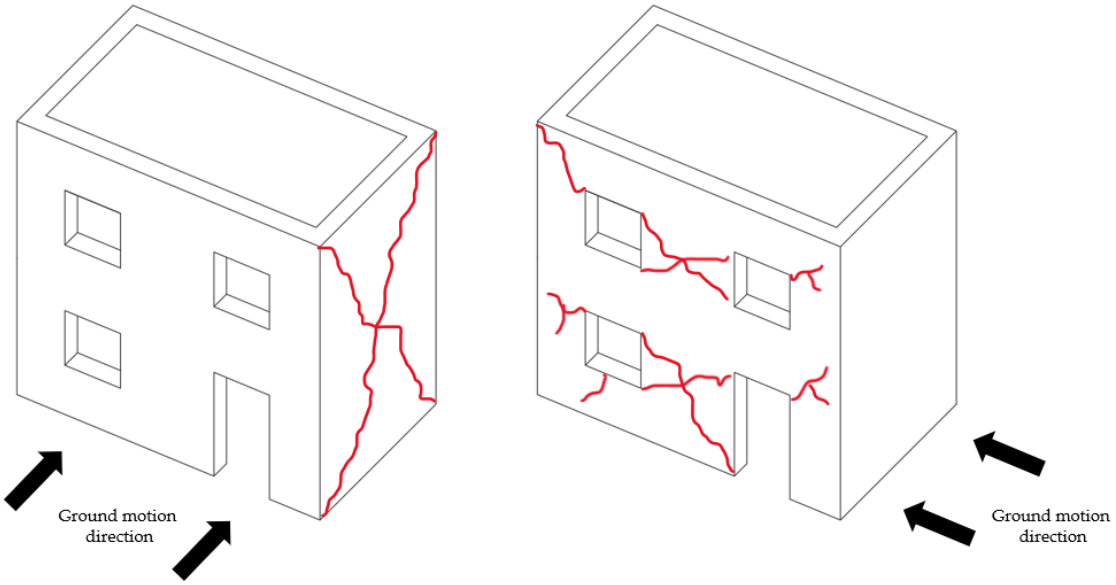

Figure 3.8 - Preferred in-plane mechanisms in an unreinforced masonry building.

Nevertheless, in walls where the composing material has poor quality causing a low shear strength, the walls can show a brittle behaviour being susceptible to collapse. Geometry properties of the walls such as openings, wall thickness, and length-height ratios, also influence the in-plane performance of the walls.

3.3. **Timber Floors Reinforcements**

As floors play such an important role in the behaviour of unreinforced masonry buildings, these elements are normally the first to be strengthened. Reinforcing and strengthening these buildings is not an easy task, as many decisions need to be done over interventions and preservation of the old structure. In this way, the strengthening methods are intended to be as less intrusive as possible. For this purpose, a set of guidelines and principles were defined. The principles give the basic concepts of conservation, and the guidelines describe the methodology that should be followed.

These principles were defined accounting for different factors like research and diagnosis needed, remedial measures and controls, and safety levels. The constant evolution of the construction technologies, which are generally going in different directions from the traditional practices, is another relevant factor, where the division between the science of construction and the art of conservation and restoration needs to be balanced.

According to [34], these principles of intervention seem to include the following ideals:

- Removability (reversibility seems to be an outdated concept);
- Unobtrusiveness, minimum repair, and respect of the original conception.
- Safety of the construction.
- Durability and compatibility of materials.
- The economy of the intervention.

The solutions need to be chosen accordingly to the needs of the building. More commonly, timber floors show damages due to deterioration of the timber elements, often caused by humidity reactions. While under seismic events, the performance of the building, as already concluded, highly depends on both quality of connections and the stiffness of the floors. All of these situations need to be analysed before strengthening interventions are designed. To keep the best preservation state of the timber floors during the buildings' period of life, periodic intervention and maintenances are normally done. These interventions depend on numerous factors, such as economic costs, patrimonial preservation measures, and structural elements to repair. Timber structures are normally affected by environmental hazards, that can jeopardize their structural capacity (Figure 3.9). In this way, the overall strengthening of timber floors should have into account both ageing and biological deterioration, vertical load-bearing capacity, and seismic load-bearing capacity.

Figure 3.9 - Timber floor with biological deterioration and ageing.

In old masonry buildings, timber floors can show deformation related to the excess of vertical loads. In this case, the loads present on these floors should be rearranged to reduce the deformation of the floors. In cases where these deformations persist, and where the structural elements show deterioration and damages, a structural intervention is required on the timber elements, to increase the global load-bearing capacity. To achieve this, various procedures can be done [29]:

- Introduction of new structural elements (Figure 3.10) - this solution can be achieved by the placement of new timber parallel beams on the structure, by reinforcing the existing ones with steel elements, or by adding new transversal elements, which will be supported by the lateral walls.

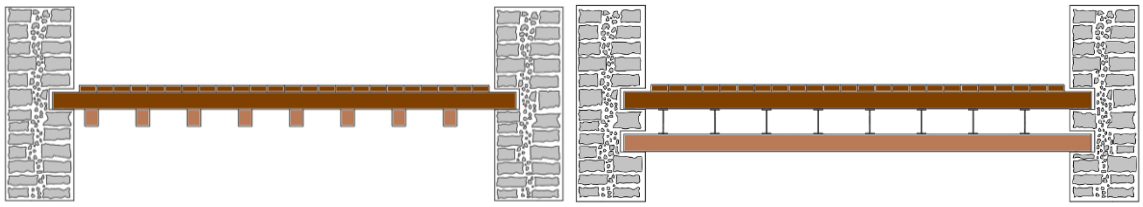

Figure 3.10 - Strengthened timber floors with the introduction of new structural elements: (a) using a new set of parallel beams and (b) using transversal steel elements.

- Introduction of new reinforcement elements (Figure 3.11) - timber and/or steel parts are connected to the existing structure, restoring the original load-bearing capacity of the floors. This procedure is very common to be used in timber elements that are deteriorated. The new and old elements can be connected using various materials, like nails, steel bolts, screws, or glues.

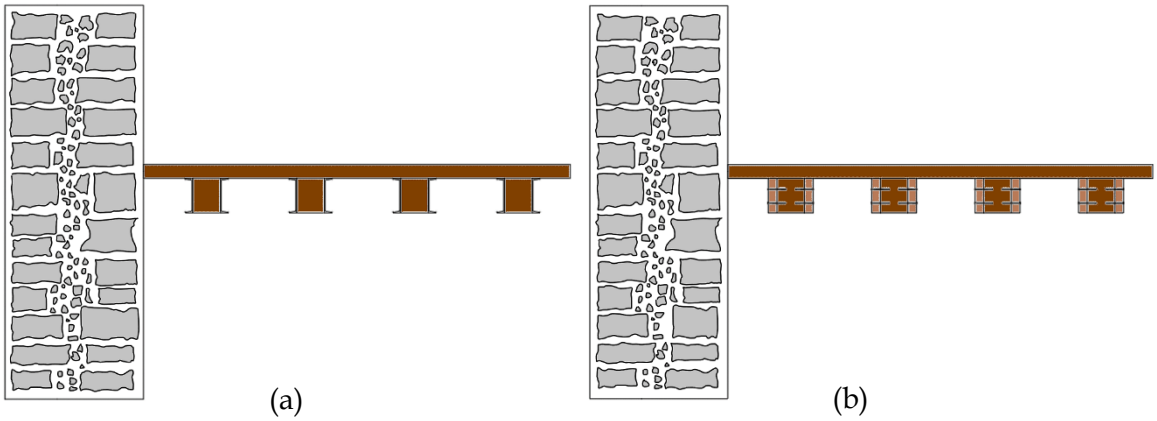

Figure 3.11 - Strengthened timber floors by the introduction of reinforcement elements: (a) using steel profiles or parts and (b) using timber profiles or parts.

- Substitution of deteriorated timber elements (Figure 3.12 and Figure 3.13) - in cases where the timber elements are irreversibly damaged, new elements can be introduced to change the damaged ones. This substitution can be done in numerous ways, with the use of new timber parts connected with nails and screws, with the usage of epoxy resin and glues to replace the damaged wood (Figure 3.13, b), or by replacement of deteriorated elements with new steel and timber profiles (Figure 3.13, a).

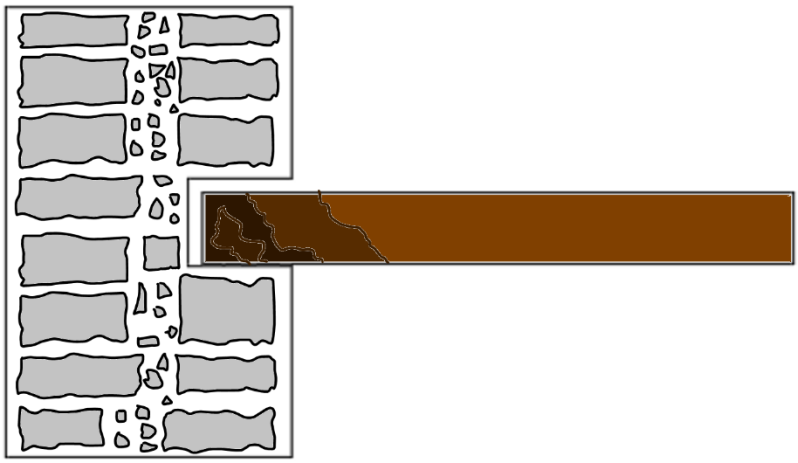

Figure 3.12 - Deteriorated and damaged timber floors.

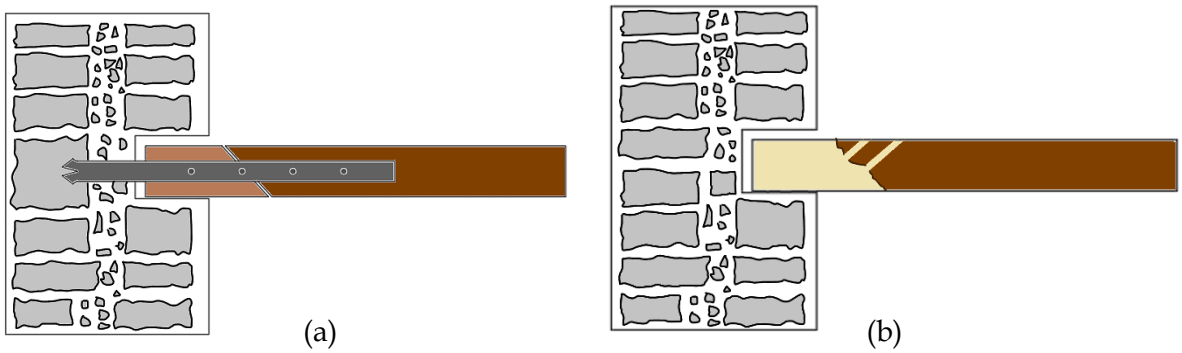

Figure 3.13 - Strengthened timber floors by substitution of deteriorated elements: (a) using steel profiles and parts, (b) using epoxy resins.

Considering seismic load-bearing capacity, as already mentioned, timber floors tend to behave like a flexible diaphragm, where both stiffness and floor-to-wall connections influence the box behaviour of the building. These procedures that were just described, although presenting local interventions, can contribute to the global response of the building. On the connections side, the proper anchoring and tying of the timber floors need to be reached.

The most common and traditional procedure is to use steel and metal elements, that work as ties and anchors, correctly fixing the floors to the walls (Figure 3.14 and Figure 3.15). This intervention not only prevents the pounding and sliding of the beams but also enhances the load distribution over the load-bearing walls, being reversible and less intrusive. These steel ties would be placed at the floor levels, inside the wall through perforation, and locked on each side of the wall, with steel anchor bars or plates. These interventions should improve the energy dissipation capability of the structure, preventing possible out-of-plane collapses [32].

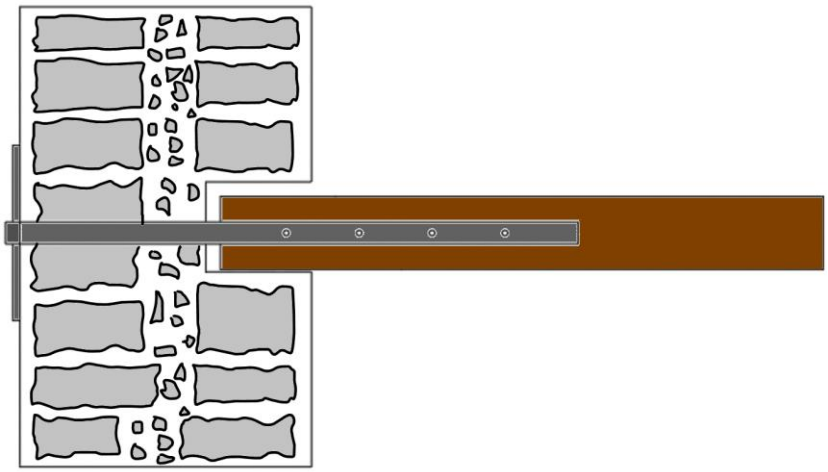

Figure 3.14 - Reinforced timber floors using steel ties and rods to enhance the connection with the load-bearing walls.

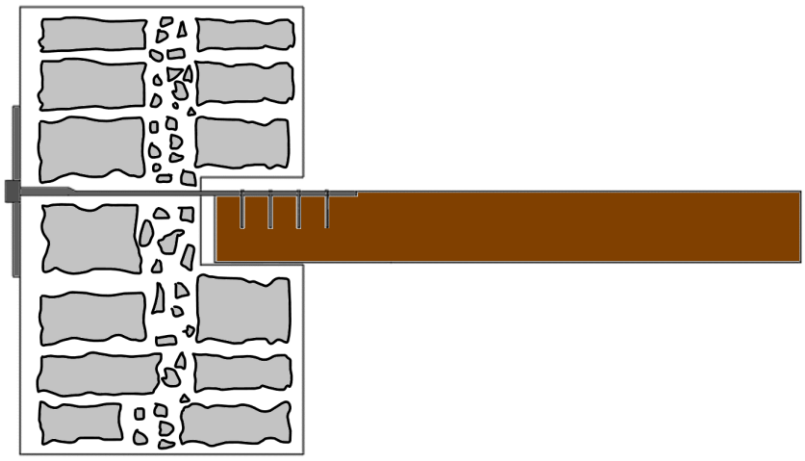

Figure 3.15 - Reinforced timber floors using steel ties, rods, and nails in a key layout, to enhance the connection with the load-bearing walls.

Pre-stress could be induced to these elements for higher fixing capacity. Although the pre-stress has consequences on the structure equilibrium and tension state, care and precautions must be taken, when designing and executing the pre-stress procedure [32].

Pombalino buildings constructed after the big 1755 earthquake in Lisbon, presented a much more complex and detailed type of connections that used these steel elements. In this system the beam joist is connected to the wall, with the help of a key anchor, that would be embedded into the wall with a steel plate on its end (Figure 3.16 and Figure 3.17). This anchoring system should be done with a plan slope of 45º and connecting at minimum 3 timber beams joists, to better distribute the seismic loads [29].

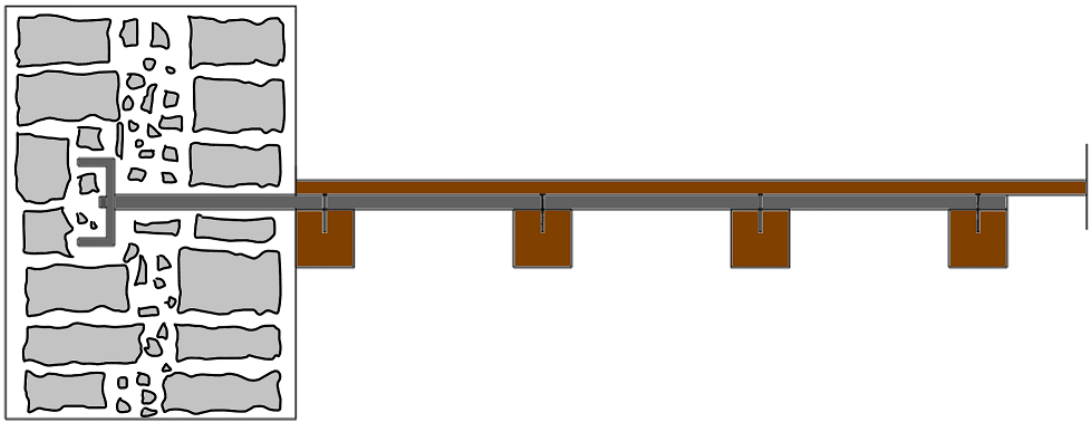

Figure 3.16 - Reinforced timber floors using the anchoring system of Pombalino buildings.

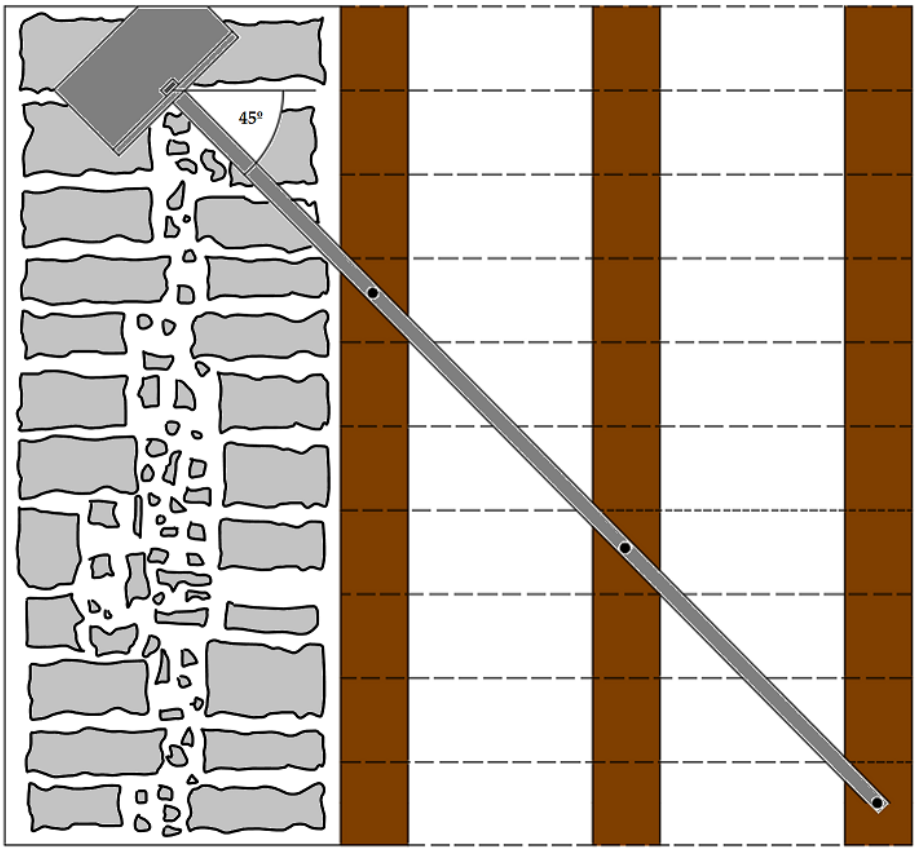

Figure 3.17 - Plan view of reinforced timber floors using the anchoring system of Pombalino buildings.

Another common type of connection intervention is the usage of expansion anchors. The anchors are fixed through the usage of an expansion mechanism where the grip of the anchor is provided by the expansion of the incorporated metal shells, cones, sleeves, or wedges. The expansion anchors can be of two categories: torque-controlled and deformation-controlled.

In torque-controlled anchors, the expansion mechanism is activated by the tightening of the nut or bolt, and the holding power of the anchor within the base material is directly related to the tightening torque used.

There are four basic types of torque-controlled expansion anchor:

- thin-walled sleeve anchors (Figure 3.18)
- thick-walled sleeve, or heavy-duty anchors
- shield anchors
- through-bolts

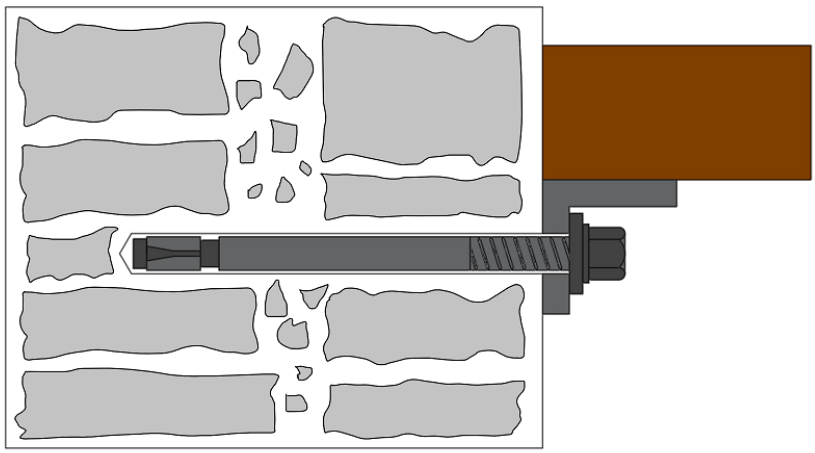

Figure 3.18 - Torque-controlled anchors - thin-walled sleeve anchors.

In deformation-controlled anchors, the expansion is controlled by the relative displacement of the expander cone within a sleeve, usually by hammering a tapered plug down inside an internally tapered shell.

Although being well suited to use in concrete, according to the guidance note published by the Construction Fixings Association (CFA Guidance Note, 2004) [35], the suitability in the masonry of expansion anchors is variable and limited:

- thick-walled sleeve anchors (whose excessive expansion can crack masonry units), through-bolts, and deformation-controlled socket anchors (with which the shock loads from hammering during setting can often crack the masonry units) are not considered suitable to use in masonry.

- the thin-walled sleeve anchors and shield anchors with diameters up to 20 mm overall have limited suitability in masonry.

More recently, cement base materials and/or resin materials have been used to enhance the interface between the steel element and the masonry. Depending on the application and on the type of material involved, injected anchoring could require different types of intervention. These types of anchors are called bonded anchors. As the name implies, these anchors are bonded to the masonry and rely on this bond for connection and grip efficiency.

The resin anchors, also known as chemical anchors, are bonded using a two-part adhesive of resin and hardener. The adhesive is normally mixed with a filler or aggregate, during installation. The type of anchors can be installed in two ways:

- Using the capsule system (Figure 3.19, a)
- Using the injection system (Figure 3.19, b)

In the capsule system, a glass, plastic, or foil tube that contains the adhesive components is inserted in the drilled hole. The mixture of the adhesive components is caused by the insertion and rotation of the anchor rod. The rod can be inserted by hammering or spinning it, depending on the type of capsule used. For this type of anchor, a caution drilling is needed, as the hole size will influence the fixing and filling of the voids. If the hole doesn't have the correct size and depth, the anchor can be incompletely bound to the base material.

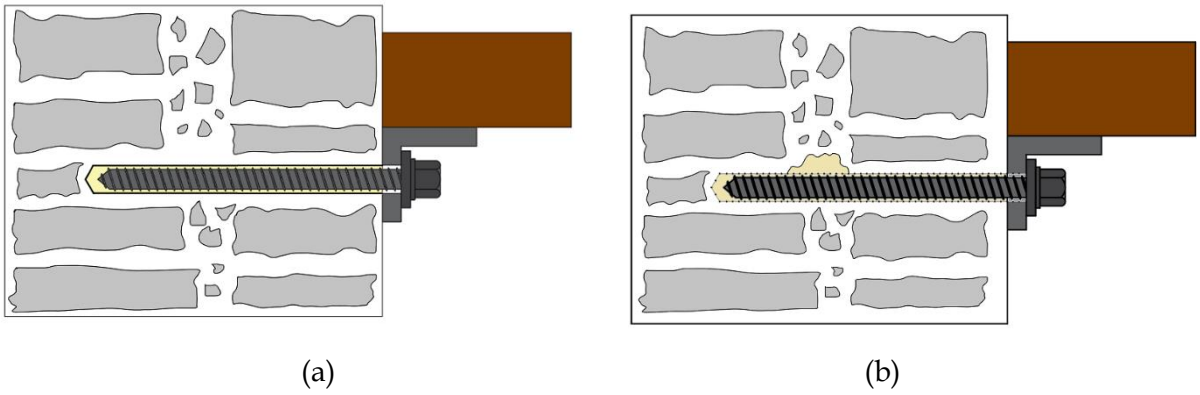

Figure 3.19 - Bonded anchors: (a) using the capsule system and (b) using the injection system.

A different procedure is used in the injection system, where the adhesive mixture is first injected into the drilled hole. The used anchor rod can be of different types. In masonry, where voids are likely, the injection system has an advantage, as the volume of resin injected can be increased to fill the voids. In this way, the hole cleaning is also slightly less critical [36].

Capsule systems are generally less suitable in masonry, for which the injection-type system is preferred, particularly with weaker and voided masonry, where it gives greater certainty of filling local voids within the masonry [37]. The injection of adhesive consolidates the masonry, as well as bonding fully to the fixing.

Anchors are required to resist forces in two directions. Pull-out forces act in the direction of the axis of the fastener, and shear forces act in the orthogonal direction of the fastener [38]. In this way, every fixing intervention using anchors has similar failure modes [39]. Concerning the resistance to tensile loading there, four main failure modes can be considered:

- Steel anchor failure - a less common failure mode, where the steel rod breaks. Is rarely seen in masonry applications and normally occurs in cases in which anchorage depth and masonry resistance are significant (Figure 3.20, a).

- Substrate masonry failure - failure mode caused by the low tensile strength of the masonry or by the lack of anchorage depth. The proximity to existing cracks in the masonry and/or other anchors can increase the possibility of the occurrence of this failure mode. The formed mechanism depends on the type of anchorage. If the anchorage does not go through the entire thickness of the wall, this failure will be characterized by a cone geometry (Figure 3.20, b and c).

- Pull-out failure - this failure mode occurs in the interface between the anchor and the masonry. In the case of chemical anchors, pull-out failure in a fastener occurs between the adhesive and the surface, or between the adhesive and the fastener (Figure 3.20, d).

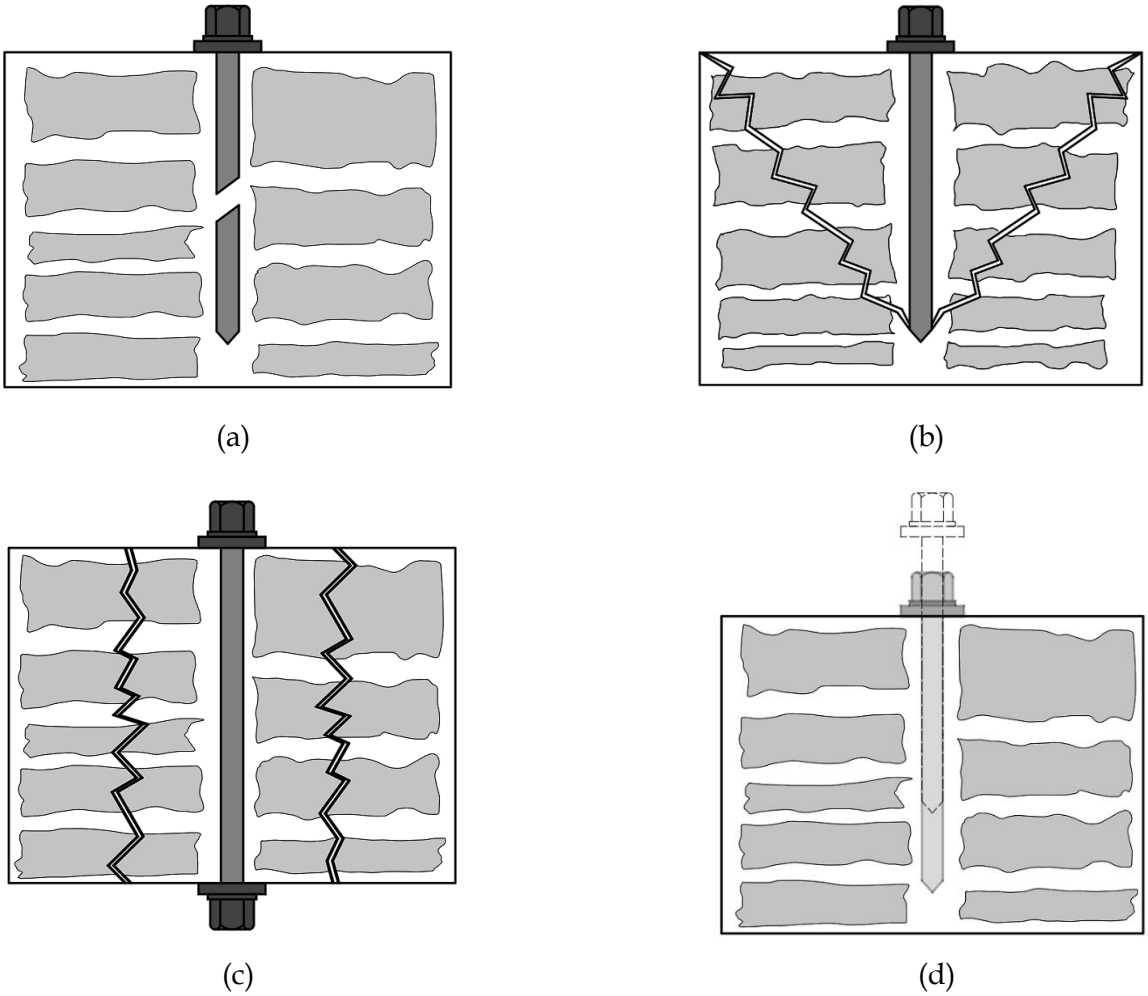

Figure 3.20 - Anchors main failure modes: (a) steel anchor failure, (b) and (c) substrate masonry failure and (d) pull-out failure.

Nevertheless, the strengthening of the connections can be insufficient to enhance the structural integrity of the building. In this way, the strengthening of the floors should be done simultaneously with the strengthening of the floor-to-wall connections. The strengthening of the floors can be done with the stiffening of the diaphragm by substituting or retrofitting the existing timber floors. This type of intervention can prevent out-of-plane mechanisms while improving the distribution of shear forces to the lateral resisting walls. The existence of excessive openings on the layout of the building combined with a poor quality of the masonry can lead to in-plane mechanisms caused by shear forces. In consequence, although being the most common strategy to increase the in-plane stiffness of the floor, in some specific cases, the increase of the floor in-plane stiffness may not induce an improvement in the global response of the building. [30]

Horizontal diaphragm action on floors or roofs is usually very weak in existing unreinforced masonry buildings because of the high flexibility of the diaphragm in comparison with the lateral resistant masonry walls. [32]

To increase their in-plane stiffness, various procedures can be done:

- Second timber boards layer (Figure 3.21) - To increase the stiffness of the floor, the second layer of timber boards can be placed on top of the existing one. The new boards should be laid diagonally to the existing ones (45º), and then connected with nails, screws, or glues. There is a considerable increase in the floor in-plane stiffness with this intervention, without causing a big self-weight increase.

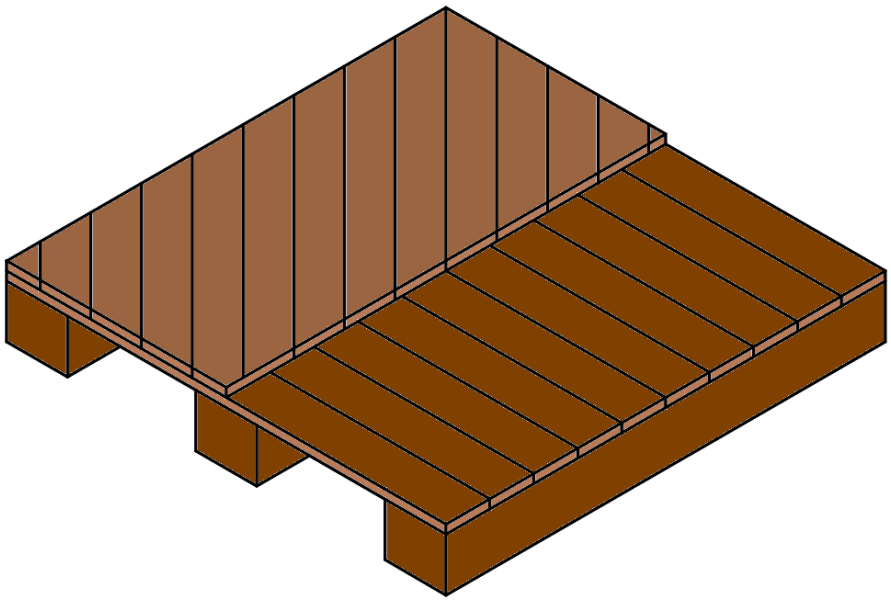

Figure 3.21 - Reinforced timber floor by adding a second layer of timber boards.

- Light steel reinforced floor (Figure 3.22) - in this method, thin steel sheets are anchored to the deck, increasing the overall stiffness of the floor. In this intervention, nails or bolts are normally used to fix the steel sheets on top of the existing timber deck.

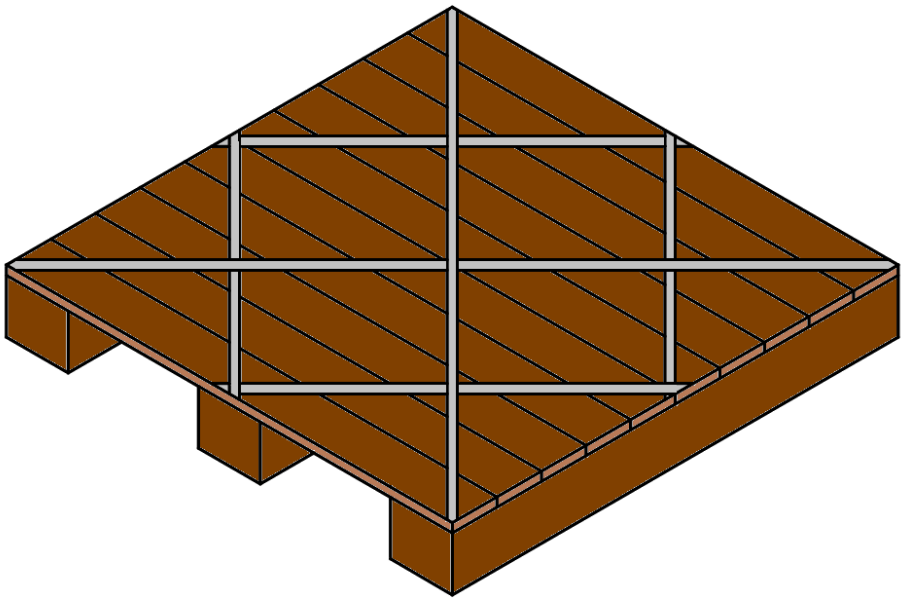

Figure 3.22 - Reinforced timber floor by adding light steel sheets.

- FRP reinforced floor (Figure 3.23) - this recent solution, consists of the placement of FRP sheets on the existing timber deck, laid diagonally, to increase the stiffness of the floor. These sheets are normally glued to wood using epoxy-based resin.

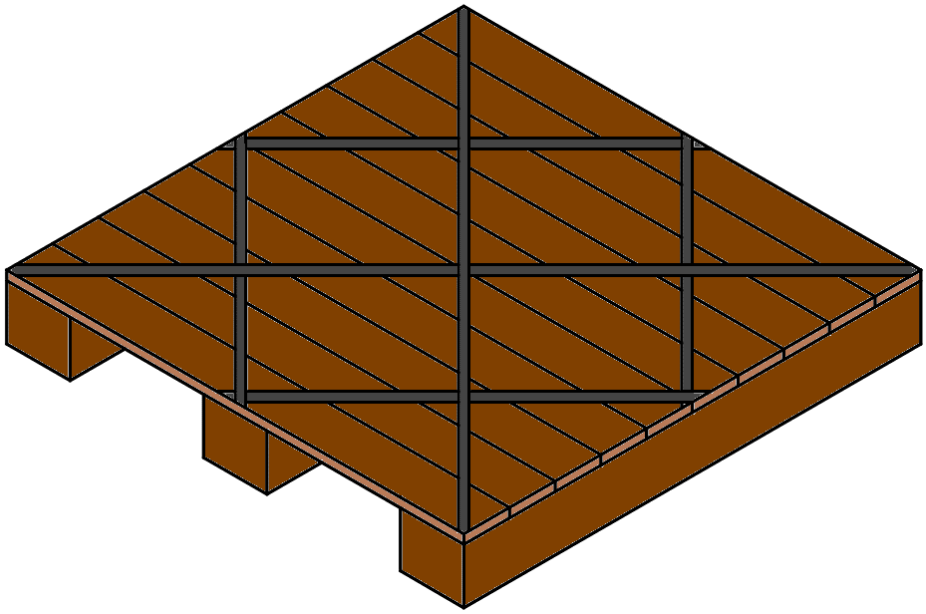

Figure 3.23 - Reinforced timber floor by adding FRP sheets and bands.

- Reinforced concrete slab (Figure 3.24) - a very traditional and common strengthening intervention where concrete is cast on top of the existing timber beams. The connections between the concrete slab and the beams are normally achieved with the help of steel bars. The stiffness and weight of the floor are highly increased.

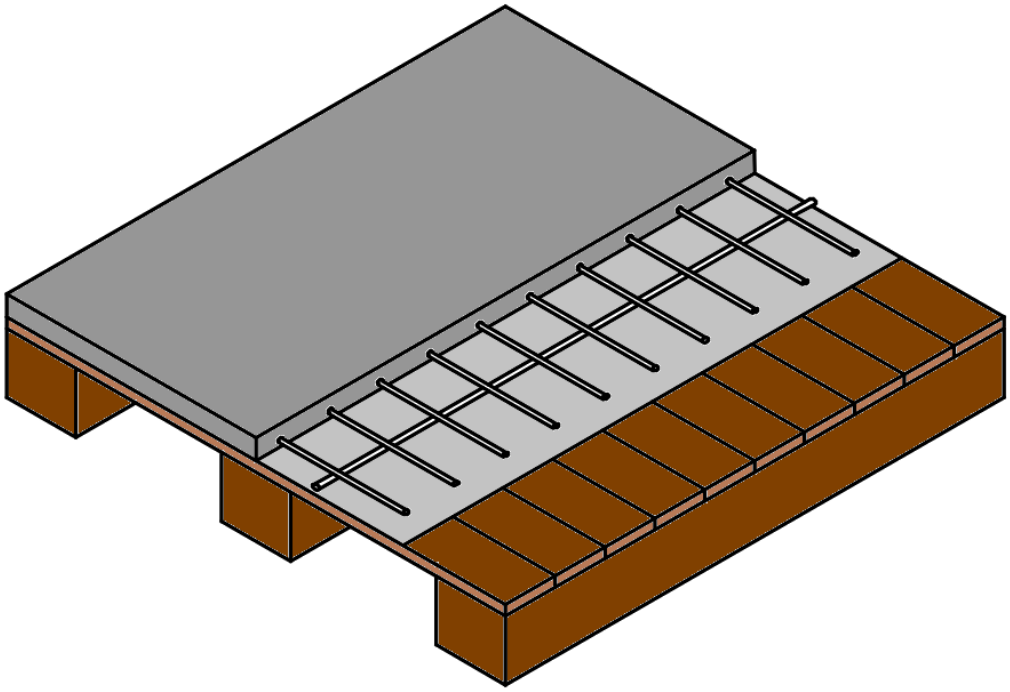

Figure 3.24 - Reinforced timber floor by adding a concrete slab on top of the existing one.

A very common and traditional intervention consists of the replacement of the timber floors or roofs with reinforced concrete slabs, typically with a perimeter reinforced concrete bond beam, where the ring beam provides the connection between the concrete slab and the wall. This procedure is done so that the structural system performs as a monolithic unit during an earthquake. However, using concrete slabs and ring beams should be considered as the last option as the increasing mass could lead to unfavourable high seismic inertia forces, which can cause higher seismic actions [32]. In cases where unreinforced masonry buildings have stiffer floors, which can be the case after using reinforced concrete in the strengthening of the floors, the high stiffness of the timber floors can influence torsion mechanisms (Figure 3.25), as the out-of-plane rotations of the building are decreased [13].

Figure 3.25 - Failure out-of-plane mechanism caused by the existence of a rigid floor.

In this way, it was already concluded that having an increase in the stiffness of the diaphragms can potentially affect the seismic behaviour and performance of the building. In this way, further scientific studies on how much extra stiffness is beneficial, need to be carried out. As this type of building can be susceptible to earthquakes, the simulation, and studies about these elements, are very important to establish appropriate retrofitting and strengthening interventions and procedures [40].

4. NUMERICAL MODELING

4.1. Introduction

The conservation and preservation of historical masonry buildings are nowadays considered a key element of cultural identity. These historical buildings can be located in earthquake-prone areas, being susceptible to damage during seismic events. In this way, the assessment of the behaviour of these constructions while under seismic ground motion is crucial. This assessment can be done in two ways: experimentally and numerically.

Numerical analyses of historic masonry buildings are not an easy assignment. Till today, few resources were used to study this type of construction. Moreover, according to [34], other difficulties are associated with these studies on historical masonry buildings, between which:

- Unknown structural information
- Unknown material mechanical properties
- Unknown existing damages
- Regulations and codes are not applicable

Even with these difficulties, in the last decades, several methods and tools were developed and are used for the assessment of historic masonry buildings. Depending on the approach, numerous factors can vary, affecting the relationship between the accuracy of the results and the time consumption. It can be assumed that different approaches can give different results, without compromising one method over the other.

All the strategies and methods are normally chosen based on the compatibility between the analysis tool and the case to assess [41]. The time consummation and financial cost are also important factors while choosing modelling methods and strategies.

4.2. **Equivalent Frame Modelling**

The equivalent frame modelling strategy is a simple and effective tool for the assessment of unreinforced masonry buildings [15], [42], [43]. This modelling technique uses a structure discretization method to create this so-called equivalent-frame idealization. In this way, the building layout and geometry must be as regular and simple as possible, meaning that small misalignments and curvatures on the walls are normally neglected. After this regularization of the geometry, the walls are meshed into spandrels and piers. Piers are considered the main load-bearing elements and will be coupled by the spandrels in the case of a seismic event. After the identification of the piers and spandrels, rigid panels are defined in the remaining masonry portions. These rigid panels or rigid zones replicate masonry panels, where according to previous earthquake observation, damage does not commonly occur. The discretization of the load-bearing walls is fully dependent on the opening layout of the walls and can be done in numerous ways. The discretization used in this thesis is presented in Figure 4.1.

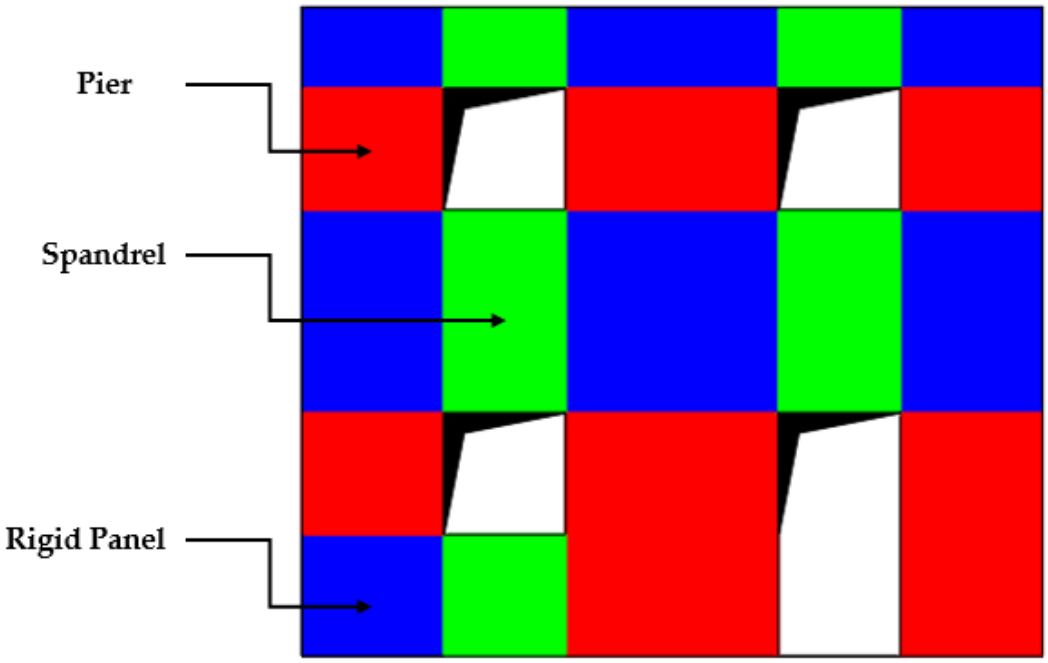

Figure 4.1 - Individuation of spandrels, piers and rigid zones.

This strategy and the existing tools for the equivalent frame modelling assume the assembly of two-dimensional frames that replicate the in-plane behaviour of unreinforced masonry buildings. With these tools, the out-of-plane behaviour is normally neglected, meaning that the floors are assumed to be adequately tied to the masonry walls.

As already described in this thesis, unreinforced masonry buildings are highly dependent on the conditions and properties of their floors and of their wall-to-diaphragm connections. Moreover, recent post-earthquake damage observations, show that out-of-plane failures are commonly the ones that lead to collapses of historical masonry buildings. In this way, ignoring the out-of-plane behaviour when modelling, can negatively affect the accuracy of the results of the global response of unreinforced masonry buildings. As a solution, a new macro-element was formulated by Vanin et al. (2020) [42], which can capture both in-plane and out-of-plane behaviour of piers and spandrels. A more detailed resume about this element is presented in the next sub-chapter.

4.3. **Macro Element**

The macro-element developed by Vanin et al. (2020) [42] is the first macro-element used in equivalent frame models that can replicate both in-plane and out-of-plane behaviour of masonry elements (Figure 4.2). This element is implemented in OpenSEES software and is defined by three nodes, two of which define the element ends. The other node defines the element geometrical centre. The nodes are standard three-dimensional nodes with six degrees of freedom, three of which are displacements, and three are rotations. In each node, sections that divide the element into two panels that only deform in shear, are defined. The shear response of the element is controlled by the middle section of the element, where a non-linear interface that acts on the masonry elements mid-section is defined [44], [45]. This response is coupled to the axial response in terms of forces. To avoid interacting between both deformations, a zero-dilatancy behaviour of the shear interfaces is defined. The flexural response is controlled by all three sections, around which the panels can rotate, with lumped flexural deformations. The uplift related to the rocking response can be properly described by suitable sectional models. In-plane and out-of-plane flexure depend directly on the defined section model.

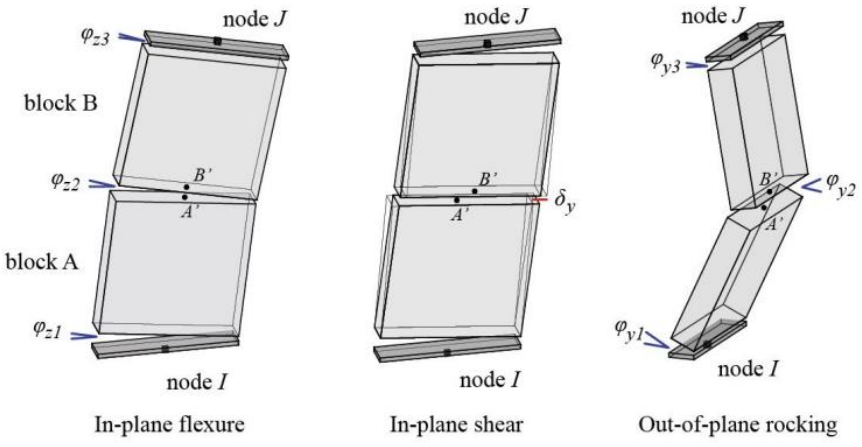

Figure 4.2 - Macro element deformation modes. [42]

The torsional behaviour is modelled linearly elastically and decoupled from all other behaviour modes. Second-order geometrical effects are accounted for through a P − Δ formulation. The masonry properties are also defined in the sections, where a no-tension material with limited compressive strength is set. Gable walls can also be modelled using this element. With this recently developed approach, both in-plane and out-of-plane failure modes can be assessed through nonlinear analyses using equivalent frame models.

4.4. **Orthotropic Membrane**

The timber floors are modelled as a linear elastic orthotropic membrane, where the direction of the main beams dictates the orientation of the larger and lower axial stiffness. The larger axial stiffness will have the same direction of the main beams and the direction of the lower axial stiffness will be the orthogonal direction to the direction of the main beams. Timber properties are needed to describe both axial stiffnesses and shear stiffness. The axial stiffness will be defined according to both parallel and perpendicular to the grain timber properties. The diaphragm shear stiffness can be calculated using a formula developed by Brignola et al., (2008) [30], that accounts for three main contributions for the shear deformations: the flexural deformation of the single board, shear deformation of the single board, and the rigid rotation of the board due to nails slip.

$$G_{eq} = \frac{\chi \cdot F_T}{Bt} \cdot \frac{L}{\Delta} = \frac{\chi}{A} \cdot \left(\frac{l}{k_{ser} s_n^{\,2}} + \frac{\chi}{GA} + \frac{l^2}{12EI} \right)^{-1}$$

Where:

$\chi = shear\ factor$; $G = shear\ modulus\ of\ timber\ planks$;
$E = flexural\ modulus\ parallel\ to\ the\ grain\ of\ timber\ planks$;
$A = area\ of\ plank\ section$;
$I = moment\ of\ inertia\ of\ plank\ section$;
$l = wheelbase\ between\ beams$;
$sn = nails\ spacing$.
k_{ser} = nail stiffness.

In this way, the timber floors are defined by shell elements to which an elastic orthotropic membrane section material is defined. The section model accounts only for membrane stresses, meaning that the bending stiffness of the floors is neglected. The order by which the shell nodes are defined affects the directions of both local axes of the element.

4.5. **Floor-to-Wall Connections**

The out-of-plane behaviour of the walls is dependent on the floor-to-wall connections, as was already described previously in this thesis. In equivalent frame models, these types of connections are normally modelled as perfectly fixed, neglecting their possible failure. As the floors are modelled with the behaviour of a linear elastic orthotropic membrane, the floor-to-wall connections need to account for the non-linear behaviour of the floor. To account for this non-linearity, a zero-length element was created, featuring possible beam slips, through a Coulomb friction mechanism (Figure 4.3). This interaction between floors and walls accounts for other conditions, such as the pounding of the beams towards the walls, and/or the loss of contact due to excessive sliding.

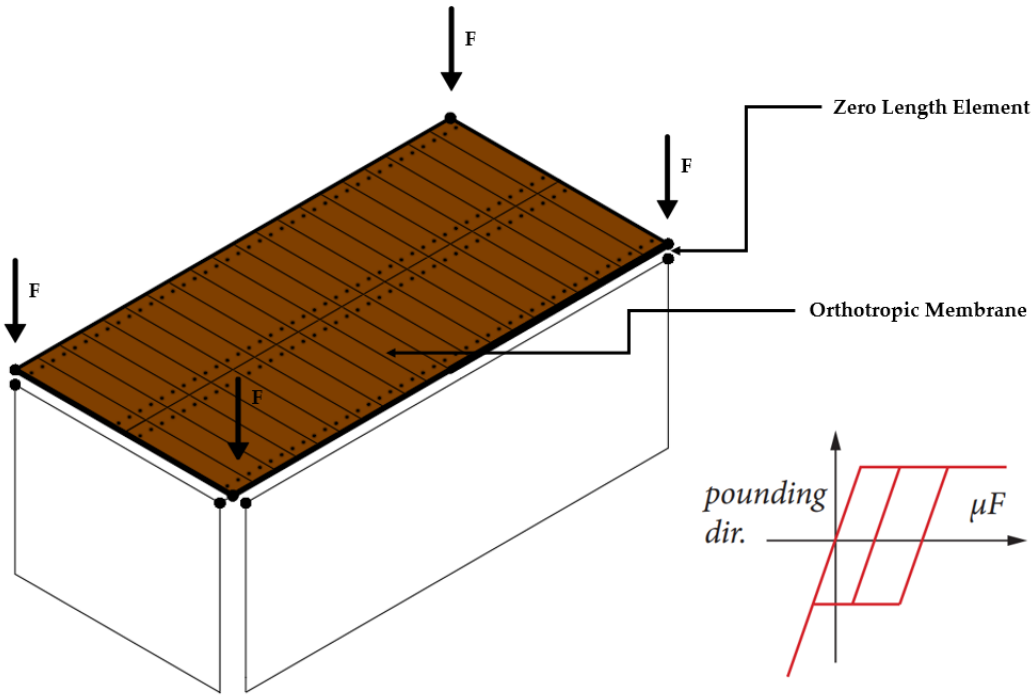

Figure 4.3 - Definition of zero-length elements for modelling the floor-to-wall connections.

To account for every possible condition, a new friction material model was implemented in the OpenSEES software. While using this material model the floor nodes are modelled separately from the wall nodes to record and extract possible relative displacements (beam sliding). The model features zero shear strength, while under traction. While under compression, the transversal forces are transferred proportionally to a friction coefficient that acts in the plane of the floors [11], [12]. The slipping of the beams is only considered to exist in the perpendicular direction to the walls, while in the orthogonal direction an elastic model provides the full transfer of the loads into the walls. The model features the loading in the positive direction through sliding (beam pulled off the support) and in the negative direction through pounding (beam pounding against the wall). A maximum value for the beam slipping can be set to the element, which will originate a collapse mechanism when exceeded.

4.6. **Wall-to-Wall Connections**

Similarly, to what happens with floor-to-wall connections, wall-to-wall connections can also be modelled through a zero-length element. The condition of the interlocking between orthogonal walls depends on various factors, such as the quality of construction and materials. If the connection is not sufficiently good, there is the probability that during a seismic event a vertical crack is formed in the interface between walls, exhibiting a nonlinear behaviour, that can lead to a possible out-of-plane failure.

This type of nonlinear behaviour can be modelled in the corner nodes of both walls with the definition of a zero-length element with appropriate tensile properties. With this element, the strength capacity of the connection is defined by integrating the tensile strength of the masonry along the section of the connection [12]. In this thesis, a 1D material model featuring a linear elastic response in compression and a damage tension law with exponential softening is used on the zero-length elements (Figure 4.4). The model material is described by its elastic characteristics, tensile strength, and the fracture energy produced when a cracking opening occurs. This fracture energy represents the area that will be under the force-displacement curve.

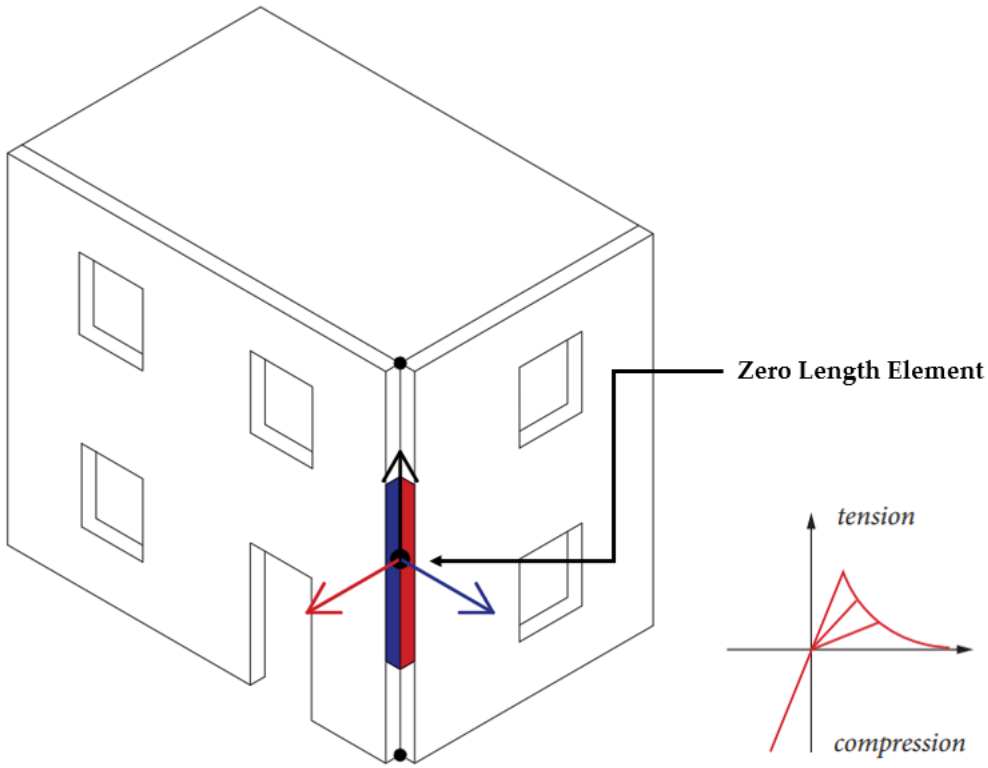

Figure 4.4 - Definition of zero-length elements for modelling the interaction between orthogonal walls.

4.7. **Rayleigh Proportional Damping**

Every structure exhibits energy dissipation. This energy loss is normally associated with the internal friction of the construction materials. As masonry walls consist of a heterogenous combination of mortar and blocks, the internal friction is assumed to be higher and hard to calculate. According to Vanin & Beyer, (2021) [46], Rayleigh damping models are especially relevant when assessing the out-of-plane behaviour of masonry walls. In nonlinear structures three approaches can be done while applying Rayleigh proportional damping [47]:

1. Damping matrix computed based on the initial stiffness
2. Damping matrix based on both initial and tangential stiffness
3. Damping matrix computed based on the tangential stiffness

According to Charney et al., (2008) [47], extreme caution should be taken when using Rayleigh proportional damping in inelastic response history analysis, particularly when the stiffness proportional part of the damping is based on the initial stiffness of the complete structure. This recommendation is associated with the possibility of the overdamping attributed to initial-stiffness proportional damping and with the numerical problems created by using tangential-stiffness proportional damping. As a solution to this issue, a recently developed secant-stiffness proportional damping model is used. This model defines a correction term that acts on the initial stiffness-matrix proportional damping present in the classical Rayleigh damping matrix. This formulation can replicate the out-of-plane behaviour with reasonable accuracy [11].

5. CASE-STUDY

5.1. Introduction

The equivalent frame models developed for the analyses done in this thesis are based on a built and strengthened specimen, that was used for a set of shake table tests [14]. Thi specimen were built in the facilities of the Laboratory for Earthquake Engineering/National Technical University of Athens (LEE/NTUA). The base building consists of a two-story plain three-leaf stone masonry prototype, constructed at a reduced scale of 1:2. The specimen dynamic characteristics were firstly measured (Figure 5.1, a). Thereafter, the as-built prototype was tested under biaxial seismic tests, increasing the intensity of the base acceleration stepwise, to allow the gradual occurrence of damages. When substantial but reparable damage was observed in the as-built specimen, strengthening, and retrofitting techniques were used to enhance and assess the response of the building (Figure 5.1, b). The strengthened specimen was then tested similarly to the as-built one. The tests ended when extensive damage was observed in the retrofitted building.

Figure 5.1 - Image of the model on the shaking table: **(a)** as-built model and **(b)** strengthened model.

5.2. **Geometry of the experimental model**

The tested specimen consists of a non-symmetrical plan masonry building with 3.65 x 2.30 m^2 timber floors (Figure 5.2). Each floor has a height of 1.60 meters, meaning that the building has a total height of 3.20 meters (Figure 5.3). The masonry walls are 0.25 meters thick and are composed of three masonry leaves.

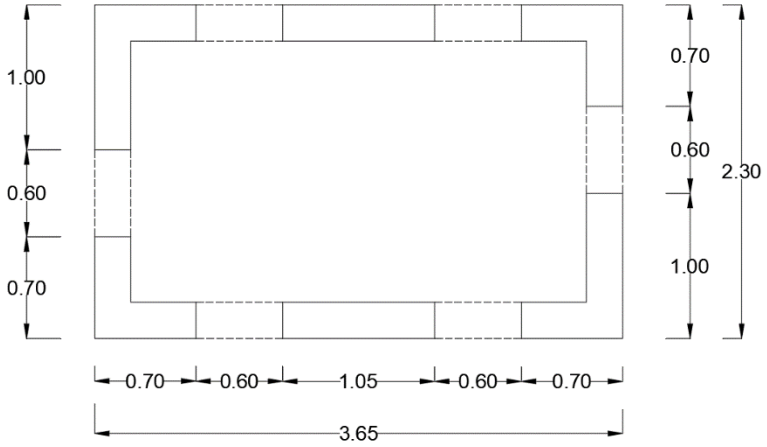

Figure 5.2 - Floor plan of the tested specimen.

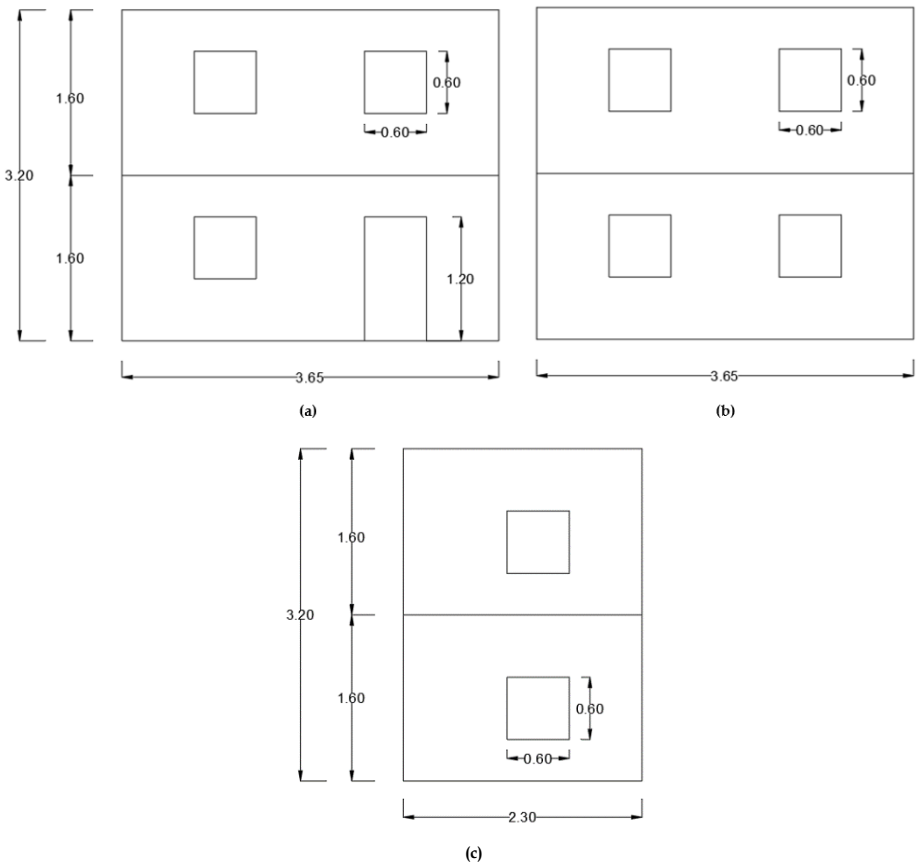

Figure 5.3 - Elevations of the tested specimen: **(a)** front facade, **(b)** back facade and **(c)** side facades.

5.3. **Masonry Walls**

The three leaves in the masonry walls had approximately the same thickness. At the corners of the specimen, stone quoins were installed crosswise throughout the height of the walls, to enhance the interlocking between orthogonal walls. Limestone-based units and mortar were used on the masonry elements. The mortar was composed of lime putty, pozzolan, and a mixture of aggregates. Both head and bed joints were set to be approximately 10 mm thick. When constructing the walls, a percentage of 40% was established for the voids, to recreate characteristics of the filling materials in real unreinforced masonry buildings.

Simultaneously to the specimen construction, two masonry wallets were tested in compression. The first wallet was tested up to collapse and the second till substantial damage occurred. After these tests, the second wallet was grouted, and re-tested, 6 months after, till failure. These tests allowed the computation of the mechanical properties of the masonry walls before and after grouting Table 5.1.

5.4. **Timber Floors**

The floors of the specimen consist of classical timber floors. The floors are composed of timber joists (60 x 100 mm^2) spaced at 340 mm, that are laid in the shorter direction (Figure 5.4). The timber joists sustain a pavement of 100 x 10 mm^2timber boards, that are nailed and laid perpendicular to the main beams. The timber joists are supported by a wooden collector beam that is set through the masonry walls. All timber elements belong to the C22 strength class (EN 338-2003).

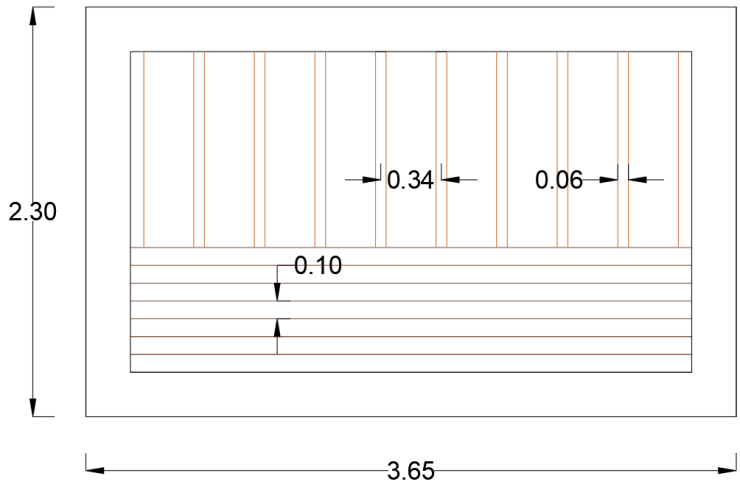

Figure 5.4 - Detailing plan of the timber floors.

5.5. **Strengthening Techniques**

After the first set of seismic excitation tests, the as-built specimen was retrofitted and strengthened. First, the damaged walls were grouted using a natural lime-based grout. This grout was composed of 90% pure NHL5 and 10% superfine natural pozzolan. This mixture was injected into the walls with the help of an ultrasound dispersion mixer by a mechanical device of low turbulence.

Table 5.1 - Mechanical properties of the tested wallettes before and after grouting.

Wallete	$f_{wc,o}$ (MPa)	$f_{wc,j}$ (MPa)	$f_{wc,j}/f_{wc,o}$	$E_{wc,o}$ (GPa)	$E_{wc,j}$ (GPa)	$E_{wc,j}/E_{wc,o}$
1-initial	4.33	–	–	0.84	–	–
2-initial/2-grouted	4.07	5.45	1.33	0.88	3.34	4.35

$f_{wc,o}$ and $E_{wc,o}$ denote the compressive strength and the modulus of elasticity of the wallettes at their original state, $f_{wc,j}$ and $E_{wc,j}$ denote the compressive strength and the modulus of elasticity of the wallettes after grouting

Simultaneously to the grouting of the walls, a second layer of timber boards was placed on the timber floors to enhance their in-plane stiffness. These additional boards were of the same specs as the ones laid down in the as-built model. The new pavement boards were laid at an angle of 45º concerning the original ones and nailed through the original boards to the existing joist beams. Moreover, the stiffened floors were fixed to the masonry walls using a 100 x 100 x 5 mm^3 steel bearing plates (placed against the exterior face of masonry) and an L80/80/8 steel element 200 mm long (placed against the interior face of masonry and bolted onto the timber floor). Both steel elements were connected using 10 mm bolts that were set through holes drilled in the masonry walls (Figure 5.5).

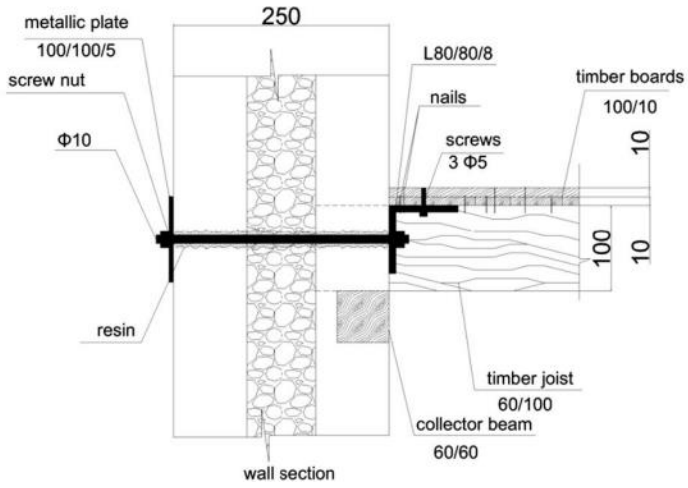

Figure 5.5 - Wall to timber floor strengthened connection detailing.

5.6. **Test-setup and instrumentation**

Sixteen accelerometers and twelve displacement transducers were placed in various locations of the specimen to measure accelerations and absolute displacements along with X and Y directions (Figure 5.7). This setup was used in both the as-built specimen and the strengthened specimen. Additionally, four displacements transducers were set in the strengthened specimen to capture possible relative displacements in the floor-to-wall connections, allowing the assessment of the quality of the connection between horizontal and vertical load-bearing elements.

Extra masses were added to the as-built specimen to replicate the real loading of unreinforced masonry buildings. Heavyweight objects were placed on each floor, adding 7.5 tonnes of mass to the first floor and 4.5 tonnes to the second floor (Figure 5.6). The total mass of the as-built specimen was approximately equal to 22.0 tones. After the strengthening of the specimen, the total mass was increased by approximately 13%, making a total of 23.5 tonnes.

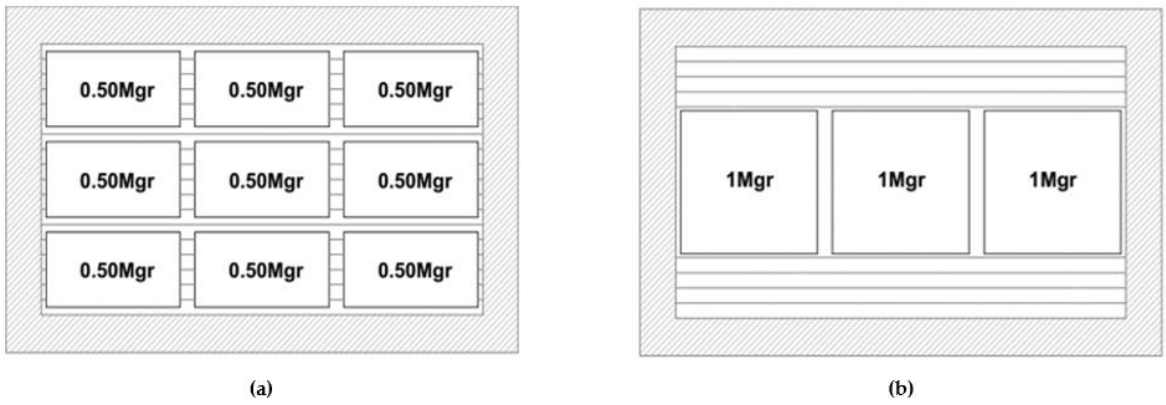

Figure 5.6 - Arrangement of additional masses: (a) 1st floor and (b) 2nd floor.

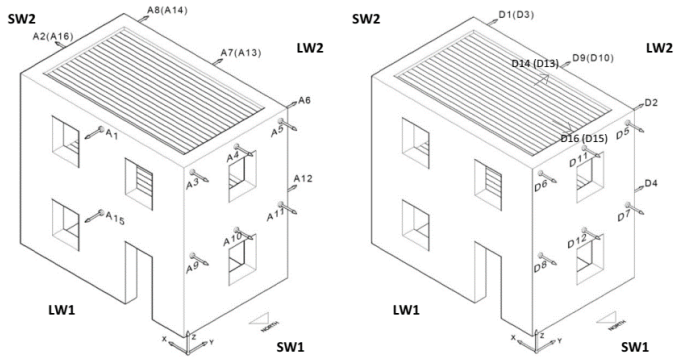

Figure 5.7 - Location of accelerometers and transducers.

5.7. **Test Procedure**

Both as-built and strengthened specimens were tested on the shaking table under biaxial excitation, along two orthogonal axes. Before the initiation of the incremental seismic tests, sine sweep excitations were used separately in each direction, to measure the dynamic characteristics of the specimens. After the sine logarithmic sweep test, the as-built building was subjected to a series of stepwise increasing base acceleration tests (Table 5.2). The ground motion input was defined by a record from the 1986 Kalamata earthquake (September 13, 1986, Ms = 6.2, max a = 0.25 g(X)/0.27 g(Y)). As already described, the tests on the as-built specimens ended when substantial damage was observed.

Table 5.2 - Test protocol for the as-built model.

No. of test	Excitation	Direction of excitation	Base acceleration (g/%)	
			X	Y
1BS	Sine sweep	X	0.02	–
2BS	Sine sweep	Y	–	0.02
3BS	Kalamata	X&Y	0.045/(18 %)	0.037/(14 %)
4BS	Kalamata	X&Y	0.10/(40 %)	0.09/(33 %)
5BS	Kalamata	X&Y	0.14/(56 %)	0.13/(48 %)
6BS[a]	Kalamata	X&Y	0.18/(72 %)	0.16/(59 %)
7BS	Kalamata	X&Y	0.22/(88 %)	0.21/(78 %)
8BS	Kalamata	X&Y	0.29/(116 %)	0.24/(89 %)

[a] Initiation of cracking

After the tests on the as-built specimen, a new set of tests were done on the strengthened specimen. First, the same record used before was used on the retrofitted specimen. As predicted, the series done on the retrofitted building reached higher maximum accelerations. To continue the series of seismic excitation tests till failure, a new ground motion input was used (Table 5.3). This new input is defined by the 1980 Irpinia earthquake (November 23, 1980, Calitri record, Ms = 6.9, max a = 0.13 g(X)/0.13 g(Y)).

No. of test	Excitation	Direction of excitation	Base acceleration (g/%)	
			X	Y
1AS	Sine sweep	X	0.02	–
2AS	Sine sweep	Y	–	0.02
3AS	Kalamata	X&Y	0.04/(16 %)	0.04/(15 %)
4AS	Kalamata	X&Y	0.10/(40 %)	0.09/(33 %)
5AS	Kalamata	X&Y	0.14/(56 %)	0.13/(48 %)
6AS	Kalamata	X&Y	0.19/(76 %)	0.17/(63 %)
7AS	Kalamata	X&Y	0.23/(92 %)	0.20/(74 %)
8AS	Kalamata	X&Y	0.29/(116 %)	0.25/(93 %)
9AS	Kalamata	X&Y	0.33/(132 %)	0.27/(100 %)

10AS	Kalamata	X&Y	0.40/(160 %)	0.32/(119 %)
11AS	Kalamata	X&Y	0.49/(196 %)	0.37/(137 %)
12AS	Kalamata	X&Y	0.55/(220 %)	0.39/(144 %)
13AS	Irpinia	X&Y	0.16/(123 %)	0.16/(123 %)
14AS	Irpinia	X&Y	0.34/(262 %)	0.29/(223 %)
15AS[a]	Irpinia	X&Y	0.48/(369 %)	0.43/(331 %)
16AS	Irpinia	X&Y	0.62/(477 %)	0.72/(554 %)
17AS	Irpinia	X&Y	0.54/(415 %)	0.66/(508 %)

[a] Initiation of cracking

Table 5.3 - Test protocol for the strengthened model.

5.8. **Numerical Model**

In this thesis, an equivalent frame model was developed to replicate the global seismic behaviour of both case-of-study specimens. Due to the geometry and openings layout of the building, the discretization of the masonry walls was simple. The height of the piers and the length of the spandrels were assumed to be equal to the size of the adjacent openings. In this way, the rigid panels were also set in the remaining masonry portions. The recently developed macro-element by Vanin et al., (2020) [42] was used, to capture both in-plane and out-of-plane of the masonry walls. As described in Figure 5.8 - Element discretization of the numerical model., the element discretization was done considering the openings of the specimen. This discretization method was chosen due to the symmetry of the facades.

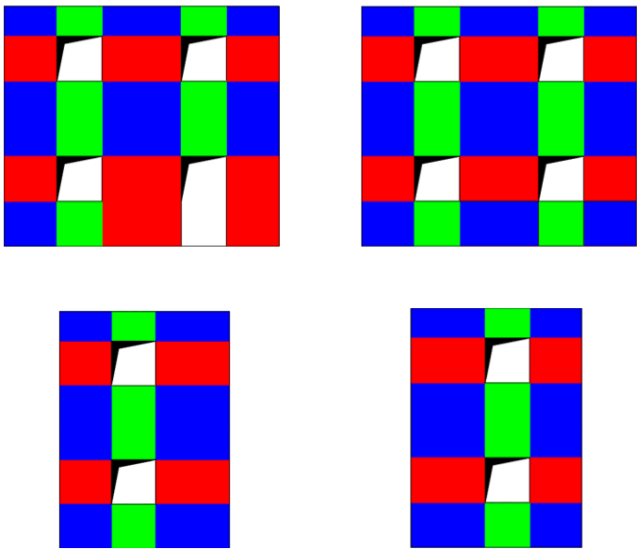

Figure 5.8 - Element discretization of the numerical model.

The masonry mechanical properties present in *Vintzileou and Mouzakis, 2014* [14], obtained from the masonry wallet tests were used to develop the masonry material model. Nevertheless, the paper contained only information on parameters related to the compression tests. In this way, other masonry mechanical properties such as cohesion and the masonry friction coefficient that defines the peak strength of the walls were obtained from previous numerical models [11], [48]. The used parameters are shown in Table 5.4. The wall-to-wall connections were modelled using the no-crushing material model that features the possible non-linearity of the connections, already described in sub-chapter 4.6.

Table 5.4 - Material properties assumed for masonry elements of the as-built model.

E (GPa)	G (GPa)	ρ (kg/m)3	fc (MPa)	τ (MPa)	μ
0.840	0.336	2200	4.33	0,175	0.200

The timber floors were modelled using a linear elastic orthotropic membrane. The timber properties were obtained from the strength class table (EN 338-2003) and formulations presented in Brignola et al., (2008). All these parameters are shown in Table 5.5. As the model was built to account for possible out-of-plane failures, the floor-to-wall connections were assumed to have a nonlinear behaviour and were modelled using a friction-based interface. This interface was modelled based on experimental tests presented in Almeida et al., (2020).

Table 5.5 - Material properties of diaphragms and the wall-to-diaphragm connections.

	E1 (GPa)	E2 (GPa)	G (MPa)	t (m)	$\mu_{friciton}$
PBM-BS	10	0.330	6.9625	0.01	0.7
PBM-AS	10	0.330	13.6425	0.02	Fixed

In the strengthened specimen model, different conditions were assumed. The used masonry mechanical properties were obtained from the tests done to the grouted masonry wallet. The new values are shown in Table 5.6. As there was no literature information on how the strengthening interventions would affect both the cohesion and the masonry friction coefficient that defines the peak strength of the walls, these values were not reduced. As a new set of boards was used in the experimental prototype to increase the in-plane stiffness of the floors, the used parameters for these elements are different in the strengthened numerical model. The floor-to-wall connections were also assumed to be fixed, as metal steel plates were used in the experimental specimen to enhance the interlocking between horizontal and vertical load-bearing elements.

Table 5.6 - Material properties assumed for masonry elements of the strengthened model.

E (GPa)	G (GPa)	ρ (kg/m)3	fc (MPa)	τ (MPa)	μ
3.34	1.336	2300	5.45	0.175	0.200

5.9. **Seismic Excitation**

The seismic ground motion records used in the experimental shake-table tests were not available for the incremental dynamic analysis performed in this thesis. To replicate the ground motion of the performed shake table tests, an open-source 1986 Kalamata earthquake ground motion record was obtained from the Engineering Strong Motion Database [50]. This record was composed of a set of three direction acceleration measurements. In this case, the signals correspondent to the vertical direction was ignored once vertical excitation was not performed in the experimental campaign. The obtained record had a PGA of 0.216 g in one direction, and 0.296 g in the orthogonal direction. Similar to what was done in the experimental campaign, the main direction record (record with the highest PGA) was defined to act in the X-direction (Figure 5.9 and Figure 5.10).

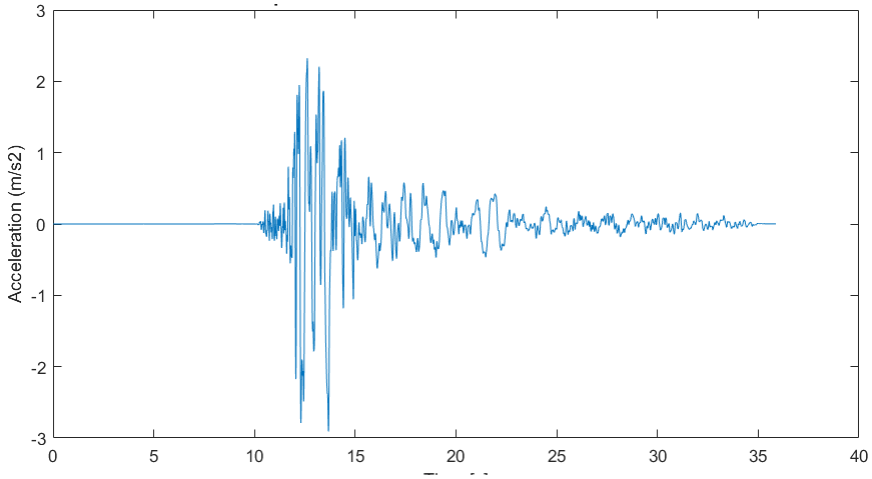

Figure 5.9 - Kalamata Earthquake - Processed acceleration time-history record - X direction.

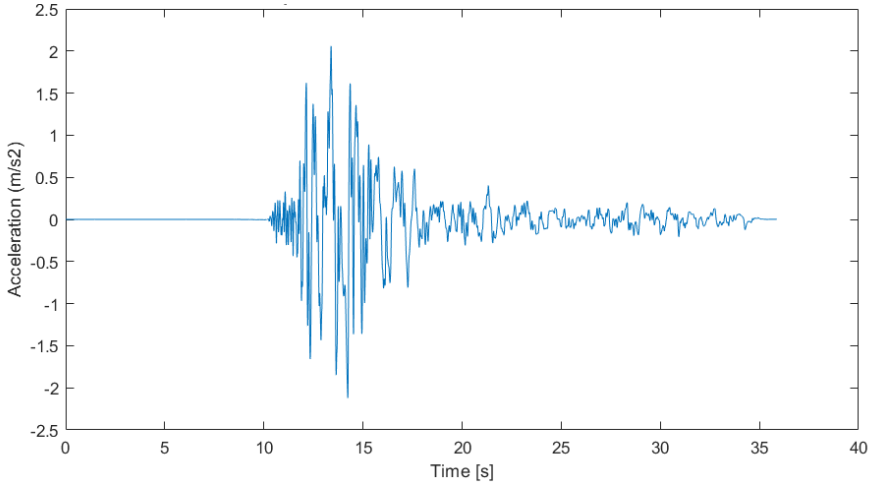

Figure 5.10 - Kalamata Earthquake - Processed acceleration time-history record - Y direction.

A set of multiplication factors were multiplied to the original ground motion record, to replicate the PGAs of the ground motion used in the test series that was already described in section 5.6. The factored records were then compiled into a single file. In this way, one long analysis that comprised all six runs was performed considering the damage evolution of the tested model. This procedure was done to both ground motion directions (Figure 5.11 and Figure 5.12).

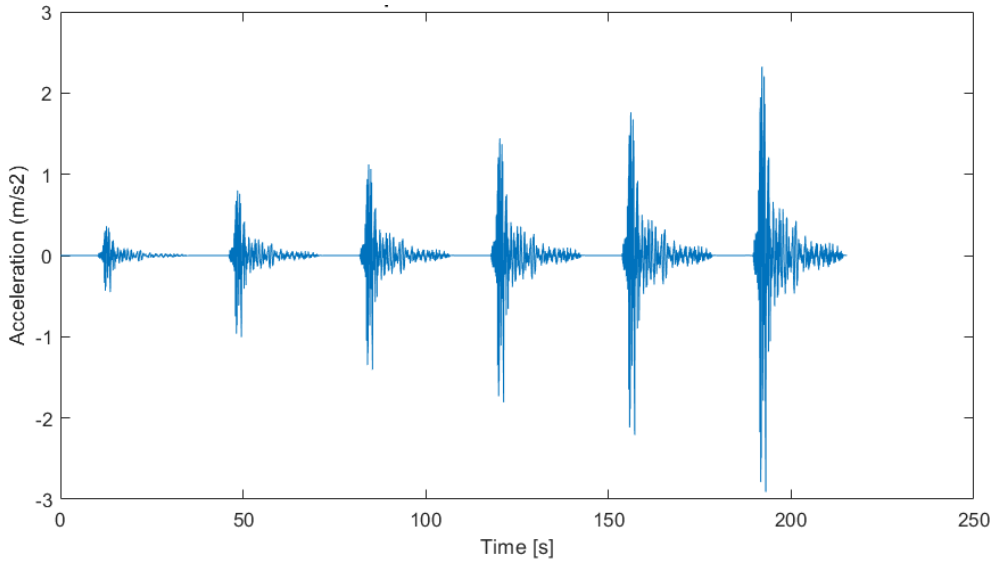

Figure 5.11 - As-built model records - 6 runs record - X direction.

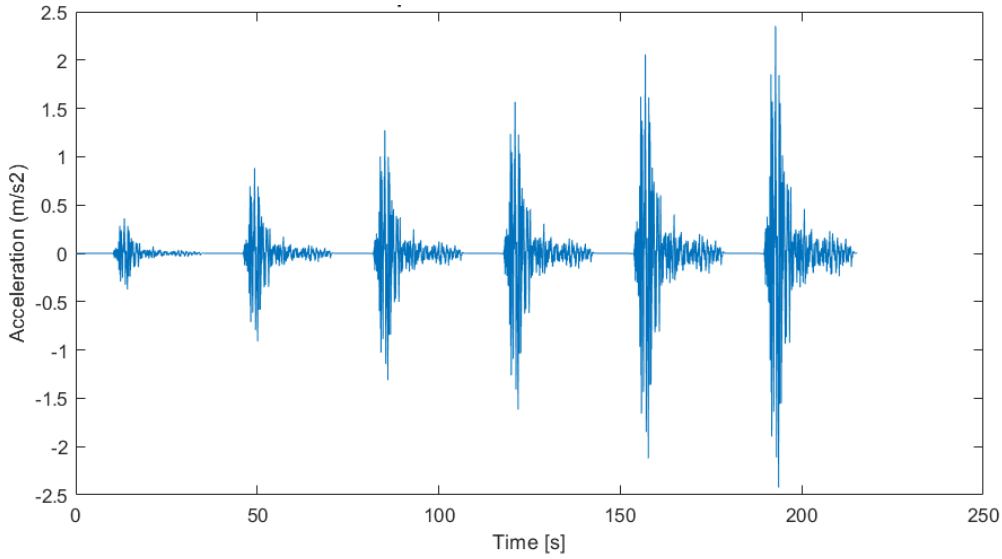

Figure 5.12 - Kalamata Earthquake - 6 runs record - Y direction.

The same procedure was used to replicate the ground motion used in the experimental campaign on the strengthened specimen. According to the paper, the signals from the Irpinia earthquake (November 23, 1980, Calitri record, Ms = 6.9, max a = 0.13 g(X)/0.13 g(Y)) were used to assess the seismic behaviour of the strengthened specimen.

In this way, a record was obtained from the Engineering Strong Motion Database [[51]]. The obtained record was composed of a set of three direction acceleration measurements. Similar to the previous case, the signals from vertical directions were ignored. The obtained record had a PGA of 0.175 g in one direction, and 0.158 g in the orthogonal direction.

Similar to what was done in the experimental campaign and for the Kalamata earthquake signals, the main direction record (record with the highest PGA) was defined to act in the X-direction. The record was processed into the correct units and cut to eliminate null records that delay the analysis (Figure 5.13 and Figure 5.14).

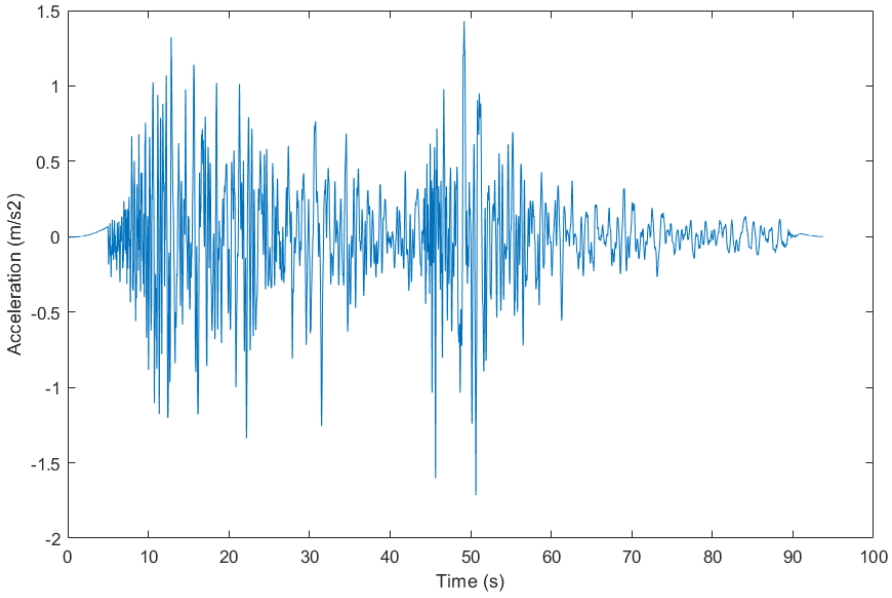

Figure 5.13 - Irpinia Earthquake - Processed acceleration time-history record - X direction.

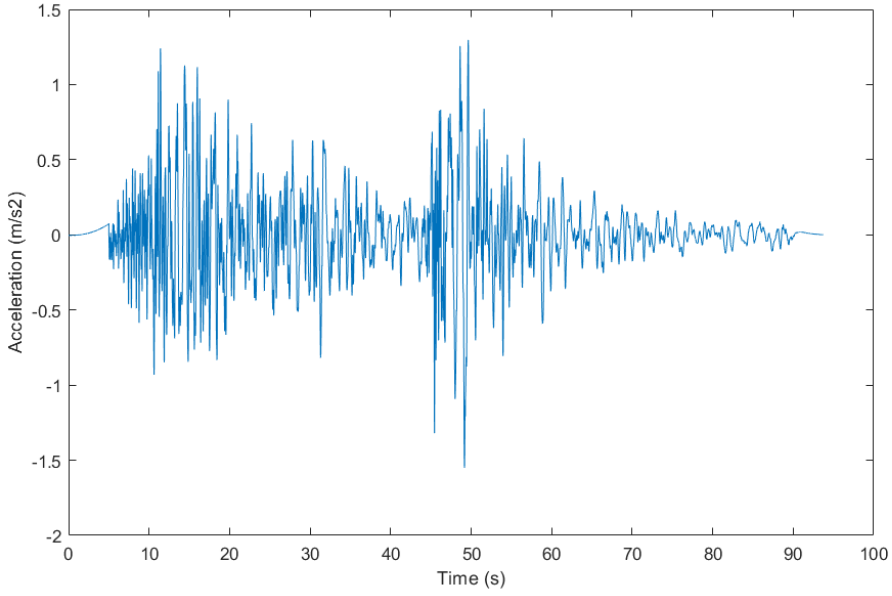

Figure 5.14 - Irpinia Earthquake - Processed acceleration time-history record - Y direction.

The seismic excitation imposed to the strengthened specimen in the experimental campaign was composed of both Kalatama and Irpinia earthquake signals. To replicate this record, a set of multiplication factors were multiplied to the original ground motion records, to replicate the PGAs of the ground motion used in the test series that was already described in chapter 5.6. As before, the factored records were then compiled into a single file. In this way, one long analysis that comprised all six runs was performed having into account the damage evolution of the tested model. This procedure was done to both ground motion directions (Figure 5.15 and Figure 5.16).

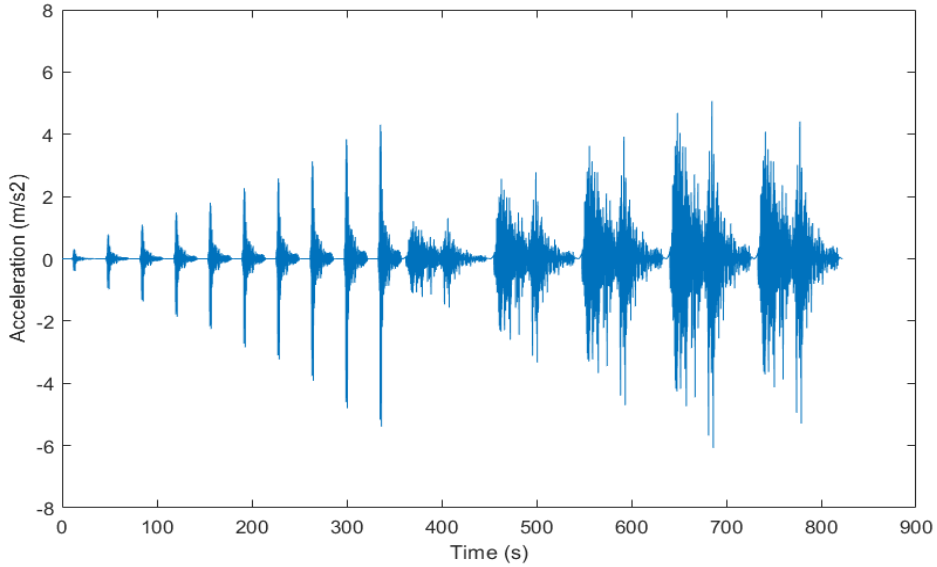

Figure 5.15 - Strengthened model records - 15 runs record - X direction.

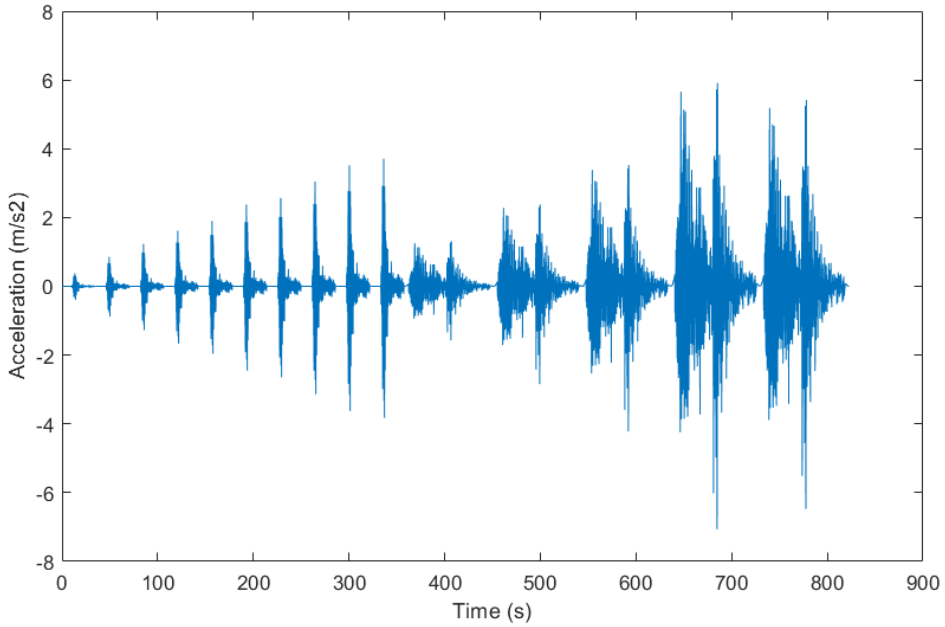

Figure 5.16 - Strengthened model records - 15 runs record - Y direction.

6.
AS-BUILT NUMERICAL MODEL

6.1. Introduction

A numerical model was created to reproduce the behaviour of the as-built specimen under seismic excitation. As already described, the model was developed based on geometry parameters and mechanical properties gathered from the paper *Vintzileou and Mouzakis, 2014* [14]. Although most of the prototype information was present and extracted directly from the paper, some uncertainties existed, especially on the properties of the connections between structural elements.

Therefore, a numerical calibration was carried out to validate the numerical model and guarantee the accuracy of the results. First, the model was calibrated based on its dynamic properties. For this calibration, a set of dynamic characteristics present in the paper was used to compare with the numerical values. Second, the numerical model was calibrated regarding the damping percentage while under seismic excitation, where the relative displacements present in the paper were compared to the ones obtained from the numerical incremental dynamic analyses.

After the calibration of the model, the same set of analyses used for the model calibration was used to extract results and data from the numerical model. To help evaluate and assess the behaviour of the as-built numerical model, the results present in the case-study paper were used for comparison, just as they did in the calibration phase.

6.2. **As-built numerical model calibration**

6.2.1. **Wall-to-wall stiffness calibration**

The base numerical model was developed considering all the parameters extracted from the paper [14]. After the development of the base model, three types of analysis were performed to evaluate its status. First, a modal analysis was performed to evaluate the dynamic properties of the model. Second, a self-weight analysis was performed to test the behaviour of the model while just considering all loads and self-weights. Lastly, an incremental dynamic analysis that replicates the experimental campaign was carried out to evaluate the performance of the model while under seismic excitation.

The results obtained from the modal analysis performed on the base numerical model showed a big difference between the numerical and experimental dynamic properties. Table 6.1 contains the experimental dynamic properties, that were calculated from the response of the as-built specimen during sine logarithmic sweep excitations, and the values extracted from the base numerical modal analysis.

	Experimental Model		**Base Numerical Model**	
	Frequency (Hz)	Period (s)	Frequency (Hz)	Period (s)
X Direction Mode	6.05	0,17	16,52	0,0605
Y Direction Mode	4.21	0,24	7,19	0.139

Table 6.1 - Dynamic properties of the experimental specimen in both directions.

These results pointed out that the numerical model was too stiff compared to the experimental prototype. In this way, a calibration was initiated considering the difference between numerical and experimental dynamic properties.

As most of the mechanical and geometrical properties were described in the paper, a decision was made that the parameters to calibrate would be the ones that were not specified and described in the research paper: the parameters related to floor-to-wall connections and the parameters related to wall-to-wall connections.

As an addition to the calibration study, the modal shapes described in the paper (Figure 6.1) were compared to the modal shapes obtained from the numerical model by computing the modal assurance criterion (MAC) coefficients [52], [53]. This method uses the numerical correlation of the mode shape vectors and is used to compare two mode shapes of the same mode in different models.

MAC coefficients can be calculated using the following formula:

$$MAC_{I,J} = \frac{|\sum_{k=1}^{n} \varphi_k^i \, \varphi_k^j|^2}{\sum_{k=1}^{n}(\varphi_k^i)^2 \sum_{k=1}^{n}(\varphi_k^j)^2}$$

- where φ_k^i and φ_k^j are pairs of identified mode shapes and n is the number of monitored degrees of freedom. $MAC_{I,J}$ is a scalar quantity assuming values between 0 and 1 for no correlation and perfect match, respectively. According to Pepi et al., (2021) [53], values greater than 0.80 indicate a good correlation between mode shapes.

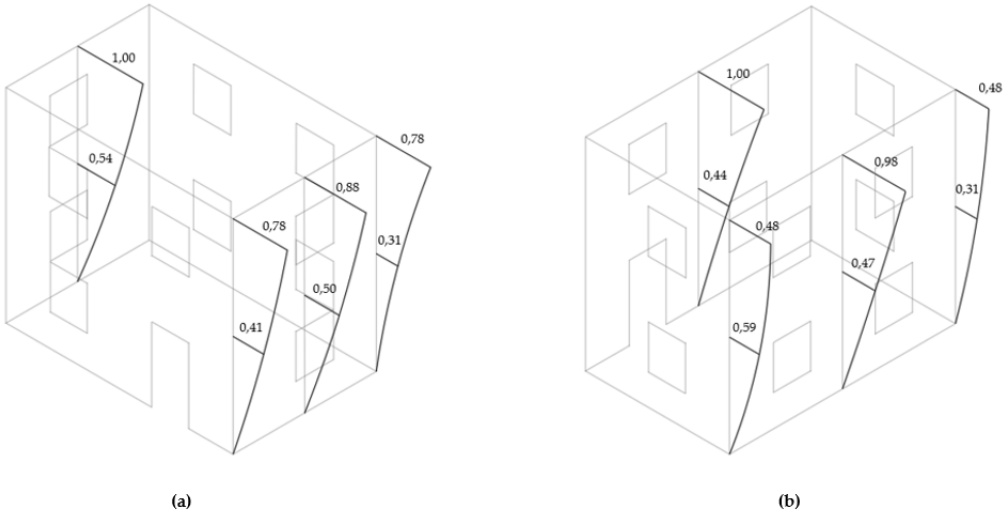

Figure 6.1 - Normal mode shapes of the as-built specimen: (a) mode shape of f=6.05Hz (X-direction) and (b) mode shape of f=4.21Hz (Y-direction)

As a first step of the calibration, the floor-to-wall connections were iterated. The calibration did not have an impact on the dynamic properties of the model, as the floor-to-wall connections were modelled considering a friction mechanism. In this way, the initial properties of the floor-to-wall connections were established, as according to Almeida et al., (2020) [49], the final and assumed value for the friction coefficient was 0.7.

As the calibration that was done to the properties of the floor-to-wall connections did not have an impact on the dynamic properties of the model, the properties of the wall-to-wall connections were iterated.

When studying these connections and their behaviour in the experimental campaign, it was noticed that the as-built specimen developed vertical cracks in the corners for rather low seismic excitation values. Separation of the masonry leaves was also observed in the experimental campaign and was more pronounced close to the corners of the building. This could imply that the deformation capacity and the interlocking of the connections between the load-bearing walls were not sufficient to prevent the formation of out-of-plane mechanisms.

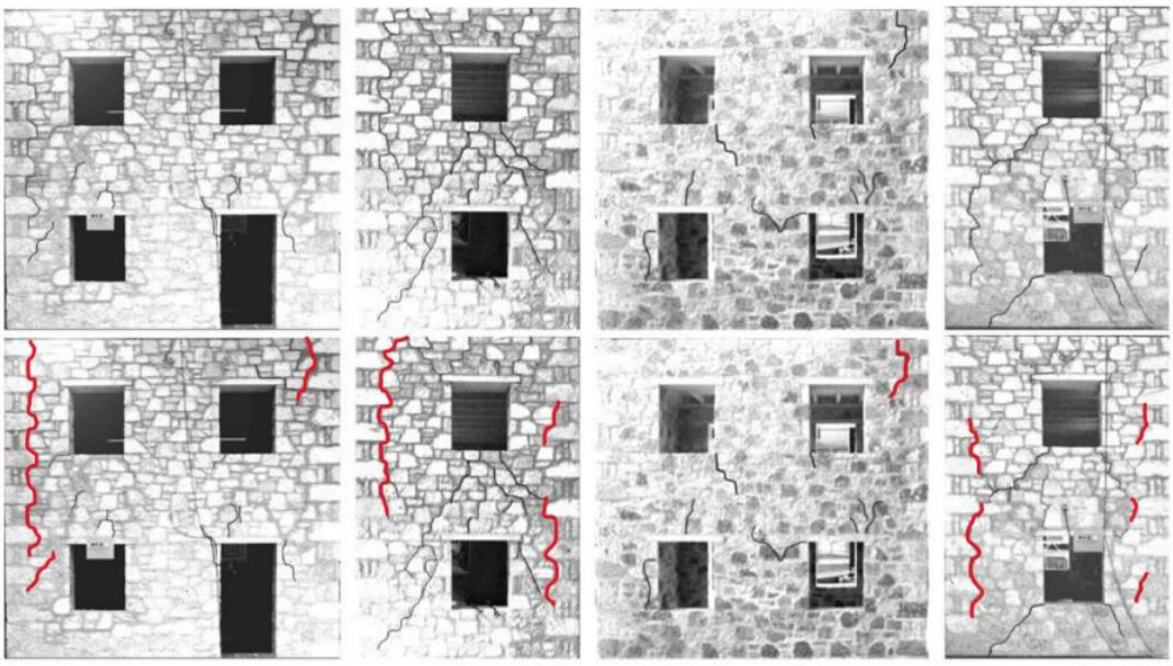

Figure 6.2 - Experimental crack map of the as-built specimen [14].

In this way, the connections between the orthogonal load-bearing walls of the experimental specimen were assumed to have poorly executed head joints, that didn't provide the correct interlocking and didn't allow the development of the mass friction mechanisms that prevent out-of-plane failure in this type of building. To account for this characteristic, a new calibration was performed to estimate the stiffness value of the wall-to-wall connections.

The study was accomplished by monitoring the evolution of the dynamic properties and mode shapes of the numerical model while reducing the wall-to-wall interface stiffness. For this purpose, a total of 15 models were developed with a decreasing stiffness of the connections, starting from $3 \times 10^9\ N/m$ (value used on the base numerical model) to $7 \times 10^5\ N/m$. Both wall-to-wall stiffness and calculated dynamic properties for this study are described in Table 6.2.

Stiffness of the interface (N/m)	X Direction Period (s)	X Direction Frequency (Hz)	Y Direction Period (s)	Y Direction Frequency (Hz)	X Direction MAC coefficient	Y Direction MAC coefficient
3,00E+09	0,0605	16,52	0,139	7,19	0,899	0,774
1,00E+09	0,0606	16,51	0,139	7,19	0,900	0,774
5,00E+08	0,0606	16,49	0,139	7,19	0,902	0,775
3,00E+08	0,0607	16,46	0,139	7,18	0,904	0,777
1,00E+08	0,0612	16,34	0,140	7,14	0,917	0,783
5,00E+07	0,0619	16,15	0,141	7,09	0,936	0,793
3,00E+07	0,0630	15,87	0,142	7,03	0,959	0,805
1,00E+07	0,0688	14,53	0,149	6,70	0,934	0,854
5,00E+06	0,0746	13,40	0,160	6,25	0,887	0,901
3,00E+06	0,0823	12,14	0,174	5,76	0,916	0,928
2,00E+06	0,0927	10,78	0,190	5,27	0,931	0,937
1,00E+06	0,118	8,49	0,228	4,39	0,940	0,928
9,00E+05	0,122	8,18	0,235	4,26	0,941	0,925
8,00E+05	0,127	7,85	0,243	4,12	0,942	0,922
7,00E+05	0,133	7,50	0,252	3,97	0,943	0,918

Table 6.2 - Evolution of the dynamic properties and MAC values during the numerical calibration

In addition to the study, a set of three curves were plotted to help understand the evolution of the dynamic characteristics of the numerical models. The first curve and the second curve describe the evolution of the natural periods and frequencies for the X and Y directional modes respectively (Figure 6.3 and Figure 6.4).

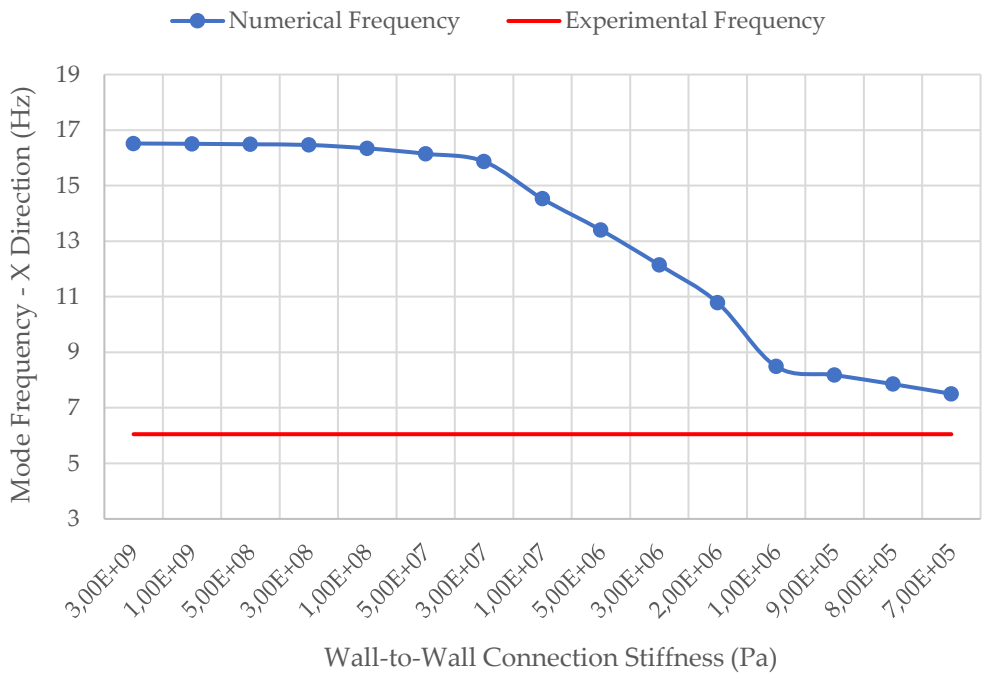

Figure 6.3 - Evolution curve of the X-direction mode frequency with decreasing wall-to-wall stiffness.

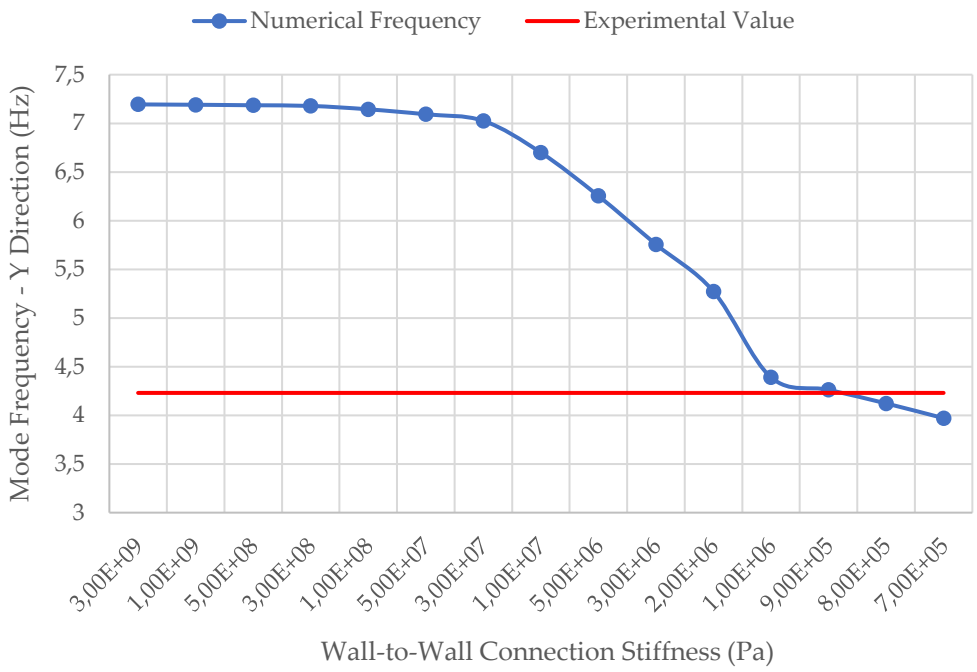

Figure 6.4 - Evolution curve of the Y-direction mode frequency with decreasing wall-to-wall stiffness.

The third curve describes the behaviour of the MAC coefficients for both directional modes during the study (Figure 6.5).

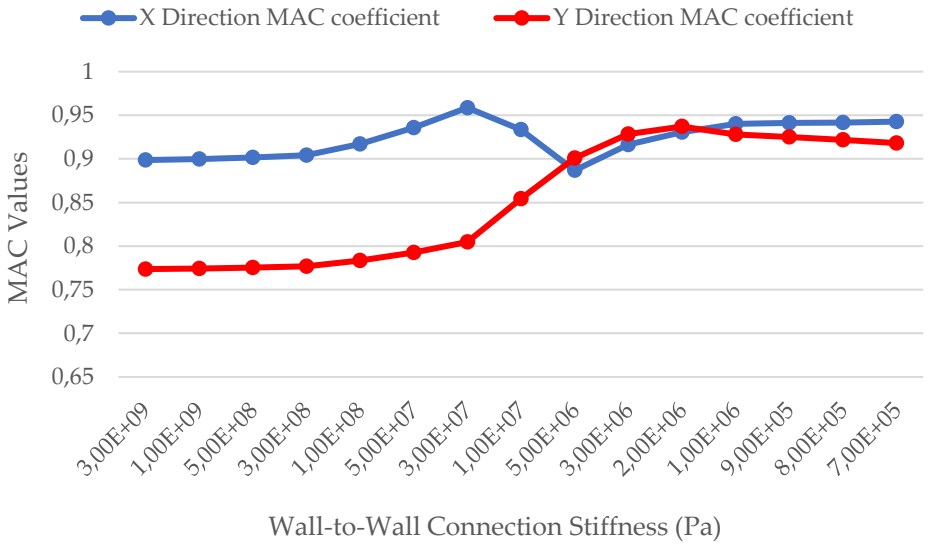

Figure 6.5 - Evolution curve of the X and Y direction MAC values with the decreasing wall-to-wall stiffness.

As can be concluded when observing Figure 6.3 and Figure 6.4, the evolution of the natural frequencies of the model is not linear with the reduction of the wall-to-wall stiffness. This non-linear behaviour of the evolution is related to changes in the mode shapes related to torsional effects.

By analysing the first and second curves extracted from the numerical modal analysis, it is concluded that the appropriate reduction of the wall-to-wall stiffness can approximate the numerical dynamic properties from the ones obtained in the experimental campaign. This approximation is especially noticeable when the value of the stiffness is reduced below $3 \times 10^7\ N/m$. The third curve, where the calculated MAC coefficients are shown, indicates that the calibration of the stiffness of the wall-to-wall interfaces improves the correlation of the mode shapes of the numerical and the experimental model.

In this way, the calibration study empirically shows that the poor interlocking and strength capacity of the wall-to-wall connections is a possible explanation for the difference between the dynamic properties of the experimental and base numerical model. This resulted in a calibration that reduces the value of the stiffness of these connections. For the final model, a stiffness of $1 \times 10^6\ N/m$ was adopted, as it guarantees a good approximation to the dynamic properties of the experimental campaign without excessively reducing the global stiffness of the model. Moreover, as can be seen in the third curve, the MAC coefficients tend to stabilize for stiffness values lower than $1 \times 10^6\ N/m$, as this was the final calibrated value for the wall-to-wall stiffness.

As the wall-to-wall connections were assumed to be poorly executed, the tensile capacity of these connections was assumed to be low. In this case and considering the experimentally observed damage patterns, the tensile capacity was set to $5\ kN$ [54].

6.2.2. **Damping calibration**

As already described, three types of analysis were performed on the base numerical model to evaluate its behaviour and performance in comparison to the results from the experimental campaign. The modal analysis was used to calibrate the dynamic properties of the model and the self-weight analysis was performed to study the possibility of collapse while just considering extra loads and the self-weights of the structural elements. The self-weight analysis was done without errors or numerical failures which gives a good indication of the stability of the model.

Regarding the incremental dynamic analysis that simulated the experimental seismic excitation, a calibration of the damping percentage was needed to validate the numerical model. In this way, a set of calibration models were created, with damping ratios between 1.5 and 5% to find the damping percentage that better fits the validation of the model. Rayleigh damping model parameters were computed such that the damping ratios at the first mode and sixth mode correspond to the damping ratio of this model. In this calibration study, a comparison between the relative displacement values that were recorded at the middle-length of the walls at both levels of the experimental specimen and the relative displacements of the numerical model in the same location was made. Figure 6.6 shows the recorded displacements at the end of the experimental campaign.

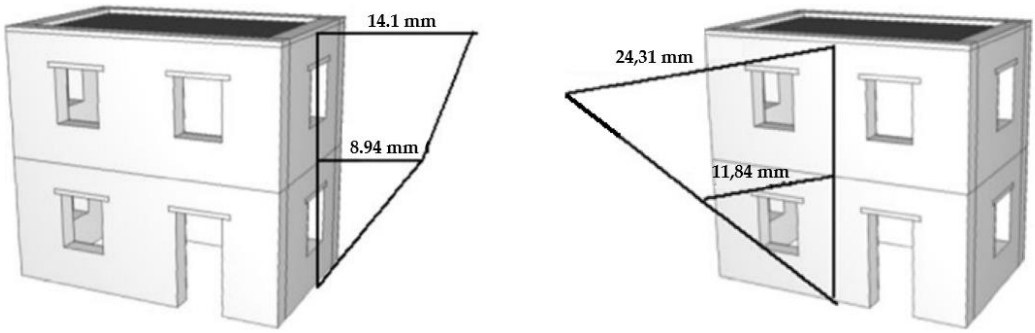

Figure 6.6 - Maximum relative displacements recorded at middle-length of the front and right facades at both levels of the as-built specimen after the end of Test 8BS (Table 5.2): (a) right facade - X-direction displacements and (b) front facade -Y direction displacements.

For the calibration study, a set of figures were created to compare the relative displacements of each numerical model with the respective experimental value. In Figure 6.7, the displacements obtained for each one of the analysed numerical models are shown. The red horizontal line represents the experimental value for each location.

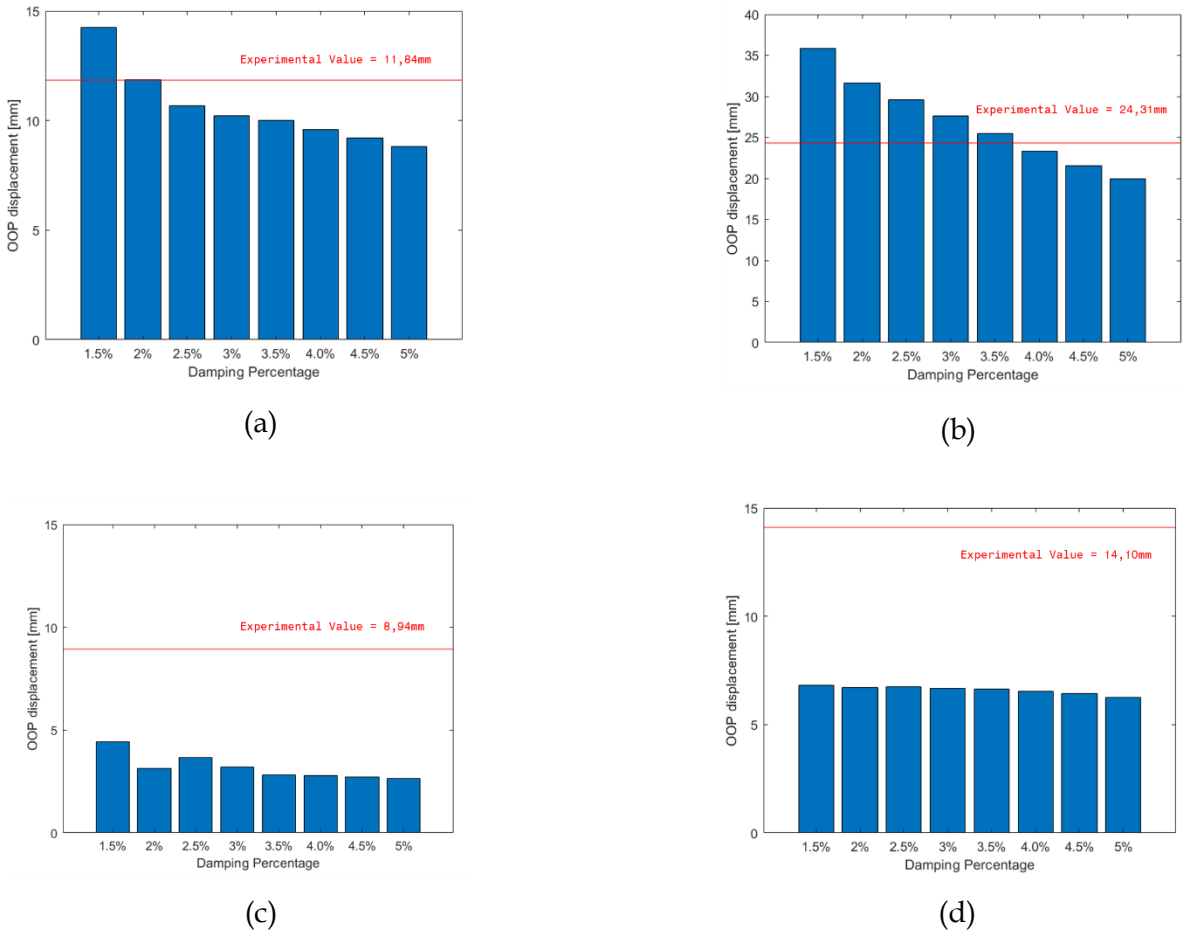

Figure 6.7 - Evolution of the out-of-plane displacements with the increasing damping percentage, measured at middle-length of the facades at both levels: (a) middle-length of the front facade - first floor, (b) middle-length of the front facade - second floor, (c) middle-length of the right facade - first floor and (d) middle-length of the right facade - second floor.

While analysing the figures, it is noticeable that the displacements of the front façade of the numerical model are close to the values measured in the experimental campaign. Nevertheless, the displacements obtained from the right facade seem to be smaller when compared to the measured values. The difference between the dynamic properties of the experimental and numerical models in the X direction and the differences between the numerical and experimental ground motion records used on the incremental dynamic analyses are possible explanations for the discrepancy between the experimental and numerical out-of-plane displacements measured in the right facade of the specimen.

The comparison between numerical and experimental maximum displacements at mid-length of the walls at both levels of the experimental specimen shows that the model best predicting the experimental values is the one developed with a 3.5% damping percentage. With higher damping ratios, the damping forces excessively reduce the displacements of the building.

6.3. **As-built numerical model results**

The results obtained from the analyses performed on the calibrated as-built numerical model are shown in this sub-chapter. While the analyses were performed on OpenSEES software, all the outputted data and results were organized and treated using MATLAB coding.

Starting with the dynamic properties of the numerical model, a set of 3D figures was created to represent the mode shapes for the X and Y directions (Figure 6.8 and Figure 6.9). Table 6.3 describes the values of the natural frequencies and periods for each directional mode. The MAC coefficients that correlate the numerical mode shapes with the experimental mode shapes are also present in this table.

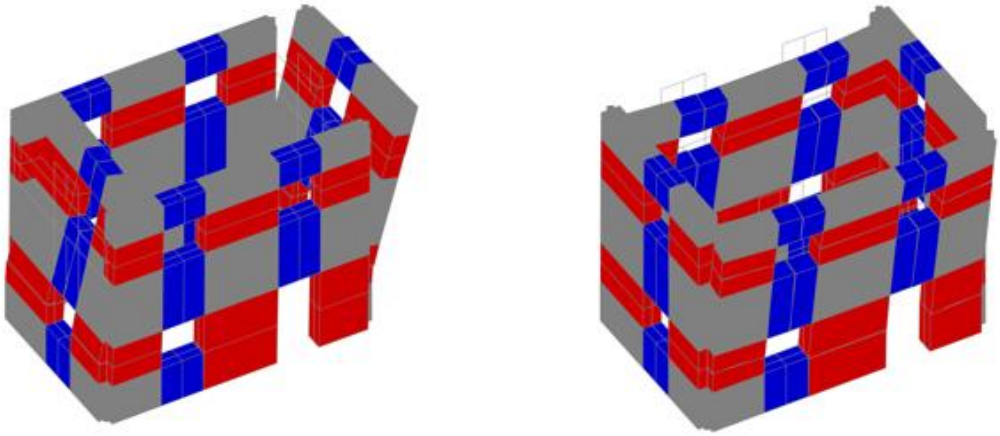

(a) (b)

Figure 6.8 - Modal deformed shapes of the as-built numerical model obtained from the MATLAB coding: (a) mode shape of f=8.49Hz (X-direction) and (b) mode shape of f=4.39Hz (Y-direction).

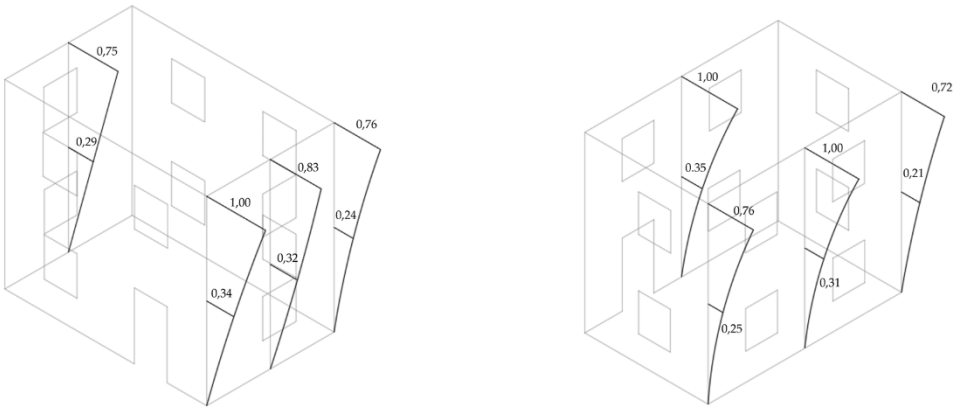

(a) (b)

Figure 6.9 - Normal mode shapes of the as-built numerical model: (a) mode shape of f=8.49Hz (X-direction) and (b) mode shape of f=4.39Hz (Y-direction).

	Frequency (Hz)	Period (s)	MAC coefficients
X Direction Mode	8.49	0.118	0.9403
Y Direction Mode	4.39	0.228	0.9279

Table 6.3 - Dynamic properties of the as-built numerical model.

The incremental dynamic analysis performed on the numerical model was crucial to study its behaviour and performance while subjected to seismic excitation. According to the case-study paper, and as it was already described in a previous section, displacement transducers were used to measure the maximum relative displacements at the mid-length of the walls at both levels of the experimental prototype. In Figure 6.10, the reader can find the maximum relative displacements for the same locations, that were extracted after the incremental dynamic analysis performed on the numerical model.

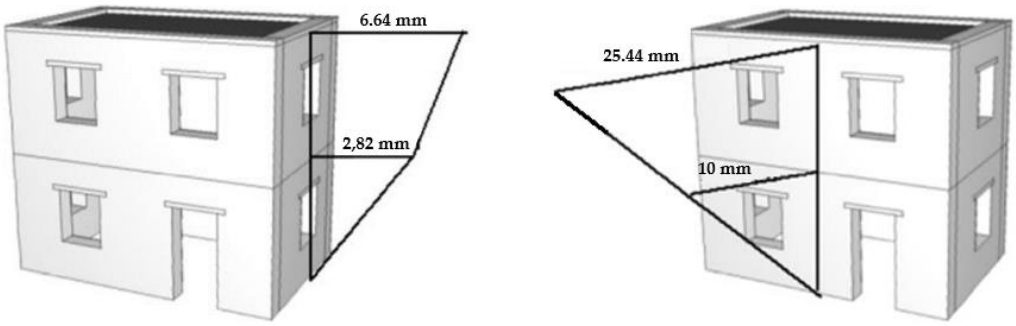

(a) (b)

Figure 6.10 - Maximum relative displacements recorded at middle-length of the front and right facades at both levels of the as-built numerical model after the end of the incremental dynamic analysis: (a) right facade - X-direction displacements and (b) front facade - Y-direction displacements.

	Experimental Displacements		Numerical Displacements	
	Front Facade (mm)	Right Facade (mm)	Front Facade (mm)	Right Facade (mm)
1st Floor	11,84	6,1	10,00	2,82
2nd Floor	24,31	12,75	25,44	6,64

Table 6.4 - Maximum relative displacements of the as-built models: Experimental vs Numerical.

In Table 6.4 a comparison between experimental and numerical maximum relative displacements is shown. Possibly due to insufficient diaphragm action and consequent out-of-plane bending combined with a poor interlock between orthogonal walls, long vertical cracks were recorded close to the corners of the experimental model. As the reader can confirm in Figure 6.11, where the deformed shape correspondent to the final run (nominal PGA of 0.29g) is plotted, the numerical results show that the specimen is subjected to high flexural drifts, especially noticeable in elements that are close to the interface between orthogonal load-bearing walls. The out-of-plane behaviour of the larger facades, detailed in the case-study paper, is also evident while analysing the deformed shape in Figure 6.11. As the accelerations were increasing with the height of the model, the flexural drifts tend to be higher in the elements located at the top of the facades.

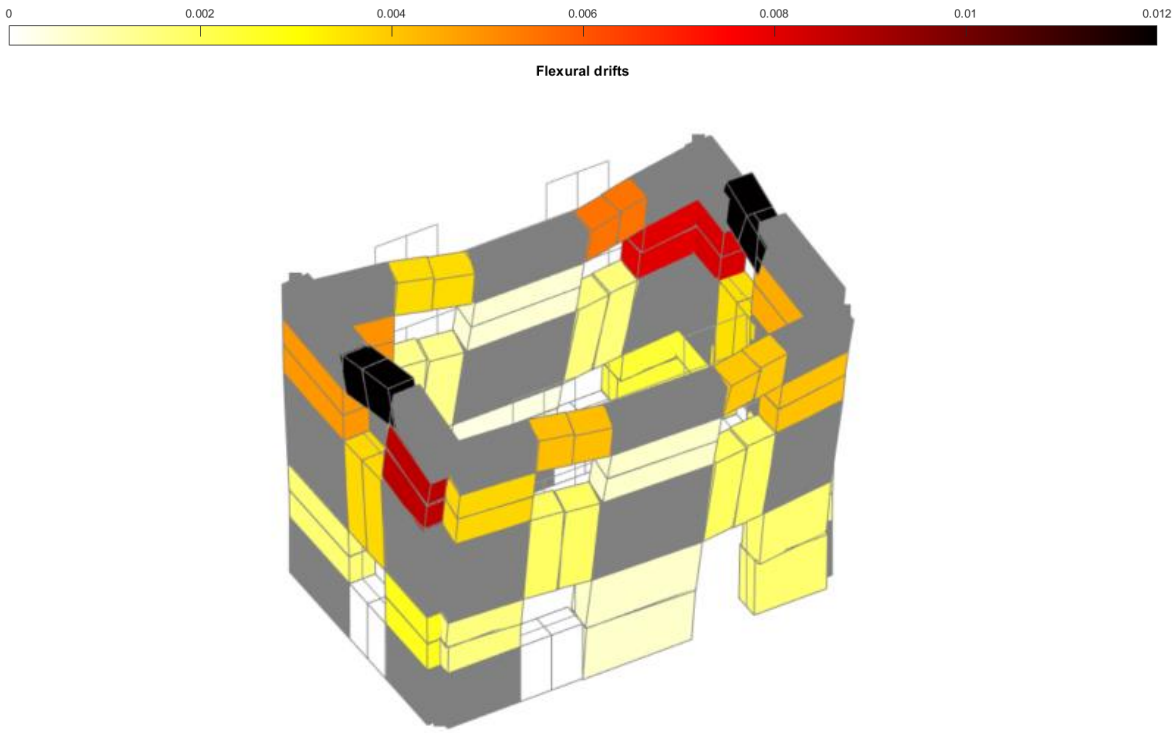

Figure 6.11 - Out-of-plane behaviour and flexural drifts of the as-built numerical model (magnification factor ×40).

As the larger facades showed out-of-plane behaviour, was predictable that the shorter façades would develop in-plane shear stresses that would be represented by shear drifts. The numerical model replicated the dominant out-of-plane behaviour of both longer facades. The flexural drifts are also more evident close to the corner of the buildings. This result matches with the separation of the masonry leaves that were observed close to the corners of the building.

According to the case-study paper, some less significant shear cracks were also noticed after the shake-table test on the as-built specimen. These cracks were located in the shorter facades and would have their origin in the corner of the openings. To get information on the shear behaviour of the numerical model, Figure 6.12 was created to represent the shear drifts of each element of the numerical model. As expected, no considerable shear drifts were detected after the seismic excitation of the model.

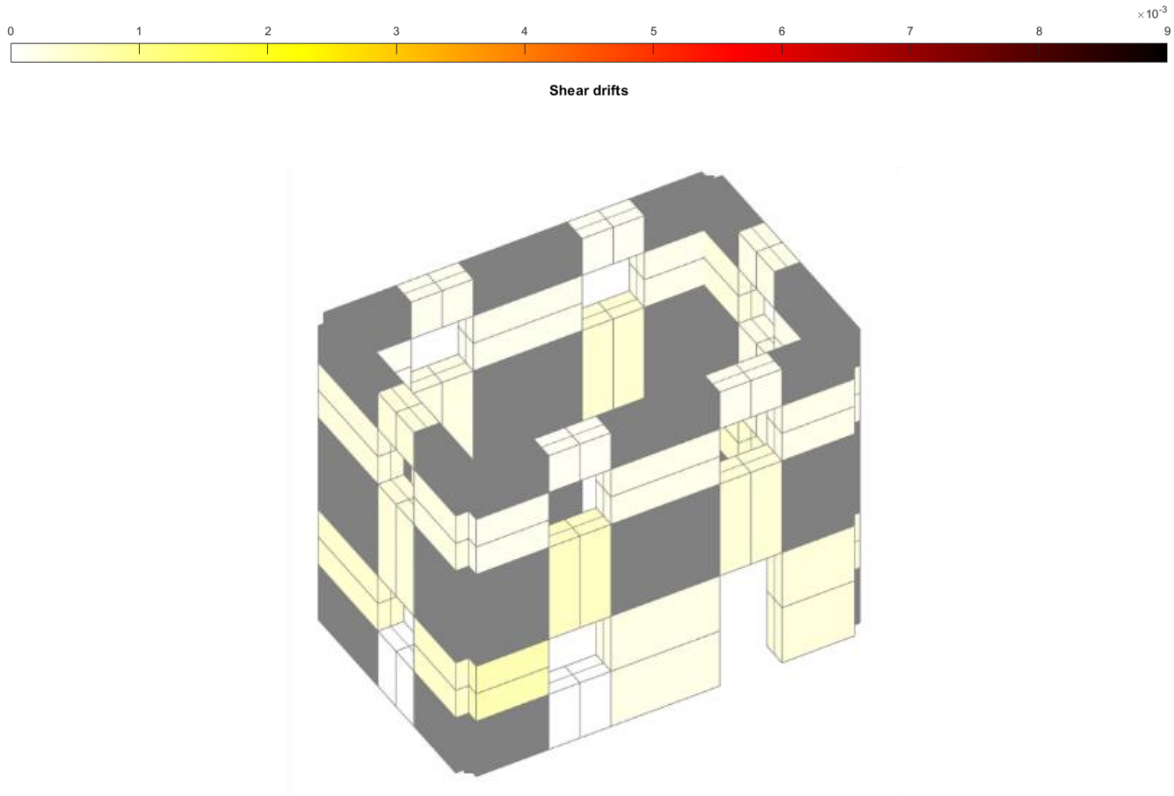

Figure 6.12 - In-plane behaviour and shear drifts of the as-built numerical model (magnification factor ×40).

To confirm that there were no errors or inconsistencies with the incremental dynamic analysis, a pair of base shear curves was plotted for each of the ground motion directions (Figure 6.13 and Figure 6.14). As an estimate of the maximum expected lateral force on the base of the structure, base shear is important to evaluate the value of seismic forces that are acting in the structure. The base shear was numerically calculated based on the forces acting in the base nodes of the model.

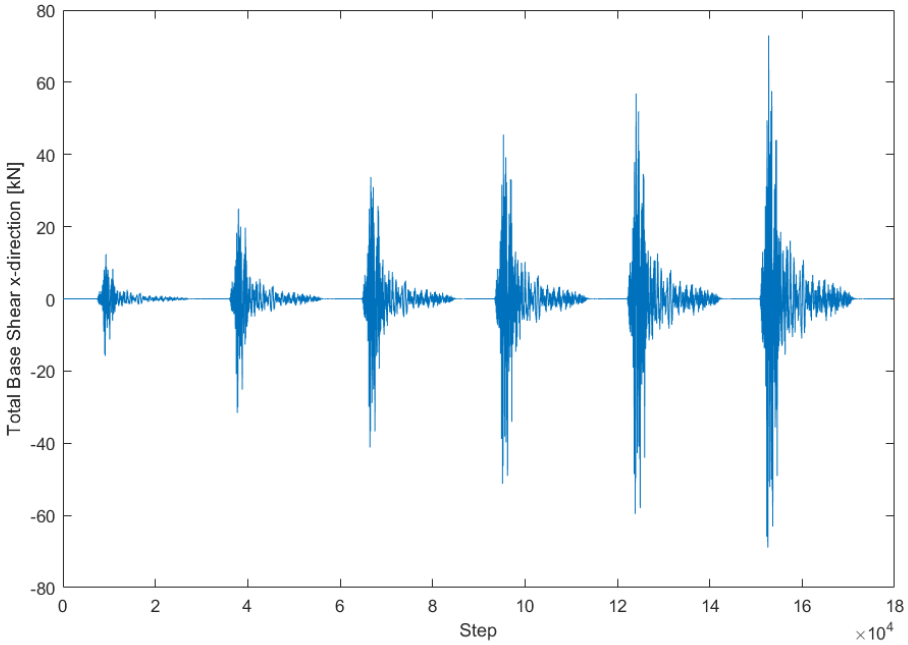

Figure 6.13 - Total base shear of the numerical model per step - X direction.

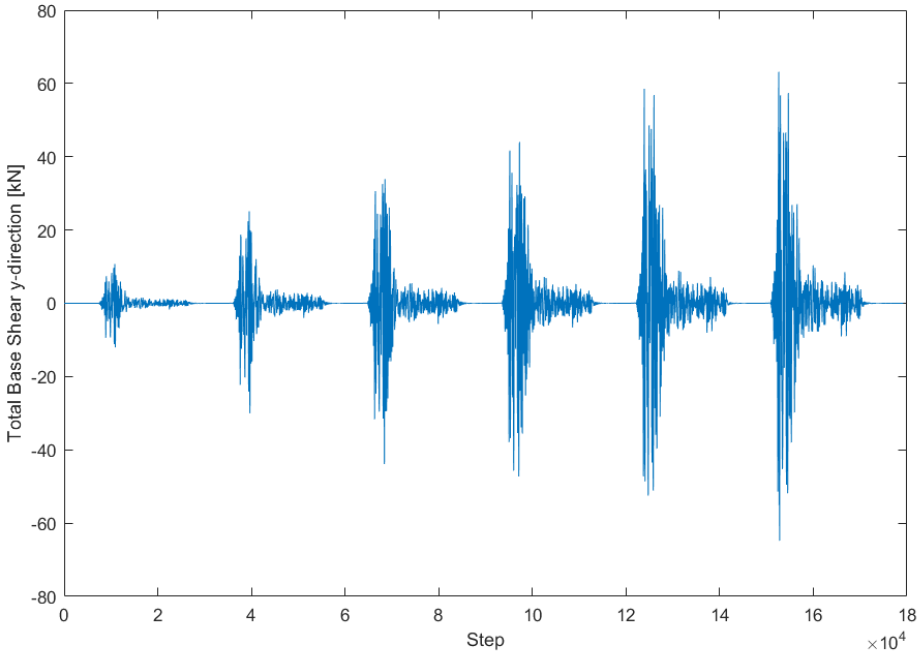

Figure 6.14 - Total base shear of the numerical model per step - Y direction.

The hysteric response of the model was also evaluated based on the data obtained from the performed numerical analyses. First, a pair of hysteric curves were plotted to show the relation between the total base shear and the average relative displacement of the roof level. These hysteresis loops were created for both directions: the longitudinal X-direction (Figure 6.15) and the transversal Y-direction (Figure 6.16). As predicted, the model shows loss of stiffness under increasing base shear and consequent occurrence of damage for both directions.

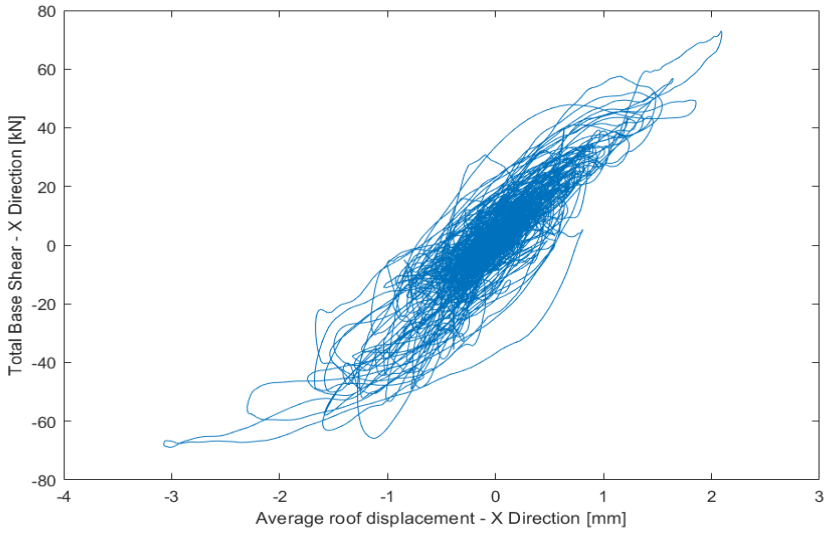

Figure 6.15 - Numerical total base shear versus roof mean relative displacement along X direction for Kalamata base motion.

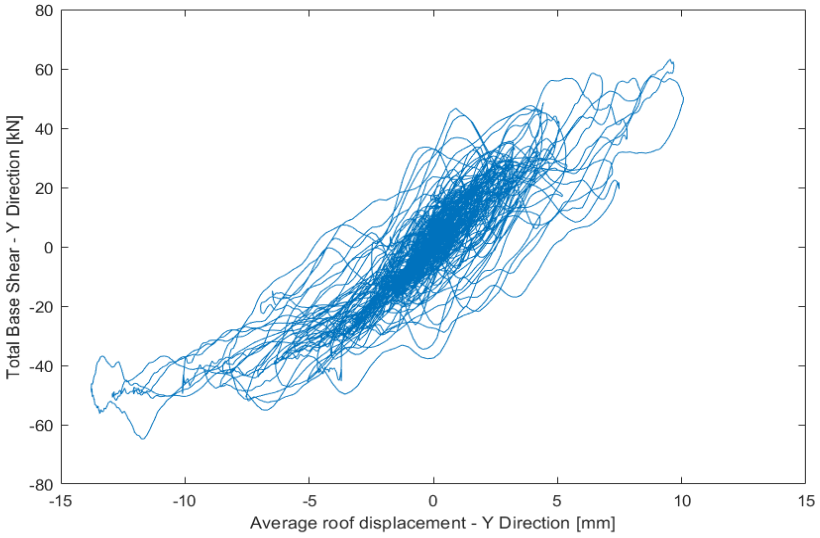

Figure 6.16 - Numerical total base shear versus roof mean relative displacement along Y direction for Kalamata base motion.

In the experimental campaign accelerations and relative displacements, for each ground motion direction, were plotted into hysteric curves (Figure 6.17 and Figure 6.19). The accelerations and relative displacements were measured at the middle length of the top of the back facade (Y direction accelerations and relative displacements) and the middle length of the top of the right facade (X direction accelerations and relative displacements).

To compare the experimental data with the results extracted from the replication of the seismic motion on the numerical model, two hysteric curves were developed similar to the ones present in the case-study paper [14](Figure 6.18 and Figure 6.20). In the curves, the data was plotted with different colours that depend on the identification of the run/test and associated nominal PGA.

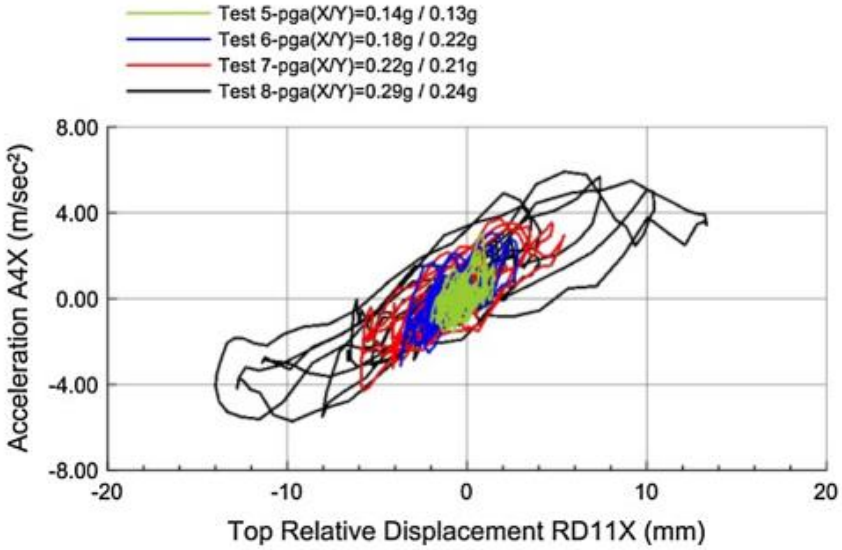

Figure 6.17 - Experimental absolute acceleration versus top relative displacement along X-direction for Kalamata ground motion [14].

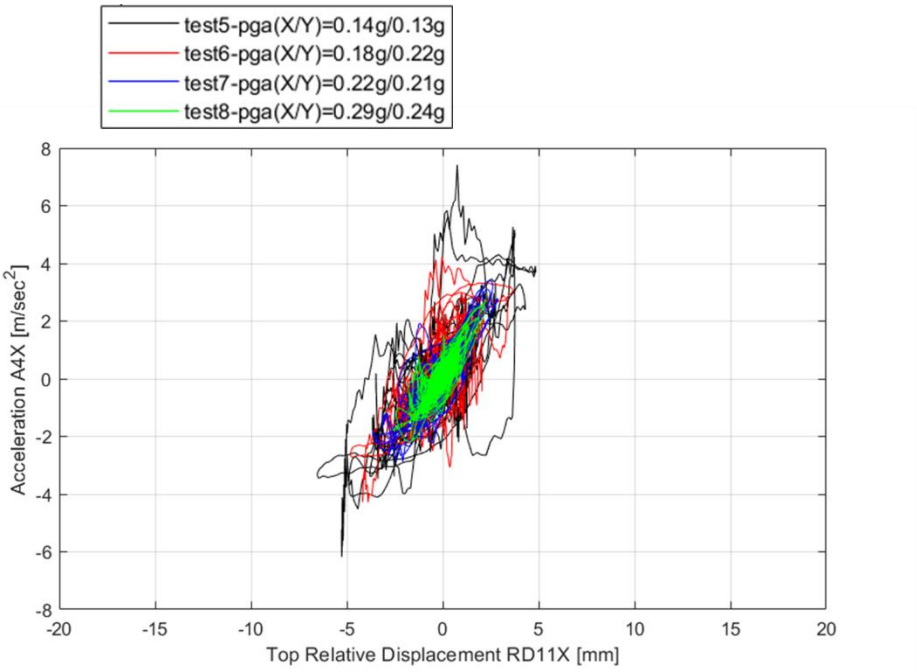

Figure 6.18- Numerical absolute acceleration versus top relative displacement along X-direction for Kalamata ground motion.

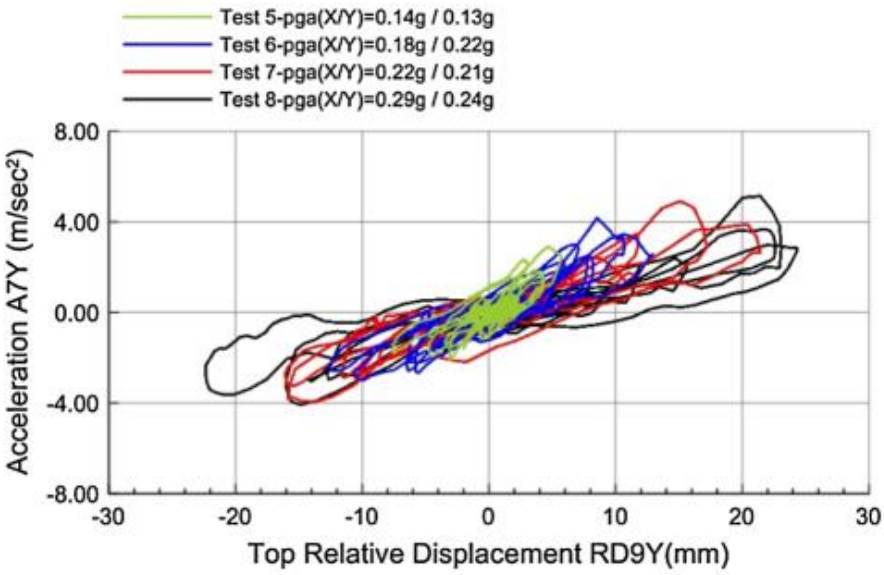

Figure 6.19 - Experimental absolute acceleration versus top relative displacement along Y-direction for Kalamata ground motion [14].

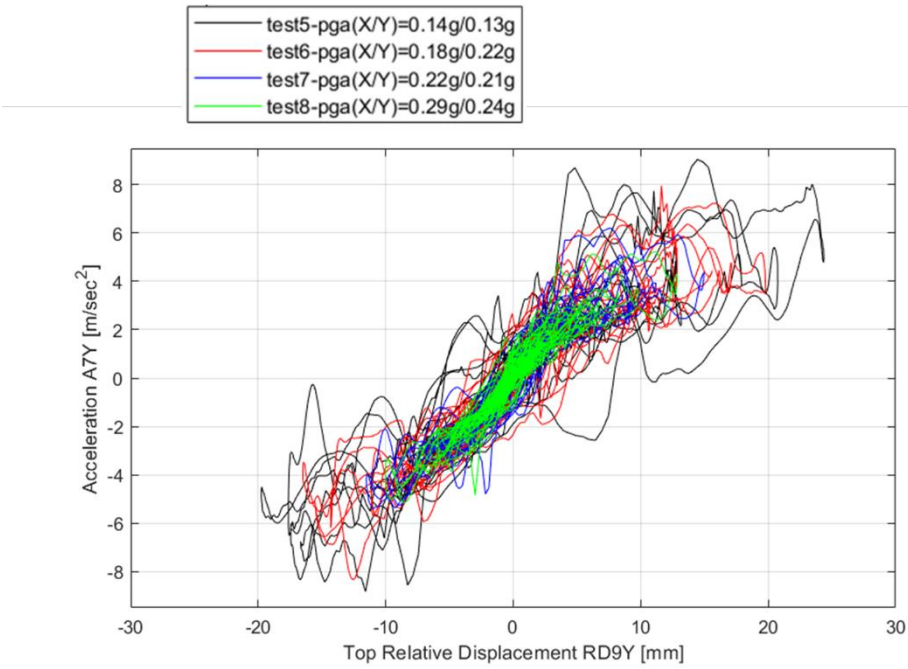

Figure 6.20 - Numerical absolute acceleration versus top relative displacement along Y-direction for Kalamata ground motion.

When comparing the experimental curves with the numerical curves, one may observe that:

- (a) as already described by the dynamic properties, the numerical model is stiffer than the experimental model in the longitudinal direction, resulting in smaller relative displacements in this direction.

- (b) acceleration spikes are noticeable in the numerical curves. These spikes can be associated with the differences between numerical and experimental ground motion records. In the experimental case, the ground motion is inputted to the shaking table as nominal PGA that will be reproduced with an error percentage. While performing the incremental dynamic analysis the inputted signals are perfectly reproduced on the model.

- (c) as predicted in the case-study paper [14], the larger displacements of the model develop along its weak Y direction, due to out-of-plane bending. The out-of-plane behaviour of the longer facades is mainly caused by the low stiffness of the timber floors and by the poor connections between the floors and the load-bearing masonry walls.

7. STRENGTHENED NUMERICAL MODEL

7.1. Introduction

A second numerical model was created to reproduce the behaviour of the strengthened specimen under seismic excitation. As done to the as-built numerical model, the strengthened model was developed based on geometry parameters and mechanical properties gathered from the paper *Vintzileou and Mouzakis, 2014* [14].

In the experimental campaign, the strengthened specimen was created by reinforcing the timber floors and grouting the walls of the damaged as-built specimen. The second layer of timber boards was added to the timber floors to increase their in-plane stiffness. To reduce the possibility of out-of-plane failures, the floor-to-wall connections were enhanced by using steel anchors and profiles. All the information and description on the reinforcement interventions was present in the paper and is already fully described in chapter 5.5. This data was used to create a new numerical model based on the as-built one. Similar to what happened to the as-built numerical model, the strengthened model was created using the OpenSEES software.

Although being based on the as-built numerical model, the strengthened model did not consider the existence of damages caused by the performed incremental dynamic analyses. This happens due to the inability of the OpenSEES software to save damage between a set of different incremental dynamic analyses where material parameters were re-iterated.

Nevertheless, a numerical calibration was carried out to validate the numerical model and guarantee the accuracy of the results. The model was calibrated based on its dynamic properties. For this calibration, a set of dynamic characteristics present in the paper was used to compare with the correspondent numerical values.

After the calibration of the model, the same set of analyses used for the model calibration was used to extract results and properties from the numerical model. To help evaluate and assess

the behaviour of the building, the results present in the case-study paper were used for comparison, just as they did in the calibration phase.

7.2. **Strengthened numerical model calibration**

7.2.1. **Wall-to-wall stiffness calibration**

As already explained, the strengthened numerical model was developed based on the as-built model and the information of all the strengthening interventions done in the experimental campaign. After the development of the base model, three types of analysis were performed to evaluate its status. First, a modal analysis was performed to evaluate the dynamic properties of the model. Second, a self-weight analysis was performed to test the behaviour of the model while just considering all loads and self-weights. Lastly, an incremental dynamic analysis that replicates the experimental campaign was carried out to evaluate the performance of the model while under seismic excitation. The results obtained from the modal analysis performed on the base numerical model showed a considerable difference between the numerical and experimental dynamic properties. Table 7.1 contains the experimental dynamic properties, that were calculated from the response of the strengthened specimen during sine logarithmic sweep excitations, and the values extracted from the base numerical modal analysis.

	Experimental Model		**Base Numerical Model**	
	Frequency (Hz)	Period (s)	Frequency (Hz)	Period (s)
X Direction Mode	10.36	0.097	10,59	0.0944
Y Direction Mode	9.95	0.1005	6,02	0.1661

Table 7.1 - Dynamic properties of the experimental specimen in both directions.

With these results was concluded that the numerical model was less stiff when compared to the experimental prototype. To solve this situation, a calibration was initiated considering the difference between numerical and experimental dynamic properties. As already detailed, no prior damages were considered while modelling the strengthened numerical model. In this way, a reduction percentage was applied on the masonry mechanical properties to have into account the existing damages of the strengthened experimental specimen.

In this way, a calibration based on the dynamic properties was carried out. As an addition to the calibration study, the modal shapes described in the paper (Figure 7.1) were compared to

the modal shapes obtained from the numerical model by computing the modal assurance criterion (MAC) coefficients [52], [53]. This method is described in sub-chapter 6.2.1.

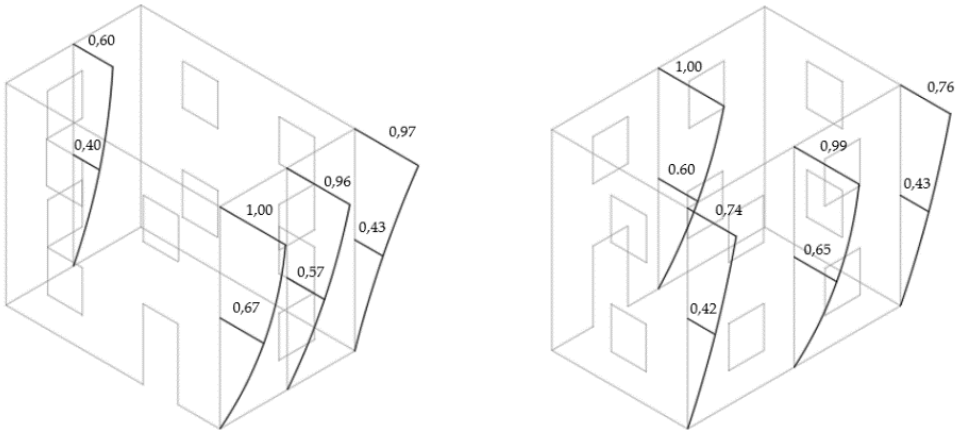

Figure 7.1 - Normal mode shapes of the strengthened specimen: (a) mode shape of f=10.36Hz (X-direction) and (b) mode shape of f=9.95Hz (Y-direction).

In the information and results obtained at the end of the shake-table test performed on the strengthened specimen present in the case-study paper, no vertical cracks or separation of masonry leaves were observed on the damages patterns of the specimen. As the masonry walls were grouted before this set of tests, enhancement of the connections between the orthogonal load-bearing walls can be assumed. In this way, the stiffness of the wall-to-wall connections was once again calibrated. To account for the prior damages on the strengthened numerical model, the reduction of the mechanical properties of the masonry walls was also calibrated.

To find the combination that gives the best results while simultaneously calibrating the damage percentage and the wall-to-wall stiffness, a total of 96 numerical models were developed. The stiffness of the connections was calibrated from the original value used on the as-built numerical model, $1 \times 10^9\ N/m$ (value used on the base numerical model) to $8 \times 10^6\ N/m$ in steps of $0.5 \times 10^6\ N/m$. The reduction of the mechanical properties of the masonry walls was assumed to be in the range of 10% to 30%. The dynamic properties of the numerical models considering a reduction of 10% on the masonry properties, while increasing the stiffness of the wall-to-wall connections, are shown in Table 7.2. To find the best combination between the calibrated parameters, the relative errors between numerical and experimental dynamic properties were calculated and are also shown in Table 7.2.

Stiffness of the interface	X-Direction Period (s)	X-Direction Frequency (Hz)	Y-Direction Period (s)	Y-Direction Frequency (Hz)	X-Direction MAC coefficient	Y-Direction MAC coefficient	X-Direction Relative Error	Y-Direction Relative Error	Average Relative Error
1,00E+06	0,0972	10,29	0,17099	5,85	0,922	0,928	0,65%	70,14%	35,39%
1,50E+06	0,0867	11,53	0,15508	6,45	0,923	0,933	10,14%	54,30%	32,22%
2,00E+06	0,0793	12,62	0,14359	6,96	0,923	0,937	17,89%	42,87%	30,38%
2,50E+06	0,0736	13,59	0,13486	7,42	0,922	0,940	23,77%	34,19%	28,98%
3,00E+06	0,0691	14,47	0,12797	7,81	0,921	0,942	28,42%	27,33%	27,88%
3,50E+06	0,0654	15,28	0,1224	8,17	0,919	0,943	32,21%	21,79%	27,00%
4,00E+06	0,0624	16,03	0,11779	8,49	0,916	0,943	35,35%	17,20%	26,28%
4,50E+06	0,0598	16,71	0,11392	8,78	0,912	0,943	38,02%	13,35%	25,68%
5,00E+06	0,0576	17,35	0,11063	9,04	0,908	0,942	40,30%	10,08%	25,19%
5,50E+06	0,0557	17,95	0,10778	9,28	0,903	0,941	42,29%	7,24%	24,76%
6,00E+06	0,0540	18,51	0,10531	9,50	0,897	0,939	44,02%	4,78%	24,40%
6,50E+06	0,0526	19,03	0,10315	9,69	0,891	0,937	45,55%	2,63%	24,09%
7,00E+06	0,0513	19,51	0,10123	9,88	0,884	0,935	46,90%	0,72%	23,81%
7,50E+06	0,0501	19,97	0,099527	10,05	0,876	0,933	48,11%	0,97%	24,54%
8,00E+06	0,0490	20,39	0,098004	10,20	0,869	0,930	49,19%	2,49%	25,84%
8,50E+06	0,0481	20,78	0,096635	10,35	0,860	0,927	50,15%	3,85%	27,00%

Table 7.2 - Evolution of the dynamic properties, MAC values and relative errors during the numerical calibration. (Assuming 10% reduction to the masonry mechanical properties).

In addition to the calibration study, a set of three curves were plotted to help understand the evolution of the dynamic characteristics of the numerical models. The first curve and the second curve describe the evolution of the natural periods and frequencies for the X and Y directional modes respectively (Figure 7.2 and Figure 7.3).

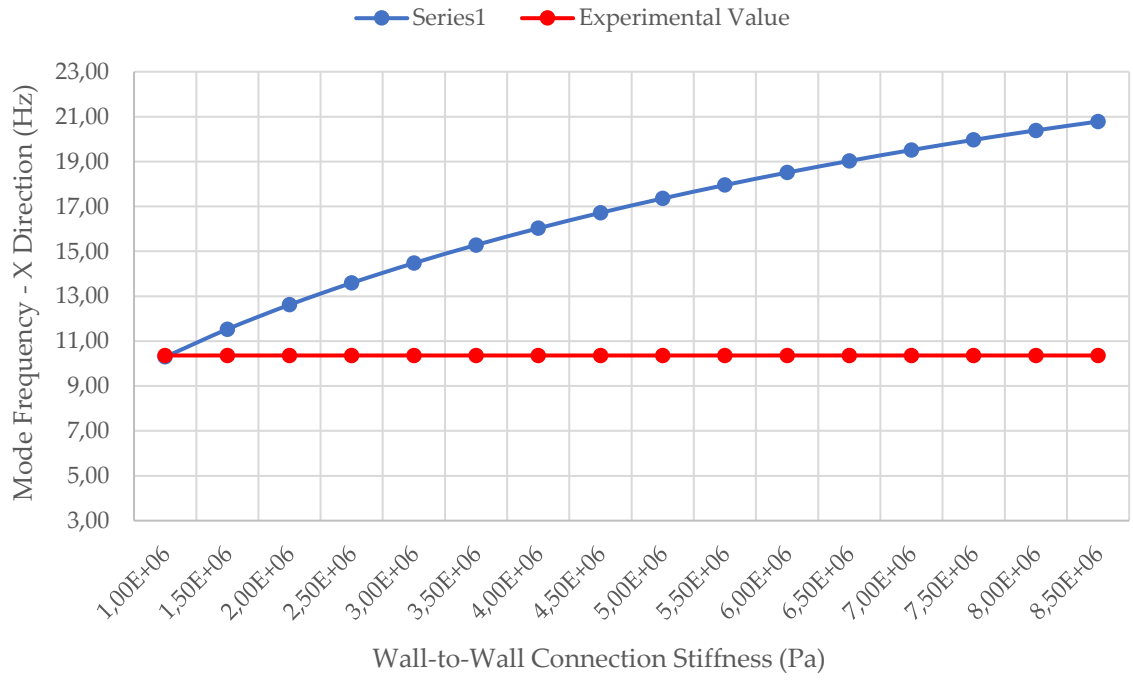

Figure 7.2 - Evolution curve of the X-direction mode frequency with increasing wall-to-wall stiffness

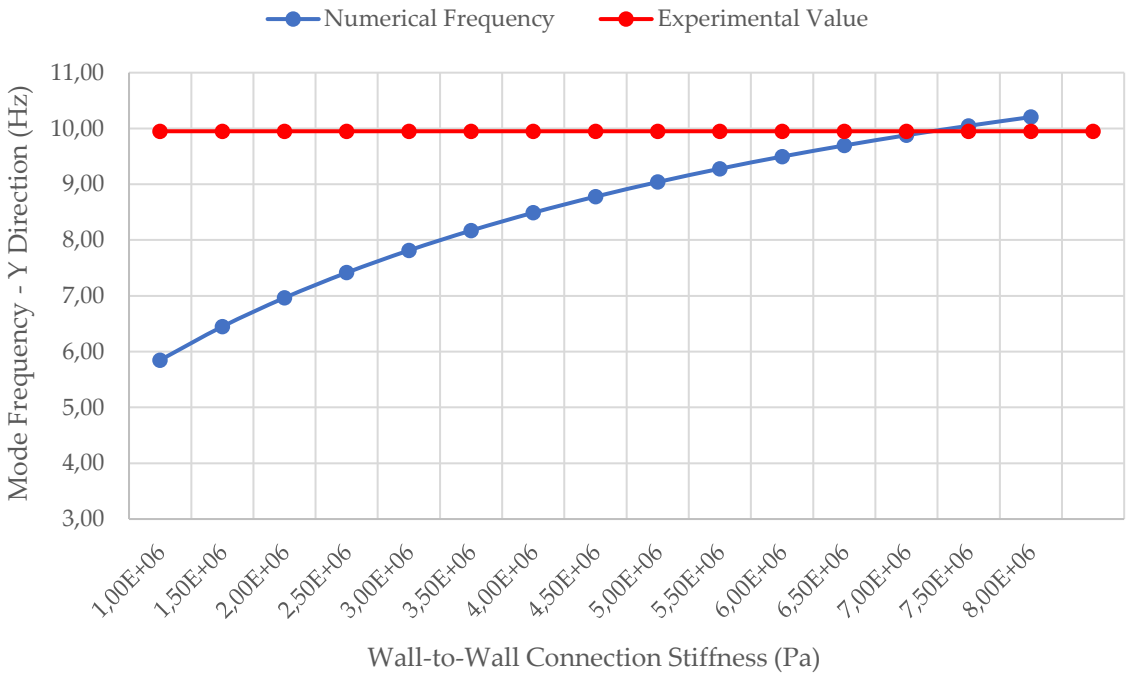

Figure 7.3 - Evolution curve of the Y-direction mode frequency with increasing wall-to-wall stiffness.

The third curve describes the behaviour of the MAC coefficients for both directional modes during the study (Figure 7.4).

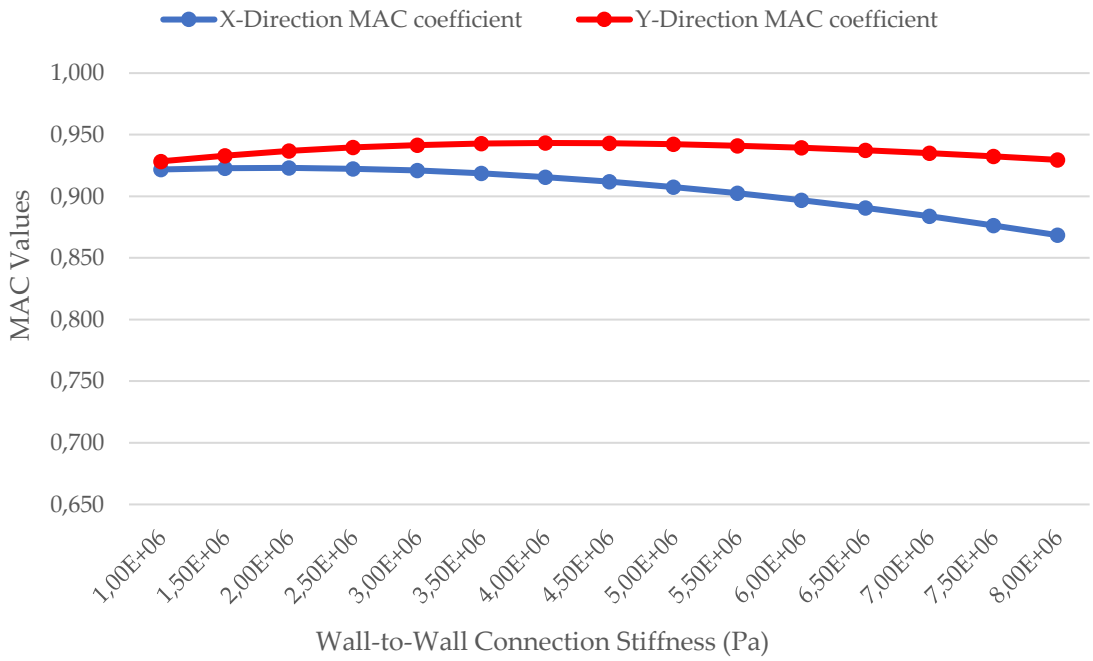

Figure 7.4 - Evolution curve of the X and Y direction MAC values with the increasing wall-to-wall stiffness.

When analysing the first and second curves extracted from the numerical modal analysis, it is noticeable that both directional frequencies increase with the increasing wall-to-wall stiffness. In Figure 7.3, where the evolution of the Y directional frequency is shown, it can be concluded that the numerical value is increasing towards the experimental one. Nevertheless, in Figure 7.2, where the evolution of the X directional frequency is shown, the difference between numerical and experimental frequency values seems to increase with the evolution of the calibration. The third curve, where the calculated MAC coefficients are shown, indicates that the calibration of the stiffness of the wall-to-wall interfaces maintains a good correlation of the mode shapes of the numerical and the experimental model.

The reduction in the mechanical properties of the masonry was assumed to be 10%. This is the percentage value that gives the smallest relative errors when comparing experimental and numerical dynamic properties. In Table 7.3, the reader can find the original and reduced mechanical properties of the masonry walls.

	E (GPa)	**G (GPa)**	**fc (MPa)**	**τ (MPa)**	**μ**
Original	3.34	1.336	5.45	0.175	0.200
Reduced (10%)	3.01	1.202	4.91	0.175	0.200

Table 7.3 - Original and reduced masonry mechanical properties used in the strengthened numerical model.

As there was no literature information on how the strengthening interventions would affect both the cohesion and the masonry friction coefficient that defines the peak strength of the walls, these values were not reduced.

Considering the enhancement of the connections between orthogonal masonry walls, and the present calibration study, a value of $5.5 \times 10^6\ N/m$ was adopted for the stiffness of these connections. This value provides a good approximation of the dynamic properties in the Y-direction. Nevertheless, there is still a considerable difference between the experimental and numerical dynamic properties in the X-direction. This difference can be associated with local damages in this direction, that were not visible or observed in the experimental campaign. Although the lowest relative error is given for stiffness of $7 \times 10^6\ N/m$, the MAC values in X-direction and the high relative error in X-direction justify the adopted solution. The MAC values provided by the adopted solution point out an excellent correlation between experimental and numerical mode shapes.

The damping percentage used on the strengthened numerical model was maintained at 3.5%, a value that was calibrated for the as-built model.

7.3. **Strengthened numerical model results**

The results obtained from the analyses performed on the calibrated strengthened numerical model are shown in this sub-chapter. While the analyses were performed on OpenSEES software, all the outputted data and results were organized and treated using MATLAB coding.

Starting with the dynamic properties of the numerical model, a set of 3D figures was created to represent the mode shapes for the X and Y directions (Figure 7.5 and Figure 7.6). Table 6.3 describes the values of the natural frequencies and periods for each directional mode. The MAC coefficients that correlate the numerical mode shapes with the experimental mode shapes are also present in this table.

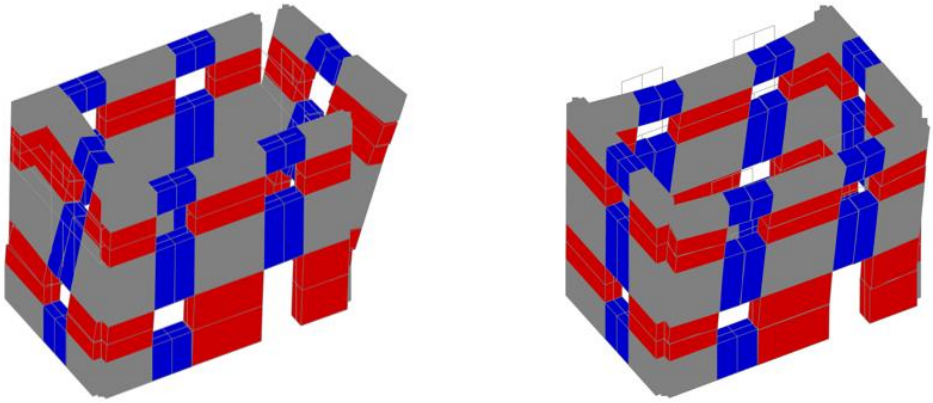

(a) (b)

Figure 7.5 - Modal deformed shapes of the strengthened numerical model obtained from the MATLAB coding: (a) mode shape of f=17.95 Hz (X-direction) and (b) mode shape of f=9.28 Hz (Y-direction)

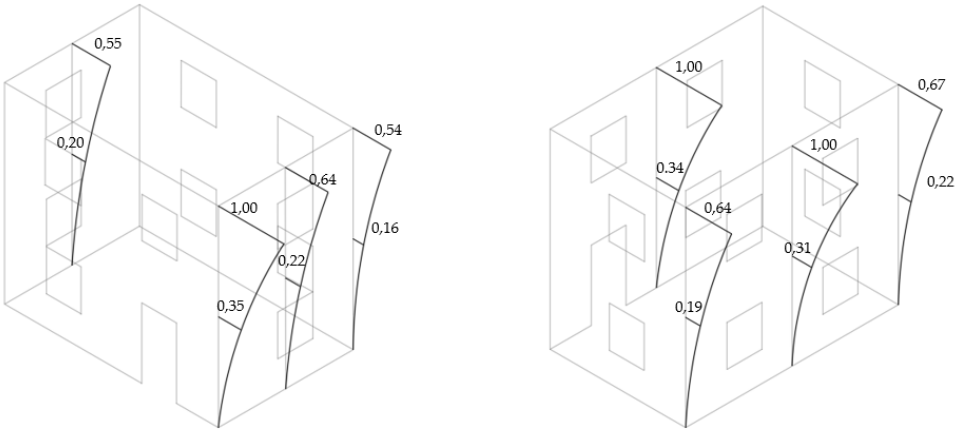

(a) (b)

Figure 7.6 - Normal mode shapes of the strengthened numerical model: (a) mode shape of f=17.95 Hz (X-direction) and (b) mode shape of f=9.28 Hz (Y-direction).

	Frequency (Hz)	Period (s)	MAC coefficients
X Direction Mode	17.95	0.0557	0.90
Y Direction Mode	9.28	0.1078	0.94

Table 7.4 - Dynamic properties of the strengthened numerical model.

The incremental dynamic analysis performed on the numerical model was crucial to study its behaviour and performance while subjected to seismic excitation. According to the case-study paper, and as it was already described in a previous section, displacement transducers were used to measure the maximum relative displacements at the mid-length of the walls at both levels of the experimental prototype. Figure 7.7 shows the recorded maximum displacements at the end of the experimental campaign. In Figure 7.8, the reader can find the maximum relative displacements for the same locations, that were extracted after the incremental dynamic analysis performed on the numerical model. Table 7.5 describes the comparison of both figures.

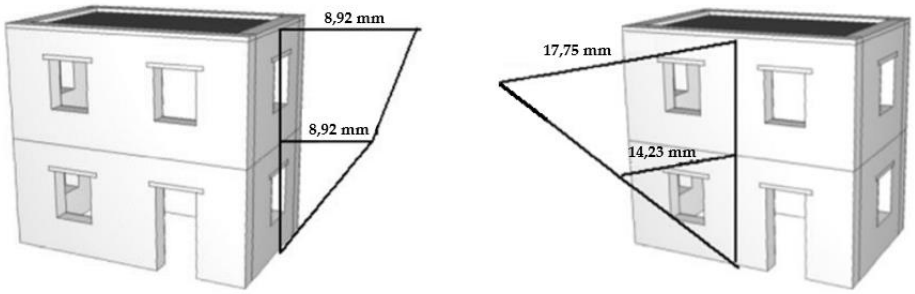

Figure 7.7 - Maximum relative displacements recorded at middle-length of the front and right facades at both levels of the strengthened specimen after the end of Test 17AS (Table 5.3): (a) right facade - X-direction displacements and (b) front facade -Y direction displacements.

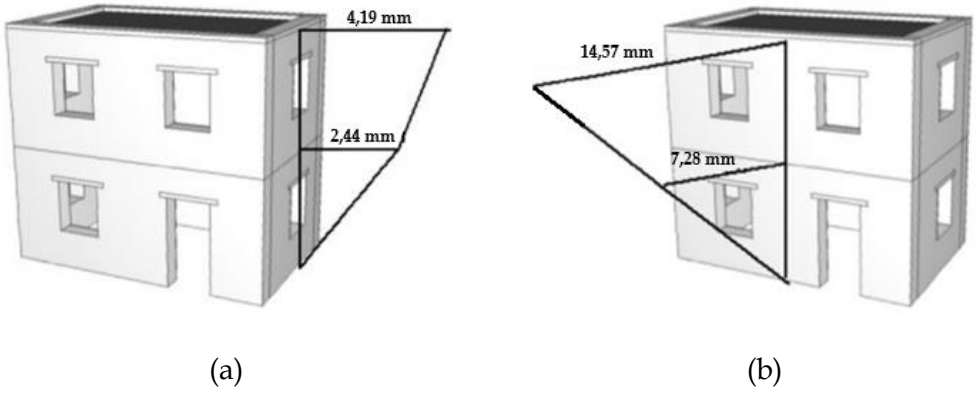

Figure 7.8 - Maximum relative displacements recorded at middle-length of the front and right facades at both levels of the strengthened numerical model after the end of the incremental dynamic analysis: (a) right facade - X-direction displacements and (b) front facade - Y-direction displacements.

	Experimental Displacements		Numerical Displacements	
	Front Facade (mm)	Right Facade (mm)	Front Facade (mm)	Right Facade (mm)
1st Floor	14,23	8.92	7,28	2,44
2nd Floor	17,75	8,92	14,57	4,19

Table 7.5 - Maximum relative displacements of the strengthened models: Experimental vs Numerical.

These results show an underestimation of the maximum out-of-plane displacements in both directions. This difference of measured maximum displacements between the numerical strengthened model and the experimental strengthened specimen is more evident in the X-direction. These results can be justified by the difference between the dynamic properties in the X-direction of the numerical and experimental models. The discrepancy between the inputted ground motion signals can also influence the difference between the maximum displacements of the numerical model and the experimental specimen. In the experimental case, the ground motion is inputted to the shaking table as nominal PGA that will be reproduced with an error percentage. While performing the incremental dynamic analysis the inputted signals are perfectly reproduced on the model.

When comparing the results of the maximum out-of-plane displacements extracted from the strengthened numerical model with the ones obtained from the as-built numerical model, it is noticeable that the maximum displacements read for the strengthened model are substantially lower than the ones calculated for the as-built model (Figure 7.8 and Figure 6.10). Considering that the strengthened numerical model was submitted to higher PGA's, it is concluded that there is an enhancement of the global seismic response when analysing the strengthened numerical model. When analysing Figure 7.9, where the deformed shape and the flexural drifts for the last run (nominal PGA of 0.66g) are shown, is concluded that the possibility of the occurrence of an out-of-place failure was reduced.

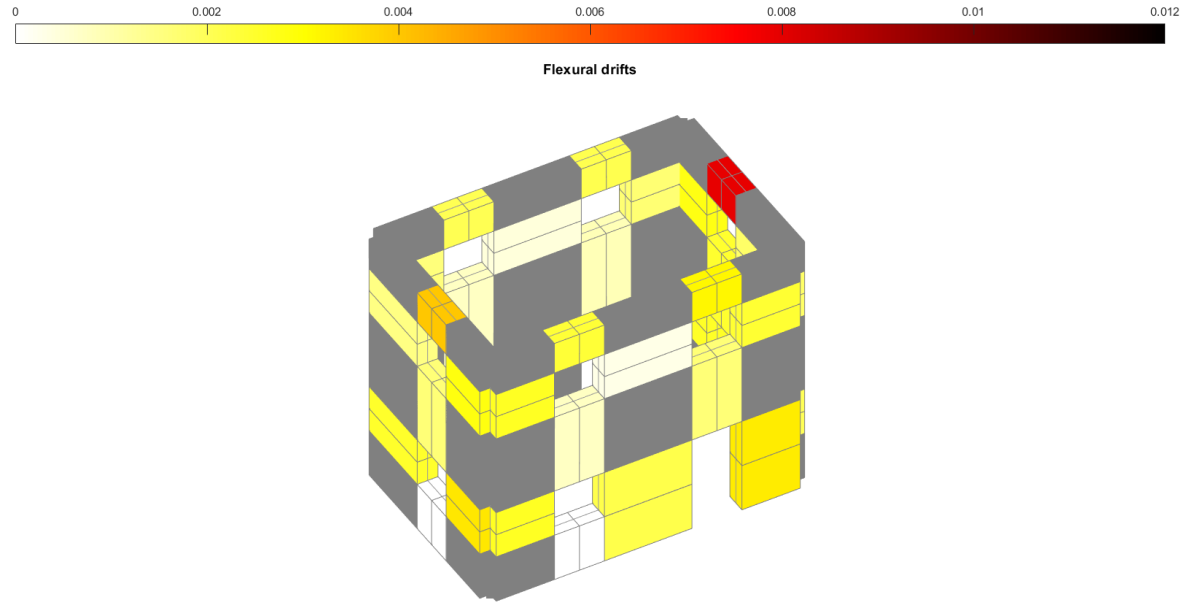

Figure 7.9 - Out-of-plane behaviour and flexural drifts of the strengthened numerical model (magnification factor ×40).

In this case, the stiffening of the timber diaphragms, combined with efficient connections between floors and load-bearing walls has led to a significant improvement of the box action of the building model, reducing the vulnerability of the long walls to out-of-plane actions.

As described in the case study paper, the strengthened specimen developed a failure mechanism characterized by in-plane bending (under the Irpinia earthquake). According to the paper, shear cracks started appearing in the building while under seismic test 15AS (Irpinia, X-0.48g and Y-0.43g, Table 5.3). To get information on the shear behaviour of the numerical model, Figure 7.10 was created to represent the shear drifts of each element of the numerical model.

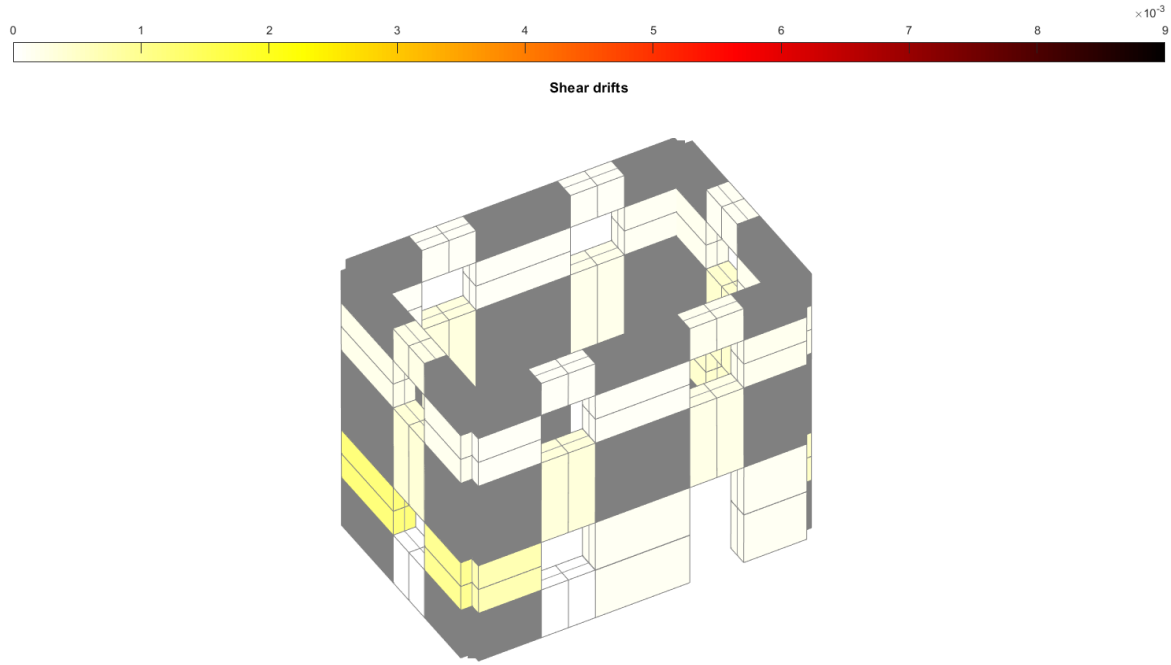

Figure 7.10 - In-plane behaviour and shear drifts of the strengthened numerical model (magnification factor ×40).

When analysing Figure 7.11, which represents the damages after the shake-table tests performed on the experimental strengthened specimen, the reader can observe that the shorter facades were more damaged than the longer facades. When analysing both flexural and shear drifts calculated from the strengthened numerical model it can also be concluded that the masonry elements with higher drifts are the ones that belong to the shorter facades. According to these results, the grouting of the walls of the as-built model and the consequent increase of the mechanical properties of the masonry made an impact on the in-plane response of the building. If we compare the figures that represent the drifts for both as-built and strengthened numerical models it can be concluded that the as-built model is showing higher drifts, especially flexural drifts. Nevertheless, these results also show a discrepancy between the experimental and the numerical strengthened model as the numerical drifts fail to represent the observed failure mechanism characterized by in-plane bending observed during the final runs of the experimental campaign.

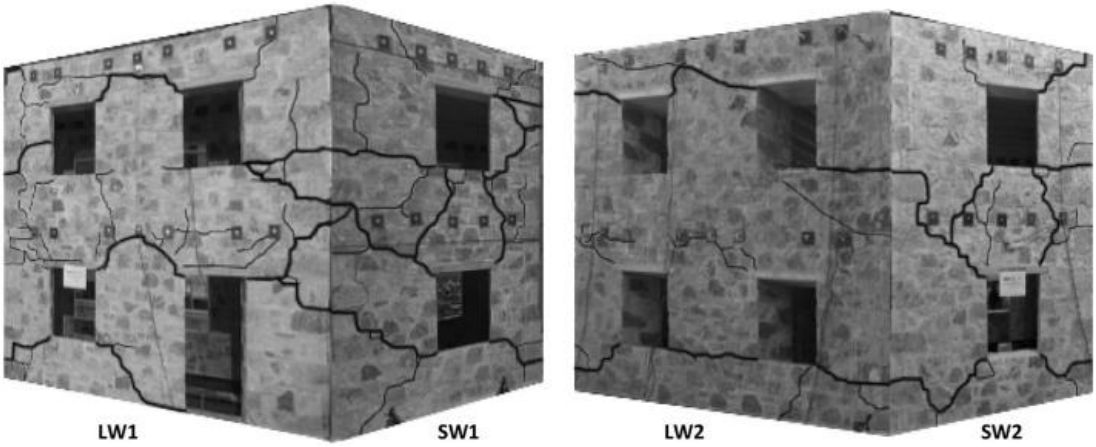

Figure 7.11 - Rigid bodies formed during Test 17AS (Irpinia earthquake: 0.54 g(X)/0.66 g(Y), Table 5.3) [14].

As done to the as-built numerical model and to control the incremental dynamic analysis, a pair of base shear curves was plotted for each of the ground motion directions (Figure 7.12 and Figure 7.13). As an estimate of the maximum expected lateral force on the base of the structure, base shear is important to evaluate the value of seismic forces that are acting in the structure. The base shear was numerically calculated based on the forces acting in the base nodes of the model.

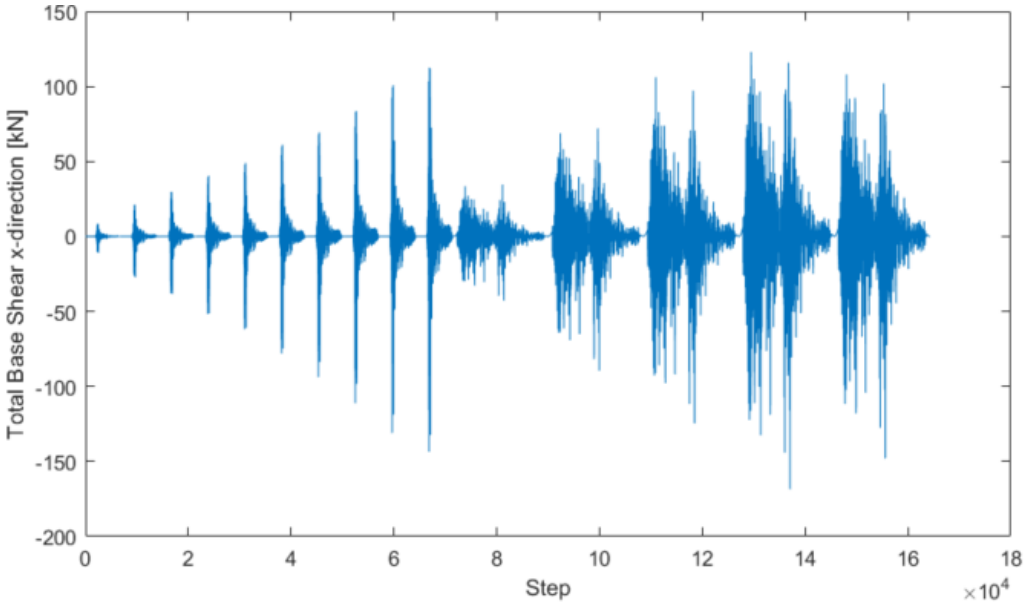

Figure 7.12 - Total base shear of the numerical model per step - X direction.

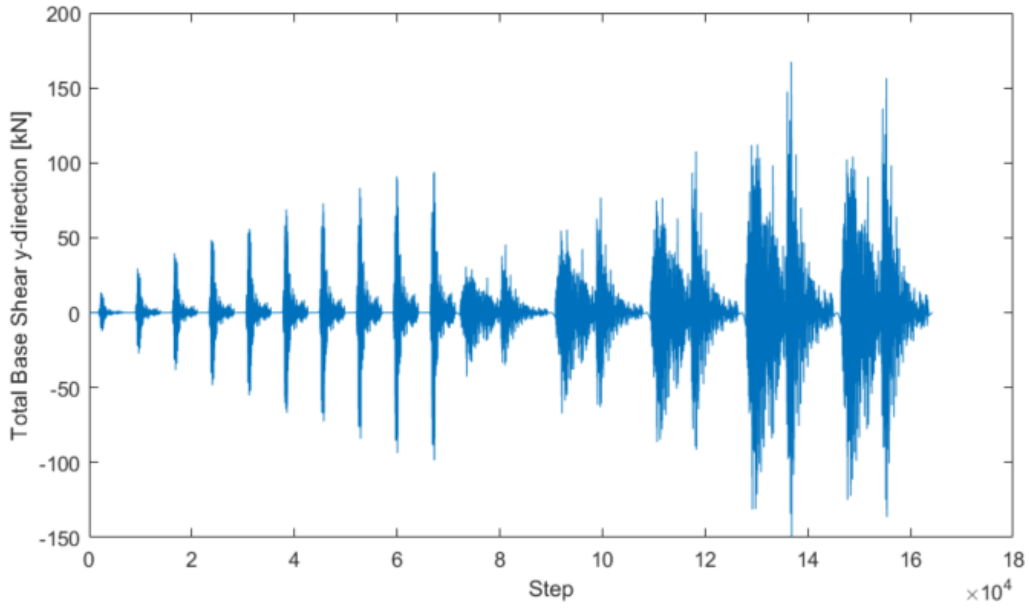

Figure 7.13 - Total base shear of the numerical model per step - Y direction.

Once again, the hysteric response of the model was evaluated. First, a pair of hysteric curves were plotted to show the relation between the total base shear and the average relative displacement of the roof level. These hysteresis loops were created for both directions: the transversal Y-direction (Figure 7.14) and the longitudinal X-direction (Figure 7.15). As predicted, the model shows loss of stiffness under increasing base shear and consequent occurrence of damage for both directions.

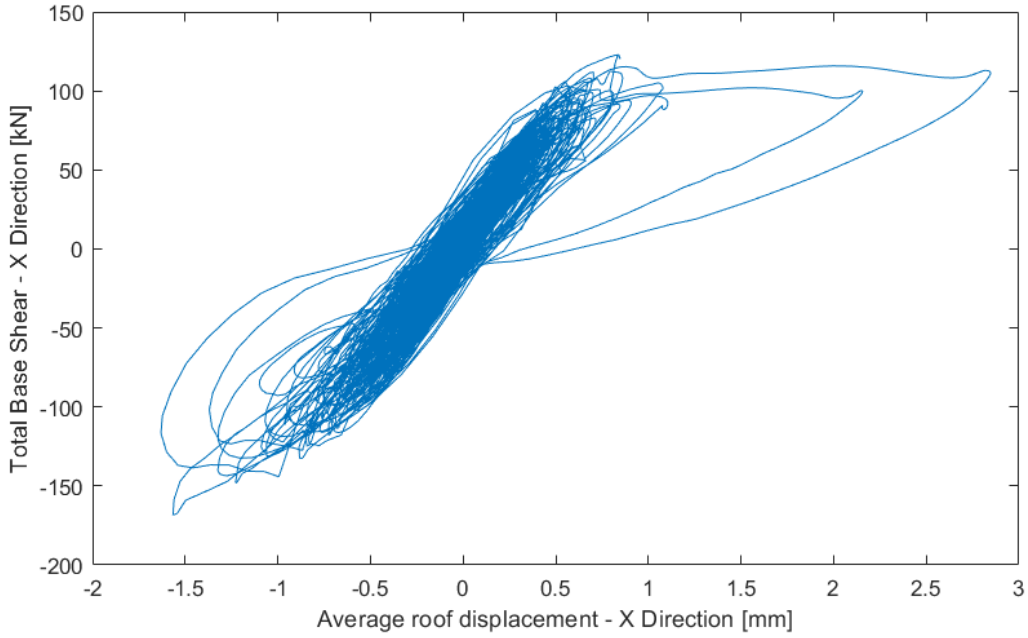

Figure 7.14 - Numerical total base shear versus roof mean relative displacement along X direction for Irpinia base motion.

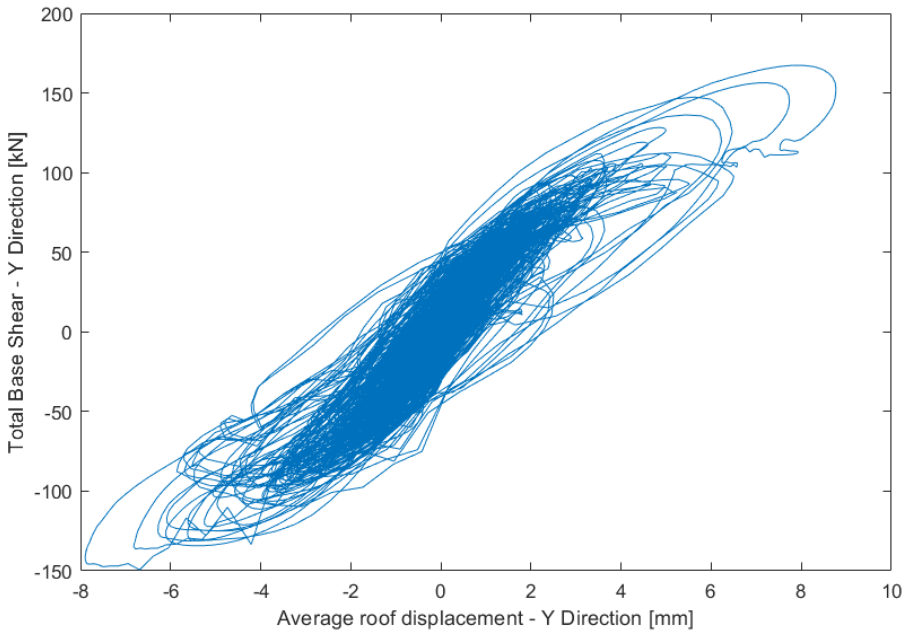

Figure 7.15 - Numerical total base shear versus roof mean relative displacement along Y direction for Irpinia base motion.

In the experimental campaign accelerations and relative displacements, for each ground motion direction, were plotted into hysteric curves (Figure 7.16 and Figure 7.17). The accelerations and relative displacements were measured at the middle length of the top of the back facade (Y direction accelerations and relative displacements) and the middle length of the top of the right facade (X direction accelerations and relative displacements).

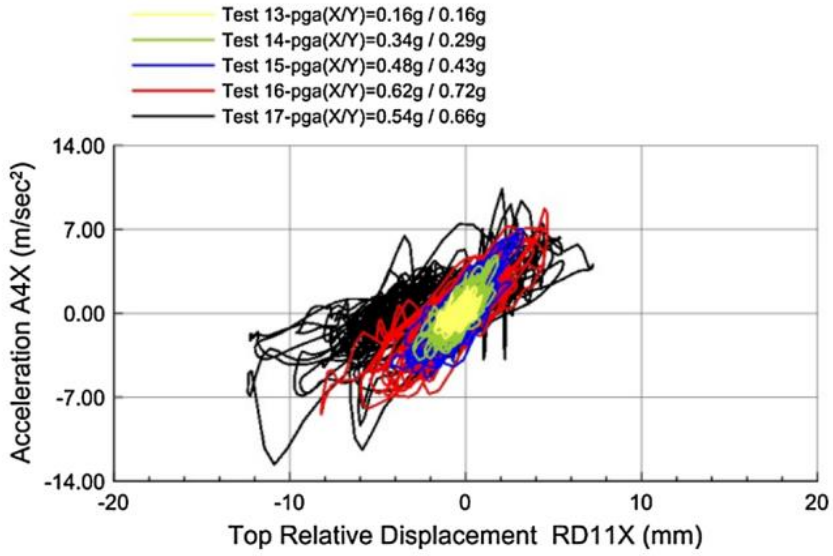

Figure 7.16 - Experimental absolute acceleration versus top relative displacement along X-direction for Irpinia ground motion [14].

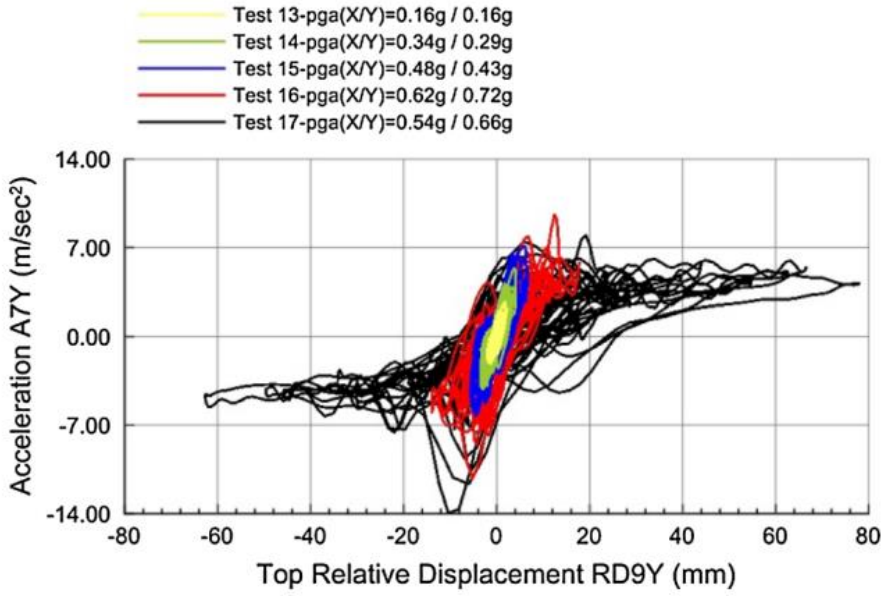

Figure 7.17 - Experimental absolute acceleration versus top relative displacement along Y-direction for Irpinia ground motion [14].

To compare the experimental data with the results extracted from the replication of the seismic motion on the numerical model, two hysteric curves were developed similar to the ones present in the paper [14] (Figure 7.18 and Figure 7.19). the data was plotted with different colours that depend on the identification of the run/test and associated nominal PGA.

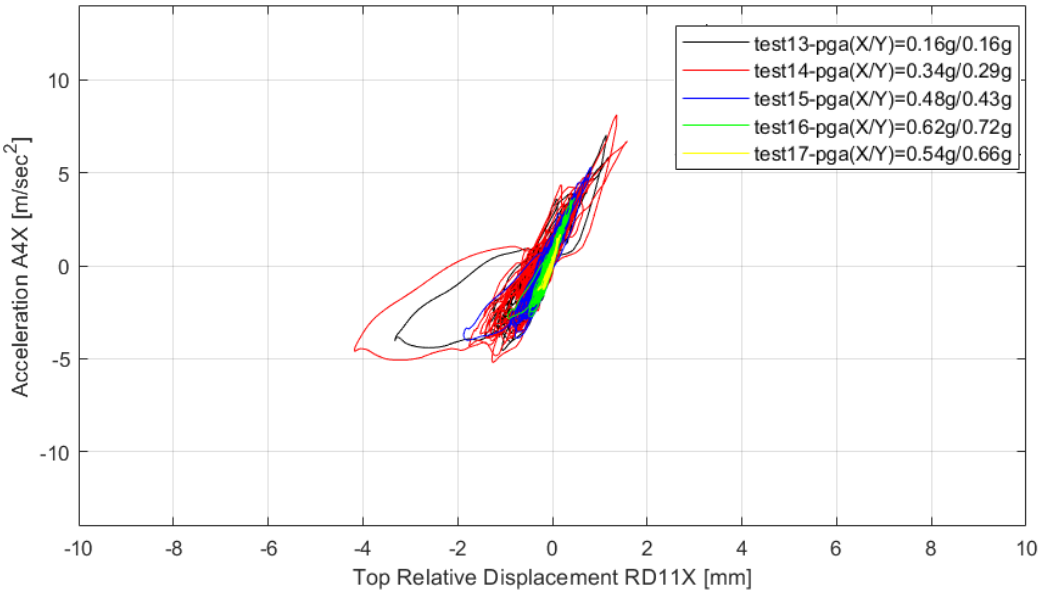

Figure 7.18 - Numerical absolute acceleration versus top relative displacement along X-direction for Irpinia ground motion.

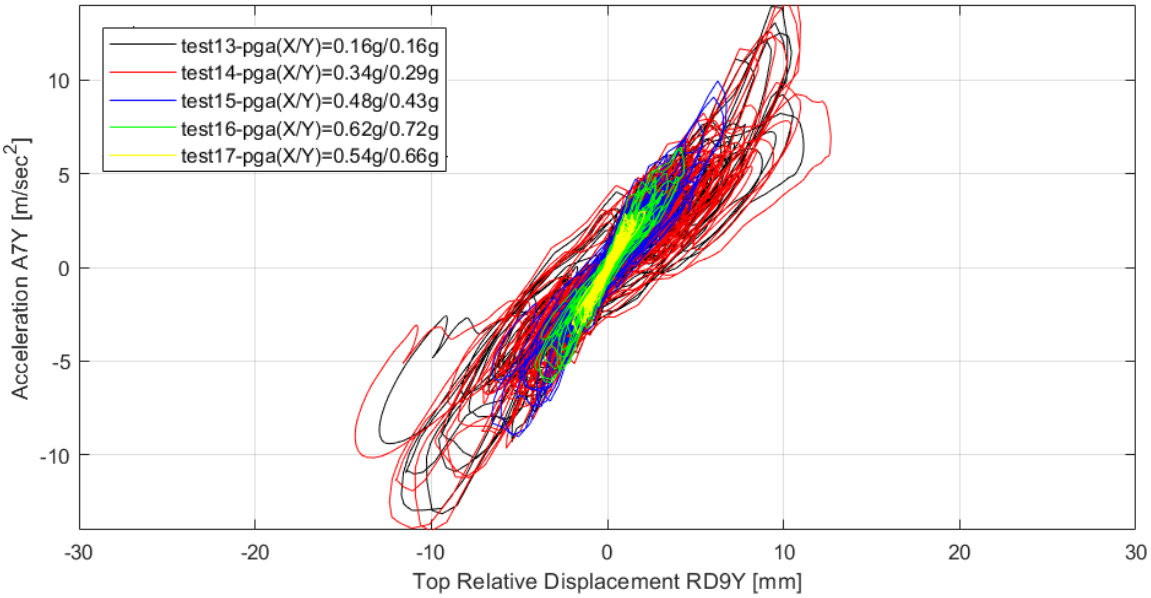

Figure 7.19 - Numerical absolute acceleration versus top relative displacement along Y-direction for Irpinia ground motion.

When comparing the experimental curves with the numerical curves, one may observe that:

- (a) as already described by the dynamic properties, the strengthened numerical model is stiffer than the experimental model in the longitudinal direction (X-direction), resulting in smaller relative displacements in that direction (Figure 7.18).

- (b) in the transversal direction, the curves seem to be similar till the last test 17AS, where the experimental model seems to show loss of stiffness, resulting in high deformations, that were caused by damage occurrence (Figure 7.19).

- (c) as predicted in the paper, the global seismic behaviour of the model was enhanced. The efficiency of the connections between diaphragms and vertical elements and the stiffening of the floors improved the box behaviour of the building reducing the probability of occurrence of out-of-plane failures (especially in the longer facades). The grouting process was used to correct local damages and failures, like the extensive detachment of the masonry leaves, and is noticeable in the increased in-plane resistance of the masonry elements.

8. CONCLUSIONS AND FUTURE WORKS

8.1. Conclusions

This thesis was mainly divided into three parts:

In the first part, a bibliographic study was performed to describe masonry buildings and explain the importance of timber floors in unreinforced masonry buildings. Due to their impact on the seismic response of unreinforced masonry buildings, the correct detailing and information on their conditions are important. As these buildings are in many cases considered cultural heritage, the conservation and preservation of their timber floors are crucial. In this way, this type of scientific study intends to validate numerical models and tools that are used to assess unreinforced masonry buildings.

The second part of the thesis was important to acquire knowledge on the case-study specimens and the modelling techniques used in the present work. In this part, a description of the used modelling techniques and on the case-study specimen was written. In recent years and supported by cultural heritage protection, new tools and methods are being developed to study and assess unreinforced masonry buildings. In this thesis, two numerical models based on two unreinforced masonry specimens were created. These specimens consist of two experimental models that were submitted to a set of shake-table tests that resulted in a scientific paper. The two numerical models were submitted to a set of analyses to study their seismic behaviour. All the results obtained from the case-study paper were used to compare the final numerical results and to validate both numerical models.

In the third part of the thesis, the numerical models were created, calibrated, and analysed. The results obtained from the OpenSEES software were then treated and organized using MATLAB coding. All the results and data regarding the numerical modelling and simulation of the experimental specimens is shown. The equivalent frame modelling approach with non-linear macro-elements proved to be efficient in simulating the shaking table tests. The new feature of capturing both in-plane and out-of-plane behaviour of the recently developed macro-element by Vanin et. al. [42]was important to simulate the real seismic behaviour of the specimens.

The effects of the three retrofit interventions (stiffening of the diaphragms, enhancement of the floor-to-wall connection and the grouting of the walls) were successfully simulated in the numerical models. The captured out-of-plane failure of the longer facades was confirmed to be sensitive to the modelling of poor vs fixed floor-to-wall connections and the stiffening of the diaphragms. The reduction of the out-of-plane behaviour of the longer facades in the strengthened numerical model caused by the appropriate fixing of the floor-to-wall connections combined with the stiffening of the diaphragms was important to understand how unreinforced masonry buildings are dependent on the conditions and detailing of their timber floors. These results are important as the floor-to-wall connections were typically modelled as a simplification of a perfect connection, generally leading to misleading box-type behaviours. The recently developed macro-element by Vanin et al. [42] enables modelling of both in-plane and out-of-plane failure modes without considering simplifications on the connections between masonry walls and timber floors.

These results are promising for future numerical simulations of unreinforced masonry buildings. Nevertheless, new tools, scientific investments and studies are required to increase the literature and knowledge to help assess and intervene in this type of building.

8.2. **Future Works**

Following the numerical work carried out, some suggestions are made for future development:

- Developing mechanical models for wall-to-wall connection parameters calibrating and validating them against experimental data.
- Perform sensitivity analysis of more modelling parameters.
- Study possible disadvantages of retrofitting techniques, such as the excessive stiffening of the diaphragms.

BIBLIOGRAPHY

[1] Miha. Tomaževič, *Earthquake-resistant design of masonry buildings*. World Scientific, 1999.

[2] K. Beyer *et al.*, "Seismic retrofit of cultural heritage buildings-when less is more," *Proceedings of the 4th Conference on Smart Monitoring, Assessment and Rehabilitation of Civil Structures*, 2017.

[3] D. D'Ayala and E. Speranza, "Definition of Collapse Mechanisms and Seismic Vulnerability of Historic Masonry Buildings," *Earthquake Spectra*, vol. 19, no. 3, pp. 479–509, 2003, doi: 10.1193/1.1599896.

[4] F. Vanin, D. Zaganelli, A. Penna, and K. Beyer, "Estimates for the stiffness, strength and drift capacity of stone masonry walls based on 123 quasi-static cyclic tests reported in the literature," *Bulletin of Earthquake Engineering*, vol. 15, no. 12, pp. 5435–5479, Dec. 2017, doi: 10.1007/s10518-017-0188-5.

[5] G. Guerrini *et al.*, "Material Characterization for the Shaking-Table Test of the Scaled Prototype of a Stone Masonry Building Aggregate," Pistoia, Italy, 2017.

[6] G. Guerrini, I. Senaldi, F. Graziotti, G. Magenes, K. Beyer, and A. Penna, "Shake-Table Test of a Strengthened Stone Masonry Building Aggregate with Flexible Diaphragms," *International Journal of Architectural Heritage*, vol. 13, no. 7, pp. 1078–1097, Oct. 2019, doi: 10.1080/15583058.2019.1635661.

[7] I. Senaldi *et al.*, "Natural Stone Masonry Characterization For The Shaking-Table Test Of A Scaled Building Specimen - 10th IMC," Milan, Italy, 2018.

[8] I. E. Senaldi *et al.*, "Experimental seismic performance of a half-scale stone masonry building aggregate," *Bulletin of Earthquake Engineering*, vol. 18, no. 2, pp. 609–643, Jan. 2020, doi: 10.1007/s10518-019-00631-2.

[9] G. Magenes *et al.*, "Experimental Characterisation of Stone Masonry Mechanical Properties National Centre for Safety of Heritage Structures View project NAM Project View project Experimental characterisation of stone masonry mechanical properties," Dresden, 2010. [Online]. Available: https://www.researchgate.net/publication/257333264

[10] M. Betti, L. Galano, and A. Vignoli, "Comparative analysis on the seismic behaviour of unreinforced masonry buildings with flexible diaphragms," *Engineering Structures*, vol. 61, pp. 195–208, Mar. 2014, doi: 10.1016/j.engstruct.2013.12.038.

[11] I. Tomić, F. Vanin, I. Božulić, and K. Beyer, "Numerical simulation of unreinforced masonry buildings with timber diaphragms," *Buildings*, vol. 11, no. 5, May 2021, doi: 10.3390/buildings11050205.

[12] F. Vanin, A. Penna, and K. Beyer, "Equivalent-Frame Modeling of Two Shaking Table Tests of Masonry Buildings Accounting for Their Out-Of-Plane Response," *Frontiers in Built Environment*, vol. 6, Apr. 2020, doi: 10.3389/fbuil.2020.00042.

[13] G. Magenes, "A method for pushover analysis in seismic assessment of masonry buildings," *12th World Conference on Earthquake Engineering*, 2014.

[14] E. Vintzileou, C. Mouzakis, C. E. Adami, and L. Karapitta, "Seismic behavior of three-leaf stone masonry buildings before and after interventions: Shaking table tests on a two-storey masonry model," *Bulletin of Earthquake Engineering*, vol. 13, no. 10, pp. 3107–3133, Oct. 2015, doi: 10.1007/s10518-015-9746-x.

[15] M. Angelillo, P. B. Lourenço, and G. Milani, "Masonry behaviour and modelling," in *Mechanics of Masonry Structures*, 2014.

[16] P. Roca, M. Cervera, G. Gariup, and L. Pela', "Structural analysis of masonry historical constructions. Classical and advanced approaches," *Archives of Computational Methods in Engineering*, vol. 17, no. 3, pp. 299–325, 2010, doi: 10.1007/s11831-010-9046-1.

[17] London: British Standards Institution, *Eurocode 8: Design provisions for earthquake resistance of structures*. 1996.

[18] B. Pantò, "La Modellazione Sismica Degli Edifici in Muratura - Un Approccio Innovativo Basato Su Un Macro-Elemento Spaziale," Tesi di Dottorato, Università degli Studi di Catania , 2007. doi: 10.13140/RG.2.2.31809.79207.

[19] Second European Conference on Earthquake Engineering and Seismology (2ECEES), "Perspectives on European Earthquake Engineering and Seismology," 2014. [Online]. Available: http://www.springer.com/series/6011

[20] P. B. Lourenco, P. Roca, J. L. González, and E. Oñate, "Experimental and numerical issues in the modelling of the mechanical behaviour of masonry," Barcelona, 1998.

[21] F. Neves, A. Costa, R. Vicente, C. S. Oliveira, and H. Varum, "Seismic vulnerability assessment and characterisation of the buildings on Faial Island, Azores," *Bulletin of Earthquake Engineering*, vol. 10, no. 1, pp. 27–44, Feb. 2012, doi: 10.1007/s10518-011-9276-0.

[22] CEN (European Commitee for Standardization), *Eurocode 6 - Design of masonry structures - Part 3: Simplified calculation methods for unreinforced masonry structures Eurocode*, vol. 2, no. 2005.

[23] M. Doleželová, J. Krejsová, and A. Vimmrová, "Influence of fine aggregate on some properties of gypsum mortars," in *IOP Conference Series: Materials Science and Engineering*, Jul. 2018, vol. 379, no. 1. doi: 10.1088/1757-899X/379/1/012005.

[24] S. M. dos S. Botas, M. do R. S. Veiga, and A. L. Velosa, "Adhesion of Air Lime–Based Mortars to Old Tiles: Moisture and Open Porosity Influence in Tile/Mortar Interfaces," *Journal of Materials in Civil Engineering*, vol. 27, no. 5, p. 04014161, May 2015, doi: 10.1061/(asce)mt.1943-5533.0001108.

[25] S. Pavía and R. Hanley, "Flexural bond strength of natural hydraulic lime mortar and clay brick," *Materials and Structures/Materiaux et Constructions*, vol. 43, no. 7, pp. 913–922, Aug. 2010, doi: 10.1617/s11527-009-9555-2.

[26] J. M. Laredo Dos Reis, "Mechanical characterization of fiber reinforced Polymer Concrete," *Materials Research*, vol. 8, no. 3, pp. 357–360, 2005, doi: 10.1590/s1516-14392005000300023.

[27] J. Válek and & R. Veiga, "Characterisation of mechanical properties of historic mortars-testing of irregular samples," *Structural Studies, Repairs and Maintenance of Heritage Architecture IX*, pp. 365–374, 2005.

[28] British Standards Institution, *Eurocode 6: Rules for reinforced and unreinforced masonry*. London: British Standards Institution, 1996.

[29] Baião M., Pinho F., and V. Lúcio, "Aspetos Da Reabilitação De Edifícios Antigos De Alvenaria," in *CIRea2012 – Conferência Internacional sobre Reabilitação de Estruturas Antigas de Alvenaria*, 2012, pp. 47–62.

[30] A. Brignola, S. Podestà, and S. Pampanin, "In-plane stiffness of wooden floor," 2008.

[31] J. Ortega, G. Vasconcelos, H. Rodrigues, and M. Correia, "Assessment of the influence of horizontal diaphragms on the seismic performance of vernacular buildings," *Bulletin of Earthquake Engineering*, vol. 16, no. 9, pp. 3871–3904, Sep. 2018, doi: 10.1007/s10518-018-0318-8.

[32] F. Solarino, D. v. Oliveira, and L. Giresini, "Wall-to-horizontal diaphragm connections in historical buildings: A state-of-the-art review," *Engineering Structures*, vol. 199. Elsevier Ltd, Nov. 15, 2019. doi: 10.1016/j.engstruct.2019.109559.

[33] L. Simões, "Ligação pavimentos/paredes de edifícios antigos. Ensaios e verificações de projeto -," Tese de Mestrado, FCT-UNL, Lisbon, 2015.

[34] P. B. Lourenço, "Computations on historic masonry structures," *Progress in Structural Engineering and Materials*, vol. 4, no. 3, pp. 301–319, Jul. 2002, doi: 10.1002/pse.120.

[35] CFA Guidance Note, "Fixings for the retention of masonry façades," Jul. 2004.

[36] L. Contrafatto and R. Cosenza, "Prediction of the pull-out strength of chemical anchors in natural stone," *Frattura ed Integrita Strutturale*, vol. 8, no. 29, pp. 196–208, 2014, doi: 10.3221/IGF-ESIS.29.17.

[37] B. Gigla, "Field pull-out tests of supplementary injection anchors in historic masonry," 1999.

[38] G. Spina, F. Ramundo, and A. Mandara, "Masonry strengthening by metal tiebars, a case study," *Structural analysis of historical constructions : possibilities of numerical and experimental techniques* -, A.A. Balkema Publishers, pp. 1207–1213, 2005.

[39] R. Muñoz, P. B. Lourenço, and S. Moreira, "Experimental results on mechanical behaviour of metal anchors in historic stone masonry," *Construction and Building Materials*, vol. 163, pp. 643–655, Feb. 2018, doi: 10.1016/j.conbuildmat.2017.12.090.

[40] I. Tomić, F. Vanin, and K. Beyer, "Uncertainties in the seismic assessment of historical masonry buildings," *Applied Sciences (Switzerland)*, vol. 11, no. 5, pp. 1–36, Mar. 2021, doi: 10.3390/app11052280.

[41] P. B. Lourenço, "Computational Strategies For Masonry Structures: Multi-scale Modelling, Dynamics, Engineerning Applications And Other Challenges," Bilbao, España, Jul. 2013.

[42] F. Vanin, A. Penna, and Katrin Beyer, "A three-dimensional macro-element for the modelling of the in-plane and out-of-plane response of masonry walls," *Earthquake Engineering & Structural Dynamics*, vol. 49, no. 14, pp. 1365. – 1387, 2020.

[43] E. Quagliarini, G. Maracchini, and F. Clementi, "Uses and limits of the Equivalent Frame Model on existing unreinforced masonry buildings for assessing their seismic risk: A review," *Journal of Building Engineering*, vol. 10, pp. 166–182, Mar. 2017, doi: 10.1016/j.jobe.2017.03.004.

[44] A. Penna, S. Lagomarsino, and A. Galasco, "A nonlinear macroelement model for the seismic analysis of masonry buildings," *Earthquake Engineering and Structural Dynamics*, vol. 43, no. 2, pp. 159–179, 2014, doi: 10.1002/eqe.2335.

[45] L. Gambarotta and S. Lagomarsino, "Damage Models For The Seismic Response Of Brick Masonry Shear Walls. Part I: The Mortar Joint Model And Its Applications," in *EARTHQUAKE ENGINEERING AND STRUCTURAL DYNAMICS*, vol. 26, 1997, pp. 423–439.

[46] F. Vanin and K. Beyer, "'Equivalent damping ratio for a macroelement modelling the out-of-plane response of masonry walls' - waiting for publication," 2021.

[47] F. A. Charney and F. Asce, "Unintended Consequences of Modeling Damping in Structures," *Journal Of Structural Engineering*, vol. 134, no. 4, pp. 581–592, Apr. 2008, doi: 10.1061/ASCE0733-94452008134:4581.

[48] A. Penna, I. E. Senaldi, A. Galasco, and G. Magenes, "Numerical Simulation of Shaking Table Tests on Full-Scale Stone Masonry Buildings," in *International Journal of Architectural Heritage*, Apr. 2016, vol. 10, no. 2–3, pp. 146–163. doi: 10.1080/15583058.2015.1113338.

[49] J. P. Almeida, K. Beyer, R. Brunner, and T. Wenk, "Characterization of mortar-timber and timber-timber cyclic friction in timber floor connections of masonry buildings," *Materials and Structures*, 2020, doi: 10.5281/zenodo.3348328.

[50] Theodoulidis and National Observatory of Athens -Institute of Geodynamics, "National Observatory of Athens Digital Broadband Network," 2004. doi: 10.7914.

[51] Presidency of Counsil of Ministers - Civil Protection Department, "Italian Strong Motion Network [Data set]. International Federation of Digital Seismograph Networks," 1972. doi: 10.7914.

[52] G. Karanikoloudis and P. B. Lourenço, "Structural assessment and seismic vulnerability of earthen historic structures. Application of sophisticated numerical and simple analytical models," *Engineering Structures*, vol. 160, pp. 488–509, Apr. 2018, doi: 10.1016/j.engstruct.2017.12.023.

[53] C. Pepi, N. Cavalagli, V. Gusella, and M. Gioffrè, "Damage detection via modal analysis of masonry structures using shaking table tests," *Earthquake Engineering and Structural Dynamics*, vol. 50, no. 8, pp. 2077–2097, Jul. 2021, doi: 10.1002/eqe.3431.

[54] POLIMI, "NIKER - Project - New integrated knowledge based approaches to the protection of cultural heritage from earthquake-induced risk," Padova, Jun. 2010.

2022

SAMUEL ALEXANDRE CORADO COSME

NUMERICAL SIMULATION OF RETROFITTED MASONRY BUILDINGS

NOVA SCHOOL OF SCIENCE & TECHNOLOGY